DEVELOPMENT OF A PORTABLE OPTICAL STRAIN SENSOR WITH APPLICATIONS TO DIAGNOSTIC TESTING OF PRESTRESSED CONCRETE

by

WEIXIN ZHAO

B.S., Huazhong University of Science and Technology, 1998
M.S., Kansas State University, 2006

AN ABSTRACT OF A DISSERTATION

submitted in partial fulfillment of the requirements for the degree

DOCTOR OF PHILOSOPHY

Department of Mechanical and Nuclear Engineering
College of Engineering

KANSAS STATE UNIVERSITY
Manhattan, Kansas

2011

Abstract

The current experimental method to determine the transfer length in prestressed concrete members consists of measuring concrete surface strains before and after de-tensioning with a mechanical strain gage. The method is prone to significant human errors and inaccuracies. In addition, since it is a time-consuming and tedious process, transfer lengths are seldom if ever measured on a production basis.

A rapid, non-contact method for determining transfer lengths in prestressed concrete members has been developed. The new method utilizes laser-speckle patterns that are generated and digitally recorded at various points along the prestressed concrete member. User-friendly software incorporating robust and fast digital image processing algorithms was developed by the author to extract the surface strain information from the captured speckle patterns. Based on the laser speckle measurement technique, four (4) successively improved generations of designs have been made. A prototype was fabricated for each design either on an optical breadboard for concept validation, or in a portable self-contained unit for field testing. For each design, improvements were made based on the knowledge learned through the testing of the previous version prototype. The most recent generation prototype, incorporating a unique modular design concept and self-calibration function, has several preferable features. These include flexible adjustment of the gauge length, easy expansion to two-axis strain measurement, robustness and higher accuracy.

Extensive testing has been conducted in the laboratory environment for validation of the sensor's capability in concrete surface strain measurement. The experimental results from the laboratory testing have shown that the measurement precision of this new laser speckle strain measurement technique can easily achieve 20 microstrain. Comparison of the new sensor measurement results with those obtained using traditional strain gauges (Whittemore gauge and the electrical resistance strain gauge) showed excellent agreement. Furthermore, the laser speckle strain sensor was applied to transfer length measurement of typical prestressed concrete beams for both short term and long term monitoring. The measurement of transfer length by the sensor was unprecedented since it appears that it was the first time that laser speckle technique was applied to prestressed concrete inspection, and particularly for use in transfer length measurement. In the subsequent field application of the laser speckle strain sensor in a CXT

railroad cross-tie plant, the technique reached 50 microstrain resolution, comparable to what could be obtained using mechanical gauge technology. It was also demonstrated that the technique was able to withstand extremely harsh manufacturing environments, making possible transfer length measurement on a production basis for the first time.

DEVELOPMENT OF A PORTABLE OPTICAL STRAIN SENSOR WITH APPLICATIONS TO DIAGNOSTIC TESTING OF PRESTRESSED CONCRETE

by

WEIXIN ZHAO

B.S., Huazhong University of Science and Technology,1998
M.S., Kansas State University,2006

A DISSERTATION

submitted in partial fulfillment of the requirements for the degree

DOCTOR OF PHILOSOPHY

Department of Mechanical and Nuclear Engineering
College of Engineering

KANSAS STATE UNIVERSITY
Manhattan, Kansas

2011

Approved by:

Major Professor
B. Terry Beck

Abstract

The current experimental method to determine the transfer length in prestressed concrete members consists of measuring concrete surface strains before and after de-tensioning with a mechanical strain gage. The method is prone to significant human errors and inaccuracies. In addition, since it is a time-consuming and tedious process, transfer lengths are seldom if ever measured on a production basis.

A rapid, non-contact method for determining transfer lengths in prestressed concrete members has been developed. The new method utilizes laser-speckle patterns that are generated and digitally recorded at various points along the prestressed concrete member. User-friendly software incorporating robust and fast digital image processing algorithms was developed by the author to extract the surface strain information from the captured speckle patterns. Based on the laser speckle measurement technique, four (4) successively improved generations of designs have been made. A prototype was fabricated for each design either on an optical breadboard for concept validation, or in a portable self-contained unit for field testing. For each design, improvements were made based on the knowledge learned through the testing of the previous version prototype. The most recent generation prototype, incorporating a unique modular design concept and self-calibration function, has several preferable features. These include flexible adjustment of the gauge length, easy expansion to two-axis strain measurement, robustness and higher accuracy.

Extensive testing has been conducted in the laboratory environment for validation of the sensor's capability in concrete surface strain measurement. The experimental results from the laboratory testing have shown that the measurement precision of this new laser speckle strain measurement technique can easily achieve 20 microstrain. Comparison of the new sensor measurement results with those obtained using traditional strain gauges (Whittemore gauge and the electrical resistance strain gauge) showed excellent agreement. Furthermore, the laser speckle strain sensor was applied to transfer length measurement of typical prestressed concrete beams for both short term and long term monitoring. The measurement of transfer length by the sensor was unprecedented since it appears that it was the first time that laser speckle technique was applied to prestressed concrete inspection, and particularly for use in transfer length measurement. In the subsequent field application of the laser speckle strain sensor in a CXT

railroad cross-tie plant, the technique reached 50 microstrain resolution, comparable to what could be obtained using mechanical gauge technology. It was also demonstrated that the technique was able to withstand extremely harsh manufacturing environments, making possible transfer length measurement on a production basis for the first time.

Table of Contents

List of Figures

List of Tables

Acknowledgements

I wish to express appreciation to my advisor, Dr. B. Terry Beck, for his friendship and guidance.

I would also like to thank Dr. Robert J. Peterman and Dr. Chih-Hang (John) Wu, with whom I have worked throughout my graduate study, for their valuable advice and insight into my research. Thank Dr. Youqi Wang and Dr. Ruth Douglas Miller for reviewing my thesis.

There are many collaborators to whom I owe my appreciation. These include Rob Murphy, Steven Hammerschmidt and Ed Volkmer, with whom I conducted extensive testing and many experiments using the laser speckle strain sensor. Trevor Heitman and Ryan Benteman also provided excellent technician support for the fabrication of the sensor. The sensor has been greatly improved due to their work.

I am also grateful of Kansas Depart of Transportation (KDOT), University Transportation Center (UTC) , Advanced Manufacturing Institute (AMI) and Precast/Prestressed Concrete Institute (PCI) for their kind financial support.

Dedication

To my wife Grace.

Chapter 1 - Introduction

1.1 Background of strain measurement for civil infrastructure

Civil engineering infrastructure comprises some of the most massively built assets in the world. For centuries, engineers have been trying to build more reliable and long-lasting infrastructure, from the Great Wall in China to the modern Interstate Highway System in the USA. Many new materials and design concepts have been proposed aimed at reducing weight, increasing spans, achieving longer infrastructure life and lower cost. However the civil engineering field has been conservative in adopting the new materials and technologies due to concern for compromising safety standards (S C Liu, 1995)(Faber & Stewartb, 2003). This resulted in a relatively slow evolution of technologies in the field of civil engineering compared to those of other disciplines such as computer science and electronic engineering. The barrier in adopting the new materials and technologies lies partly in the lack of convenient and reliable methods to evaluate their performance and implement safety control.(S C Liu, 1995)

In addition, civil infrastructure is usually designed with a large margin of safety, with the nominal load 2 or 3 times of the actual load (A.A. Mufti, 2008). However, the aging of the structure and excessive usage always lead to a reduced factor of safety. For instance, it is reported that more than 200,000 bridges in United States and 30,000 bridges in Canada are operating at a deficient condition due to the inadequate maintenance and excessive loading. (Mufti, 2003). It is risky to keep the aged civil infrastructures in service without reliable information of them.

Either to design and build civil infrastructures of extended lifetime without compromising the safety or increased cost, or to effectively qualify their performance in the term of safety, it is important to find a convenient way to collect the information about the structure performance, either at time of the construction or at the time of service. One of the factors that are always used to evaluate the performance of concrete member is the stress or strain information in the member. For example, the evaluation of the bridge health is usually done by measuring the in situ strain responding to traffic flow. (Ceravolo, 2005).

Of particular importance to civil infrastructure is prestressed concrete, which is usually fabricated by casting concrete mix around already tensioned steel strands. After the casting process is complete and the concrete has hardened, a detensioning procedure is undertaken by cutting the reinforcing strands at both ends of the concrete beam to release the tension. The stress transferred from the strands to the concrete is developed gradually from each end of the beam, where the stress is zero, and to the location far away from the end, where the stress is at its full value. The distance required to develop this stress is defined as "The transfer length", which is used to evaluate the quality and performance of concrete members. To estimate the transfer length, the surface strain profile of the prestressed concrete beam must be measured.

Many methods are available to measure strain either on the surface or in the body of the concrete structures. The strain measurement under laboratory conditions is usually straightforward, but it is much more difficult when applied in the field due to the fact that most of the strain measurements of structure materials must be done in a harsh environment, or require long term monitoring. In addition, it is recognized that a measurement technique that aimed to make its way to the diagnostic testing of large concrete structures, must be easy to use. Most civil engineers, particularly field engineers, are not experts in sophisticated sensor technology. Therefore, it is important to provide them with a practical solution instead of just a laboratory device with nanometer level resolution but could not be readily used in the field with minimum training. To be incorporated into the diagnostic testing of modern concrete structures seamlessly, the sensor must be able to provide rapid working speed and not require any special training of the workers.

The characteristics desired for a strain sensor suitable for diagnostic testing of prestressed concrete members in the field include:

- Robustness
- Portability
- Adequate sensitivity and dynamic range
- No contact to the surface
- Insensitivity to out-of-plane motion of the surface
- Insensitivity to environmental temperature fluctuation
- Removable from the surface during downtime

1.2 Literature review of strain measurement techniques

In this section, several available strain measurement techniques are discussed.

1.2.1 The Whittemore gauge

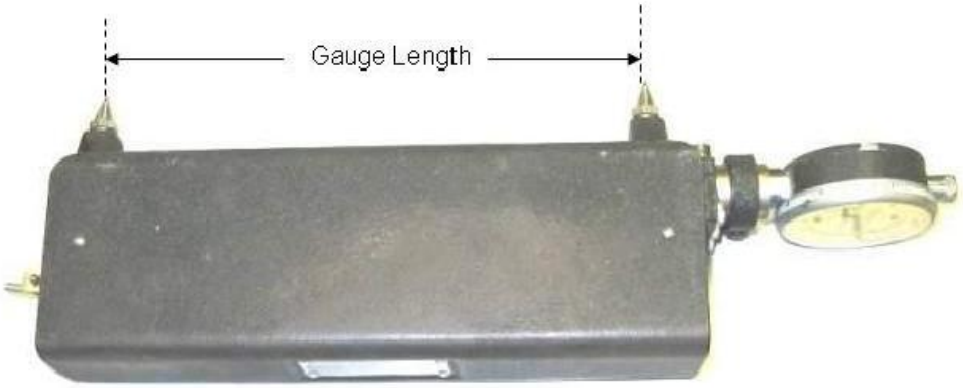

Figure 1-1 Whittemore gauge

The Whittemore gauge as shown in Figure 1-1 is a mechanical strain gauge that has been widely used for measuring surface strain of concrete structures for decades. Before a strain reading can be made, small steel circular buttons with a precision pinhole at the center, called "points", are bonded on the concrete surface by using epoxy as shown in Figure 1-2. The Whittemore gauge measures the distance between the pinholes of successive pairs of points. Prior to the surface deformation, a set of reference length measurement are made, representing the unstrained positions of the points. Then a second measurement is taken after the surface deformation. The difference between the second measurement and the reference length is divided by the gauge length 203.2mm (8"), giving the strains on the concrete surface. When a reasonable strain profile is required, tens of points must be bonded onto the concrete surface, which is very time-consuming and labor-intensive. Furthermore, the measurement results are heavily influenced by the users' habits and skills. Experience shows that different users can produce readings that are greatly different. It requires a considerable amount of training and experience to achieve consistent and repeatable results.

Figure 1-2 Prestressed concrete with metal points mounted on the surface

1.2.2 Electrical resistance strain gauge

Another traditional gauge used to measurement concrete surface strain is the electrical resistance strain gauge (MUSPRATT, 1969). It employs the principle that metallic conductors subjected to mechanical strain exhibit a change in their electrical resistance. By converting mechanical strain into an electronic signal, the electrical resistance strain gauge can measure strain to quite high resolution.

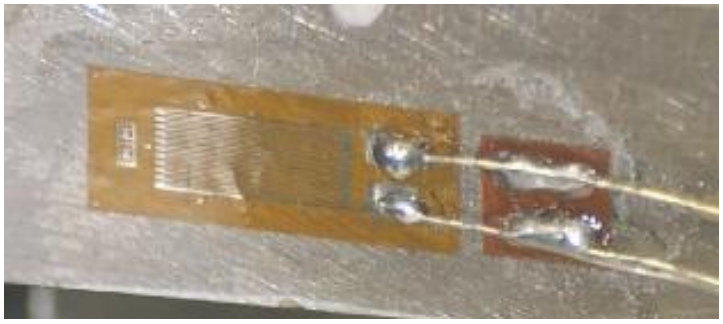

Figure 1-3 Electrical resistance strain gauge

In general, the electrical resistance strain gauge is precise, reliable and easy to use. However, the technique has several disadvantages.

- The technique requires gluing the gauge on the specimen surface. Since the gauge has contact with the specimen surface, it may influence the surface strain and cause measurement error.
- It is difficult to bond the gauge to the rough surface such as concrete.
- Temperature, material properties and the adhesive that bonds the metallic conductors to the surface all affect the detected resistance, and hence can interfere with the accuracy of the strain measurement. (A. L. Window, 1982)
- The electrical resistance strain gauge is sensitive to electromagnetic interference (EMI), which could cause measurement error when used in the industrial environment where many types of EMI inducing equipment are present, such as motors or electrical heaters.
- In a harsh environment, the glue may debond and the gauge may break off from the specimen surface, making the measurement impossible.
- In the case of large and suddenly changing surface strain, the gauge may suffer from “creep effect”. Experiments have shown that the reading of the electrical resistance strain gauge tends to decrease from an initial value if the specimen surface is subjected to a suddenly large load. The creep effect is caused by the partial debonding of the glue that bonds the gauge to the surface, which results in measurement error (Brinson, 1984).

1.2.3 Vibrating wire strain gauge

The vibrating wire strain gauge operates on the principle that the natural frequency of a pretensioned wire is affected by the stress applied to it. The relationship between the natural frequency f and the stress σ is described by (A. L. Window, 1982)

$$f = \frac{1}{2l}\sqrt{\frac{\sigma}{\rho}} \tag{1.1}$$

where ρ is the wire material density and l the length of the wire.

The vibrating wire gauge is very simple in design. Two anchors are installed on the specimen surface and the two ends of the wire are attached to the anchors. Once the stress σ of the wire is known using Equation (1.1) , the strain of the surface can be found too, assuming the wire deformation faithfully follows the surface deformation. The advantage of the wire vibration gauge is that the gauge (wire) can be removed from the specimen, which makes it a suitable tools for long-term monitoring of strain change in the concrete structure. The major drawback of the wire vibration gauge is its sensitivity to ambient temperature. It is reported that a 1 degree temperature change causes a $20\mu\varepsilon$ change in the strain measurement (Neild, 2005). In some situations the specimen temperature changes rapidly, either due to ambient temperature change, or due to active heating to the concrete mix to expedite the cure process. Unless the thermal expansion factor of the specimen is the same of that of the wire, measurement error is introduced. It is possible to compensate the error caused by the temperature change, but doing so greatly complicates the system.

1.2.4 Fiber optics strain sensor

Fiber optics based measurement techniques are very versatile. As many as 60 different quantities, including temperature, pressure and strain can be measured by fiber optics. (Fuhr, 2000). For strain measurement, Fiber Bragg Grating is one of the most popular methods in recent years. The optical fiber used in this method is fabricated in a way that there is a periodic

variation of the refractive index in the fiber core, called a “Bragg grating”. Suppose the grating interval is G, as shown in Figure 1-4, The Bragg wavelength is calculated by

$$\lambda = 2 \cdot n \cdot G \tag{1.2}$$

where n is the average refractive index.

When incident light passes through the Bragg grating, only the light of the wavelength equal to the Bragg wavelength will be reflected and the light of the wavelength other than the Bragg wavelength transfers through. Since the Bragg wavelength λ is dependent on the Bragg grating interval G, which is in turn directly related to the applied strain, the applied strain can be determined by measuring the Bragg wavelength, i.e. the wavelength of the reflected light.

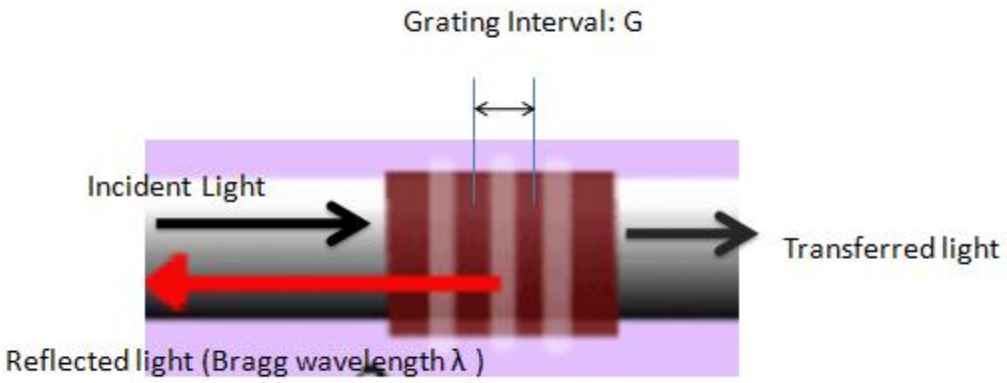

Figure 1-4 Fiber Bragg Gratings (Merzbacher, 1996)

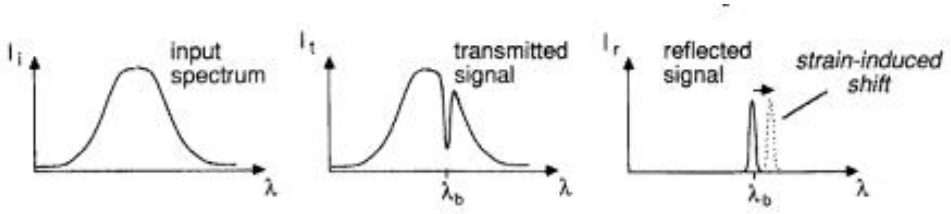

Figure 1-5 Transmission and reflection of Fiber Bragg Grating (Merzbacher, 1996)

Fiber Bragg Grating method has several advantages over the traditional eletrical resistance strain sensor. First, it is immune to electromagnetic interference from the industrial enviroment (Merzbacher, 1996). In addition, it does not suffer from any light intensity fluctuation in that it measures the strain based on the change of the reflected light wavelength, which is an absolute quantity. However, there are several drawbacks associated with the Fiber Bragg Grating method.

- To measure the specimen strain, the optical fiber can be either be mounted onto the surface or embedded in the body of the specimen. When the fiber is embedded in the concrete mix, the alkaline chemical environment starts to erode the thin coating that protects the fiber core. For long term strain measurement, the aging of the fiber might be a problem or even cause the loss of the measurement. The protection of the leads of the fiber that exit from the concrete surface is also a concern in field applications of the method.
- It is questionable how faithfully the strain of the fiber follows the change of the strain of the specimen. The loss of grip (debond) between the fiber and the concrete mix might happen, causing a difference of the strain between them.
- It is reported that when the FBG fiber is not aligned to the principal stress direction of the host material, the strain detected by the FBG sensor will be much different than that of the host material. (Hong-Nan Li, 2007)

1.2.5 Video extensometer

A video extensometer measures the surface strain by tracking the coordinates of contrasting marks placed on the specimen. The gauge marks can be in the form of grid of dots or lines as shown in Figure 1-6, with the dot diameter or line thickness ranging from half millimeter to a couple of millimeters. The video image captured by the digital camera is analyzed by the image processing algorithms to locate the centers of the dots or the edges of the lines. During the test, the centers of the dots or the edges of the lines are followed automatically by the software. Their coordinate changes are used to extract the specimen strain information (Malo, 2008).

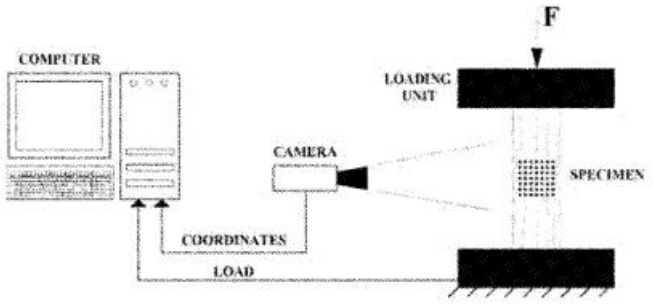

Figure 1-6 Video extensometer configuration (Malo, 2008)

Since the surface strain is measured by tracking a center of the mark, fine marks must be applied to the surface, such as a 7x7 grid of 0.5 mm diameter dots as described in wood surface strain measurement (Malo, 2008). For a material with irregular or soft surface, the application of marks may not be practical.

Some other Video extensometers, such as the MTS LX Laser Extensometer (MTS LX laser extensometer, 2009), use tapes instead of marks to tag the surface displacement. The tape that attaches to the specimen surface has strip spacing on it. The extensometer determines the surface strain by measuring the extension of the strip spacing. The technique is not a real non-contact measurement method since the tape contacts the specimen surface. It is possible that the strip and the specimen extend or shrink by different amounts due to a creep effect, so that the strain measured from the tape does not faithfully represent the actual specimen strain. The resolution is limited by tape strip spacing and usually low.

1.2.6 Laser speckle strain measurement

Speckle is generated by illuminating a rough surface with coherent light as shown in Figure 1-7. The random reflected waves interfere with each other, resulting in a grainy image, as shown Figure 1-8. The speckle pattern could be thought of as a “fingerprint” of the illuminated area in the sense that the speckle pattern produced by every surface area is unique. Furthermore, when the surface area undergoes movement or deformation, the speckle pattern in the image plane will also move or deform accordingly.

Most optical speckle methods for in-plane displacement or deformation measurements are based on the same principle. That is, the grainy speckle pattern image is recorded before the

surface is deformed and after the surface deformation. The deformation or displacement components can then be extracted by comparing the speckle patterns before and after a surface deformation. This is typically done statistically using a cross-correlation technique to measure the speckle displacement. (See Section 2.4 for detailed discussion of cross-correlation technique)

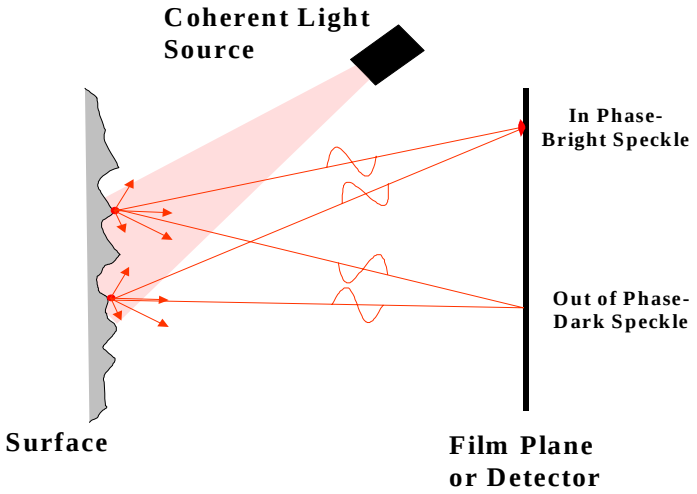

Figure 1-7 Speckle Generation Principle

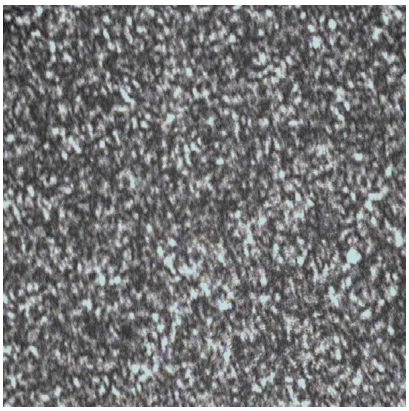

Figure 1-8 Speckle Pattern

There exist two basic categories of speckle technique for surface strain measurement: electronic speckle pattern interferometry (ESPI) and digital speckle photography (DSP). They relate to different methods of producing and processing the speckle image. The ESPI technique measures the object surface displacement or deformation by detecting the corresponding phase change of the light wavefronts reflected from the surface, just as a conventional Michelson interferometer does. The image taken in an ESPI system, called a "speckle interferogram", is produced by interfering the speckle radiation reflected from an object surface with a reference

light field, either a uniform coherent light beam or another speckle field (Dainty, 1975). In practice, the speckle interferograms are taken both before and after the object displacement or deformation. A characteristic fringe pattern can be obtained by subtracting the two speckle interferograms. The fringe spacing corresponds to a 2π phase change of the wavefronts resulted from the object surface deformation, as is the case with a Michelson interferometer with a mirror displacement. Thus the surface deformation and displacement can be readily determined by counting the number of fringe changes. As an interferometry method, the ESPI technique has high resolution on the order of a fraction of a light wavelength, and the resolution is not limited by the resolving power of the imaging system (Samala, 2005) (Helena (Huiqing) Jin, 2006). As fringe counting is involved, this method has a 2π ambiguity limitation; that is, the periodical fringe pattern resembles itself whenever it shifts by an integer multiple of 2π phase. There is no easy way to determine the phase change uniquely. Another limitation is in the upper bound of the deformation that can be measured, due to the limited number of visible fringes on the detector (typically a CCD array) (C. Joenathan, 1998).

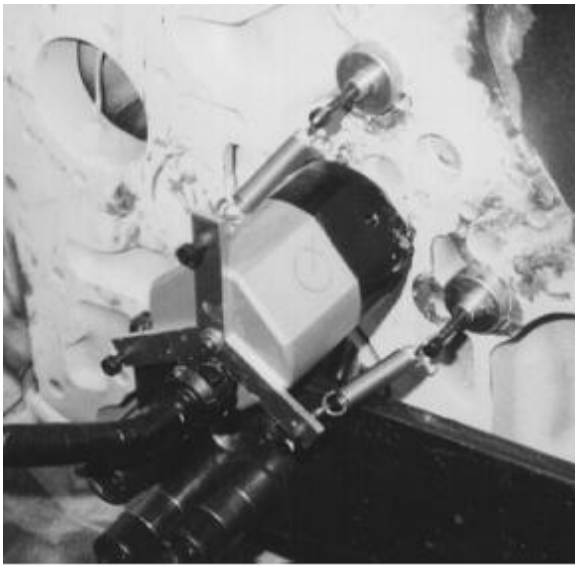

Figure 1-9 Microstar® Strain gauge

Fig 1-9 shows a commercial full field strain sensor named Microstar® based on ESPI technique. It has the ability to automatically analyze the geometry and the deformation of the surface area of interest within 100nm resolution. Due to its miniature size, the sensor can be easily attached to the components during testing and has received a wide acceptance in

automobile and aerospace industries.(L.X. Yang, 1999)(R.Wegner, 1999). The Microstar® strain sensor requires stringent alignment with the specimen surface and must be fixed onto the specimen surface throughout the measurement process to prevent rigid relative movement. This drawback makes it impractical to be used for strain measurement for civil engineering structure, where either long term monitoring of the surface strain is required, or enormous shock happens to the subject such that the sensor must be removed to avoid damage. For instance, a prestressed concrete beam is subjected to a nominal 30,000lb sudden force during the detensioning of the steel strands and this may damage the sensor if left on the concrete surface.

The DSP technique, on the other hand, is based on intensity correlation. By comparing two speckle images, taken before and after surface deformation, the in-plane displacement vector resulting from the loading can be determined. Once the complete displacement field is obtained, it can be differentiated to obtain an in-plane strain map. DSP generally has lower resolution than ESPI, but larger dynamic range. The resolution is limited by the speckle size, which typically ranges at the micrometer level, and the resolving power of the imaging system. There exists some strain measurement devices in the market utilizing DSP technique. One of them is ME-53 extensometer (ME-53 Laser speckle extensometer manual)(Eduard Schenuit, 2008) from Messphysik company. It has two variations. One version consists of two cameras and a servo drive that controls the motion of the cameras for a large gauge length setup, as shown in Figure 1-10; the other version consists of a single camera for small area surface strain measurement. The ME-53 laser speckle extensometer makes non-contact strain measurement based on the DSP technique and does not require any surface marking. However it is mainly designed for laboratory use. The sensors must be mounted on a vertical track and the specimen must be installed on a laboratory bench. This is to prevent the relative rigid motion between the sensor and the specimen. Although the DSP technique is designed to measure in-plane movement, it is also commonly sensitive to surface tilt (yaw and pitch), which brings error into the strain measurement. The bulky size of the system also makes the system impractical for use in the field. Furthermore, a calibration procedure involving displacement of the camera by a certain known distance using the servo system that comes with the system must be conducted by the end user prior to the measurement. In addition, whenever the distance between the sensor and the specimen surface changes, the system must be re-calibrated.

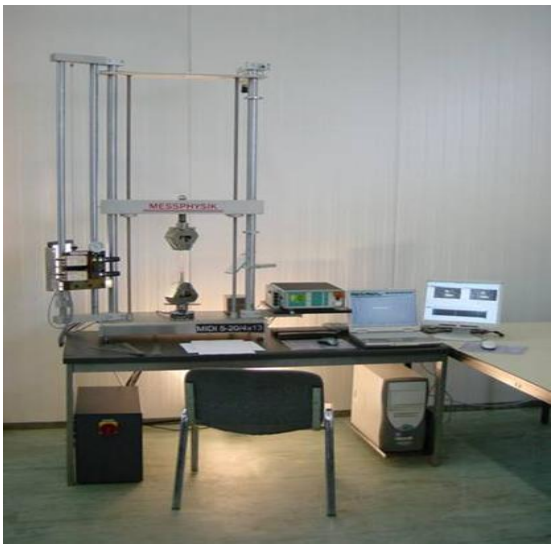

Figure 1-10 ME-53 laser speckle extensometer

1.3 Overview of dissertation

The importance of having a reliable and robust strain measurement technique for either factory monitoring or "field testing" of concrete structural members has been described above. The current available methods are either more opted for laboratory testing or are too slow to allow online monitoring.

The work presented in this dissertation illustrates the development of a general strain measurement technique based on the laser speckle principle that is able to rapidly and accurately determine concrete surface strains. An understanding of the relationship between the multi-degree motion of the subject surface and the induced motion of the speckle pattern is required in order to make the laser speckle measurement technique applicable to the typically harsh industrial environment. A portable prototype incorporating unique modular design concept and self-calibration feature has been fabricated. The portable design enables flexible adjustment of the gauge length and easy expansion to a rosette strain measurement configuration.

Extensive testing has been conducted in the laboratory environment to validate the sensor. Furthermore, the laser speckle strain sensor was applied to transfer length measurement of common prestressed concrete beams, and prestressed concrete cross-ties in the field. The sensor yielded unprecedented measurements of transfer length in just a few minutes, compared to the hours that are needed if using the current accepted method of measurement.

Through this testing with different applications, it has been shown that the newly developed portable laser speckle strain sensor can not only serve as an accurate instrument in the civil engineering laboratory where the deflection characteristics of a concrete member are needed, but also can be readily used in the harsh environment of the prestress concrete industry, with minimum surface preparation and staff training. It also has the potential to rapidly process a large quantity of data points in an industrial setting.

It should be noted that, as far as the author is aware, the new developed sensor is the first device to successfully employ speckle method to determine transfer length of prestressed concrete. Furthermore, this development represents the first time that such a method has been demonstrated successfully in a harsh industrial environment with sufficient resolution and accuracy, to make automated transfer length measurement possible in the concrete railroad cross-tie manufactory industry.

The chapters in this dissertation are arranged as follows:

- **Chapter 2: Theoretical background of the laser speckle strain measurement**
  Theoretical modeling of the speckle will be presented, using Fourier optics. The principle behind the 5-axis motion measurement, which serves as the foundation of the design of the laser speckle strain sensor, will be discussed. The digital image correlation technique, which is the crucial part of the data analysis, will also be presented.
- **Chapter 3: Hardware design of the optical strain sensor**
  Various different hardware designs of the laser speckle strain sensor will be described in detail. Their advantages and drawbacks will be compared. Technical detail of the individual components including laser head, CCD camera, lens and the alignment mechanism used by the sensor will be presented.
- **Chapter 4: Software development of the optical strain sensor**
  The preprocessing of the captured speckle images will be presented. A detailed explanation of how the digital correlation procedure is conducted to extract the relative shifting of the speckle patterns in sub pixel resolution will be presented, along with the various techniques that are implemented to speed up the correlation computation.

- **Chapter 5: Calibration**

  The general procedure for the calibration of the laser speckle strain sensor will be presented. Then the effect of the sensor misalignment will be investigated. An improved calibration method that is able to correct the error caused by the orientation difference of the two camera coordinates will be presented.

- **Chapter 6: Conclusion**

  The work that has been done for the development of the laser speckle strain sensor will be summarized. The recommendation of future work based on the efforts presented here will be discussed.

The appendices at the end of the dissertation contain the references cited in the text. The hardware components list and the specifications for the sensor, along with the uncertainty analysis, are also included. An operation manual for the laser speckle strain sensor and the software source code are attached to the end of the dissertation.

Chapter 2 - Theoretical background of laser speckle strain measurement technique

Speckle is generated by illuminating a rough surface by coherent light. The reflected light interferes constructively and destructively, creating a grainy pattern at the observation plane. In this chapter, Fourier optics, statistical tools and imaging theory are used to explore the various characteristics of the speckle. The characteristics of the speckle are described mathematically and the optimal spatial sampling resolution is obtained. Furthermore, the theory of 5-axis motion measurement technique will be described. The 5-axis motion measurement was developed at the early stage of the optical strain sensor development. It is important to the strain sensor development in that the object surface during deformation is usually subjected to 6 degrees of freedom movement. However, only the in-plane displacement information is used to calculate the strain. The motion of other axis, especially the out-of-plane rotations act as error source to the strain measurement. The 5-axis motion measurement system is able to separate the 5-axis movement so that the movement of each axis can be measured independently, thus the effect of the out-of-plane rotations can be eliminated for the strain measurement. To the end, the digital image correlation technique is discussed. It is an image process technique that estimates the relative shift of the speckle image pairs taken before and after the surface deformation, such that the displacement or strain information can be extracted.

2.1 Mathematical description of the speckle phenomenon

Speckle is generated by illuminating a rough surface with coherent light, as shown in Figure 1-7. The random reflected waves interfere with each other, resulting in a grainy image, as shown Figure 1-8.

Figure 2-1 shows an imaging system of recording the subjective speckle filed by a CCD camera. The object plane XY is illuminated by a laser light beam. The reflected laser lights from the rough object surface is collected by the lens and then imaged onto the camera plane xy from the object. The distance between the lens and the object plane is d_o and the distance between the

camera plane and the lens is d_i. For surface deformation measurement, the speckle images are recorded twice by the camera, before and after the surface deformation.

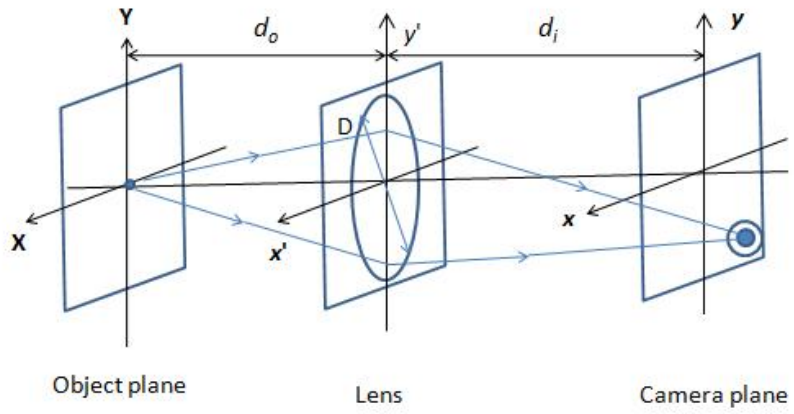

Figure 2-1 Imaging system of recording the speckle pattern

The amplitude response of a point source at coordinate $(0,0)$ on the object plane XY, which is also the impluse response function of the optical imaging system, is defined as (Goodman, 1996)

$$h(x,y)=\int_{-\infty}^{+\infty}\int P(\lambda d_i x',\lambda d_i y')\exp[-j2\pi(xx'+yy')]dx'dy' \tag{2.1}$$

where $P(\lambda d_i x',\lambda d_i y')$ is the pupil function

$$P(\lambda d_i x',\lambda d_i y')=\begin{cases}1 & \sqrt{x'^2+y'^2}\le\dfrac{D}{2\lambda d_i}\\ 0 & \text{otherwise}\end{cases} \tag{2.2}$$

where D is the diameter of the lens pupil and (x',y') is the coordinate on the lens plane.

Denoting $\rho=\sqrt{x'^2+y'^2}$, we have

$$x'=\rho\cos\theta \qquad y'=\rho\sin\theta \tag{2.3}$$

Further define $r=\sqrt{x^2+y^2}$

$$x=r\cos\xi \qquad y=r\sin\xi \tag{2.4}$$

Substituting Equation (2.3) and Equation (2.4) into Equation (2.1), and implementing the polar integral,

$$h(x,y)=\int_{0}^{\frac{D}{2\lambda d_i}}\int_{0}^{2\pi}\exp[-j2\pi\rho r\cos(\xi-\theta)]\rho d\theta d\rho \tag{2.5}$$

Since the Bessel function of the first kind is defined as

$$J_0(u)=\frac{1}{2\pi}\int_{0}^{2\pi}\exp[-ju\cos(\theta)]d\theta \tag{2.6}$$

we have,

$$h(x,y)=2\pi\int_{0}^{\frac{D}{2\lambda d_i}}J_0(2\pi\rho r)\rho d\rho \tag{2.7}$$

Further using the integral identity of the Bessel function of the first kind,

$$\int_{0}^{u}u'J_0(u')du'=uJ_1(u) \tag{2.8}$$

Equation (2.7) can be simplified to be

$$h(x,y)=\frac{J_1(2\pi Dr/\lambda d_i)}{\pi Dr/\lambda d_i} \tag{2.9}$$

Since the optical imaging system is shift-invariant, meaning that the shifting of the input in some direction shifts the output by the same distance and direction, for a point source location at the coordinate (X,Y) on the object plane, the amplitude response at coordinate (x,y) on the camera plane is

$$h(x,y;X,Y)=h(x-X,y-Y) \tag{2.10}$$

Since the optical imaging system is a linear system, the complex amplitude at coordinate (x,y) on the camera plane is the superposition of amplitude response of all the point light sources (X,Y) where $-\infty<X<+\infty$ $-\infty<Y<+\infty$.

Assuming

$$u_o(X,Y)=f(X,Y)\exp[-j2\pi\phi(X,Y)] \tag{2.11}$$

The convolution of the object intensity with the point spread function is

$$u_i(x,y) = \int_{-\infty}^{\infty}\int h(x-X, y-Y)u_o(X,Y)dXdY \tag{2.12}$$

Denoting the Fourier transform of $u_o(x,y)$, $u_i(x,y)$ and $h(x,y)$

$$U_o(\omega_x,\omega_y) = F\left[u_o(X,Y)\right] \tag{2.13}$$

$$U_i(\omega_x,\omega_y) = F\left[u_i(x,y)\right] \tag{2.14}$$

$$H(\omega_x,\omega_y) = F\left[h(x,y)\right] = P(\lambda d_i\omega_x, \lambda d_i\omega_y) \tag{2.15}$$

where

$$P(\lambda d_i\omega_x, \lambda d_i\omega_y) = \begin{cases} 1 & \omega_x^2+\omega_y^2 \le (\dfrac{D}{2\lambda d_i})^2 \\ 0 & \text{otherwise} \end{cases} \tag{2.16}$$

The convolution form in Equation (2.12) can be expressed in frequency domain as,

$$U_i(\omega_x,\omega_y) = H(\omega_x,\omega_y)U_o(\omega_x,\omega_y) \tag{2.17}$$

The intensity at point coordinate (x,y) on the camera plane is,

$$s(x,y) = \left|u_i(x,y)\right|^2 = u_i(x,y)u_i^*(x,y) \tag{2.18}$$

where $u_i^*(x,y)$ is the conjugate of $u_i(x,y)$.

Therefore, the Fourier transform of $s(x,y)$ can be represented as the convolution of $U_i(x,y)$ and $U_i^*(x,y)$

$$\begin{aligned} S(\omega_x,\omega_y) &= F\left[s(x,y)\right] \\ &= F\left[u_i(x,y)u_i^*(x,y)\right] \\ &= U_i(\omega_x,\omega_y) * U_i^*(-\omega_x,-\omega_y) \end{aligned} \tag{2.19}$$

Substituting Equation (2.17) into Equation (2.19),

$$S(\omega_x,\omega_y) = \left[H(\omega_x,\omega_y)U_o(\omega_x,\omega_y)\right] * \left[H^*(-\omega_x,-\omega_y)U_o^*(-\omega_x,-\omega_y)\right] \tag{2.20}$$

Observing that $u_o(X,Y)$ is the reflected laser light beam intensity from the rough object surface, due to the random feature of the surface profile, both the amplitude term and phase term are modulated randomly. Therefore $u_o(X,Y)$ can be regarded as a random function.

Therefore Equation (2.20) is simplified as

$$S(\omega_x,\omega_y) = H(\omega_x,\omega_y) * H^*(-\omega_x,-\omega_y) \tag{2.21}$$

Since $h(x,y)$ is symmetric, we have $H^*(-\omega_x,-\omega_y) = H^*(\omega_x,\omega_y)$

$$S(\omega_x,\omega_y) = H(\omega_x,\omega_y) * H^*(\omega_x,\omega_y) \tag{2.22}$$

Thus

$$s(x,y) = \left|h(x,y)\right|^2 \tag{2.23}$$

Substituting Equation (2.9) into Equation (2.23), we get the intensity distribution of the subjective speckle pattern,

$$s(x,y) = s(r) = \left[\frac{J_1(2\pi Dr/\lambda d_i)}{\pi Dr/\lambda d_i}\right]^2 \tag{2.24}$$

where $r = \sqrt{x^2+y^2}$, and x, y are the coordinates at the image plane, J_1 is the standard Bessel function of the first kind, D is the lens pupil diameter, d_i is the image distance, λ is the light wavelength. The intensity distribution function of the subjective speckle pattern is plotted in Figure 2-2. According to the Rayleigh criterion (Hecht, 1998), the average speckle size is determined as the value of r where the value of the function $s(r)$ drops to its first local minimum. By setting $J_1(\frac{2\pi Dr}{\lambda d_i}) = 0$, the solution is found to be

$$\frac{2\pi Dr}{\lambda d_i} = 3.83 \tag{2.25}$$

which in turn gives

$$r = 1.22\frac{\lambda d_i}{D} \tag{2.26}$$

This is the average size of the speckle on the camera plane.

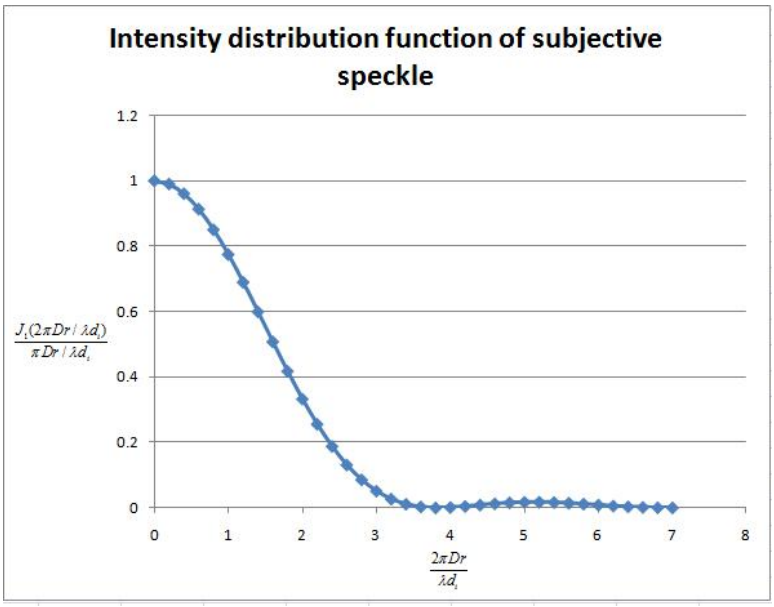

Figure 2-2 Plot of speckle intensity distribution function

2.2 Review of the 5-Axis motion measurement system

Axial strain measurement is accomplished by taking the differential of the relative displacements between two points on the object surface. A typical speckle measurement is fulfilled by first illuminating the associated specimen surface with coherent light (laser). The random reflections from the surface features (roughness) generate a grainy speckle pattern image at the camera plane. This speckle pattern could be thought of as a "fingerprint" of the illuminated area, in the sense that the speckle pattern produced by a given surface region is unique. Furthermore, when the surface undergoes movement or deformation, the speckle pattern in the image plane will also move or deform accordingly. This tracking feature is the basis of the displacement measurement of the laser speckle technology.

However, the speckle displacement at the camera plane usually is not only sensitive to the object surface displacement, but also to other axis movements of the object surface; especially the out-of-plane rotations (tilt and yaw), which result in error in the strain measurement. To extract the displacements accurately without being affected by other axis movements, a 5-axis motion measurement technique was developed that is able to separate the 5-

axis movement so that the movement of each axis can be measured independently, thus the effect of the out-of-plane rotations are mostly eliminated.

The 5-axis measurement principle is based on the fact that for subjective speckle there exist two characteristic planes behind the lens, a ‘tilt-only plane’ and a ‘translation-only plane’, such that the speckle image at the tilt-only plane is only sensitive to the tilt of the specimen, and the speckle image at the “translation-only” plane is only sensitive to the translation of the specimen. (D.A.Gregory, 1976). These planes are shown in Figure 2-3.

The 5-axis motion measurement technique was developed during the early stage of the laser speckle strain sensor development (Zhao, 2006). The principle of the 5-axis motion measurement was later applied to the design of the optical strain sensor in which the camera is positioned at the ‘translation-only plane’ of the optical system to eliminate the effect of the surface motion other than the in-plane displacement. A detailed discussion of the 5-axis motion measurement technique can be found in author’s M.S. thesis (Zhao, 2006).

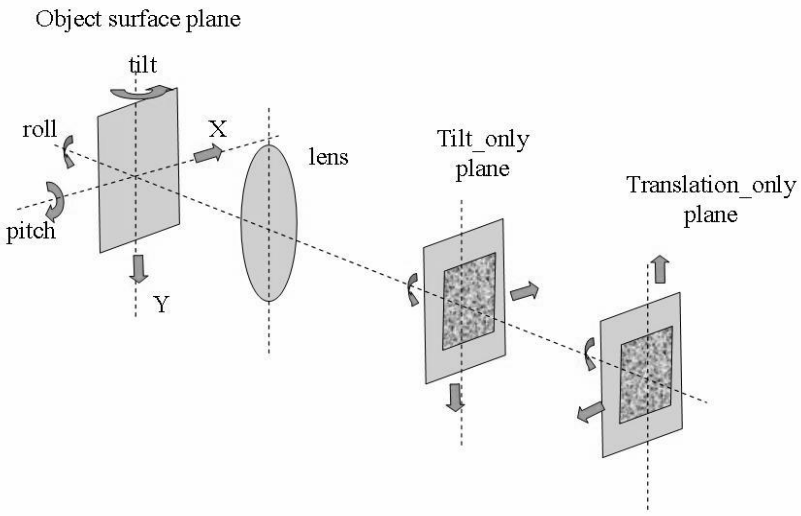

Figure 2-3 Tilt-Only Plane and Translation-Only Plane

2.3 Insensitivity of system sensitivity to out-of-plane movement

During the operation of the optical strain sensor in the field, in some situations the sensor does not work in a stationary manner. For example, for the prestressed concrete beam strain measurement, the sensor is required to be removed from the concrete beam surface before the

detensioning, and then be put back on the surface after the detensioning, due to the fact that the detensioning process involves a release of a 30000*lbs* (13607 kg) traction force, which could damage the sensor if left on the concrete surface. Thus the repositioning of the laser speckle sensor will cause the distance between the lens of the optical system to the concrete surface to vary inevitably. This arises a problem that the change of the object distance will affect the system sensitivity.

Figure 2-4 shows the measured systematic sensitivity to object translation at different object-sensor distances. It shows that the system sensitivity varies significantly when the sensor is at different depth positions relative to the object plane. This is obviously an undesired characteristic for a sensor.

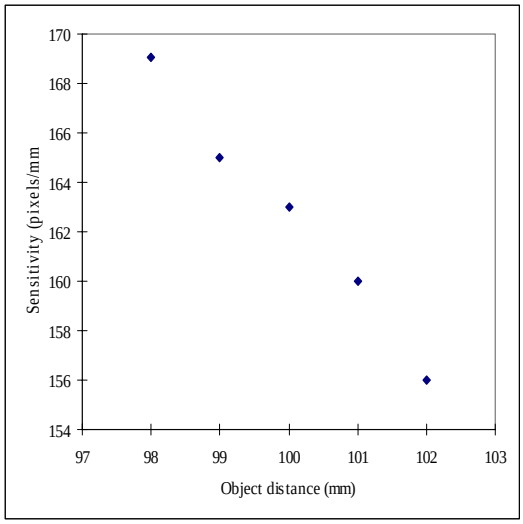

Figure 2-4 System sensitivity changes due to the object distance change (Zhao, 2006)

However, it is proved that under the condition of collimated and normal illumination, the system sensitivity becomes insensitive to the out-of-plane object movement (Zhao, 2006). Experiments, as shown in Figure 2-5, have confirmed this behaviour. In the range of 6mm variation of object distance, the systematic sensitivity has no significant variation.

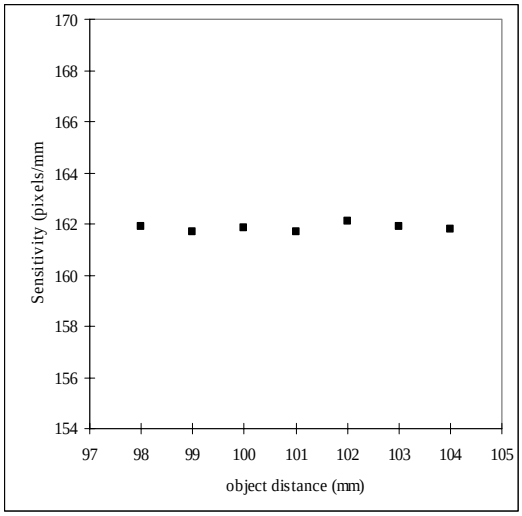

Figure 2-5 Invariance of system Sensitivity (Zhao, 2006)

2.4 Digital correlation technique

As discussed previously, the shift of speckle image captured by the camera is proportional to the translation of the object surface under a specific imaging setup. The issue of detecting the surface motion is thus actually one of evaluating the relative shift of the speckle image pairs taken before and after the surface deformation. This is done by using the digital correlation technique.

Suppose we have two speckle images I_1, I_2 of the object surface taken before and after the surface deformation. The traditional cross-correlation function is defined by

$$Corr(x, y) = \sum_{i=1}^{N} \sum_{j=1}^{N} I_1(i, j) I_2(x + i, y + j) \tag{2.27}$$

By varying the values of x and y, the maximum value of the correlation function $Corr(x, y)$ can be found, and its coordinates give the relative components of the image displacement. The disadvantage of the function above is that it is subjective to changes in image intensity amplitude, generally caused by change in lighting conditions across the image recording sequence, which are very likely to happen during a typical concrete beam strain test

measurement period that might last for months. To overcome the shortcomings associated to the traditional correlation method, adapted digital correlation algorithms are more often used.

2.4.1 Normalized correlation

This method calculates the mean of the speckle image I1 and I2, then determines their normalized version I1' and I2'. The correlation coefficient is then obtained similar to Equation (2.27). The result is normalized again to obtain the normalized cross-correlation coefficient.

$$R(x,y)=\frac{\sum_{i=1}^{N}\sum_{j=1}^{N} I_1'(i,j)I_2'(x+i,y+j)}{\sqrt{\sum_{i=1}^{N}\sum_{j=1}^{N} I_1'(i,j)^2 \sum_{i=1}^{N}\sum_{j=1}^{N} I_2'(x+i,y+j)^2}} \tag{2.28}$$

where

$$I_1'(i,j)=I_1(i,j)-\frac{\sum_{i'=1}^{N}\sum_{j'=1}^{N} I_1(i',j')}{N*N} \tag{2.29}$$

$$I_2'(x+i,y+j)=I_2(x+i,y+j)-\frac{\sum_{i'=1}^{N}\sum_{j'=1}^{N} I_2(x+i',y+j')}{N*N} \tag{2.30}$$

A perfect match will give a peak equal to 1 and a complete no match will give a peak of 0. The normalization operation used by this method helps reduce effects of the image intensity variation to the matching of the image pairs.

2.4.2 Phase correlation

Although the normalized correlation algorithm works quite well on the regular images, it was observed that it works poorly on the speckle image. This is due to the unique characteristics of the speckle pattern, which is a grainy pattern without any repeated feature. If the speckle pattern is transformed to the frequency domain, it can be observed that considerable information of the image is stored in the high spatial frequency domain, contrary to the regular image for which most information is stored in the low spatial frequency domain. The intensity of every speckle element in the pattern does not carry much information due to the fact that its intensity tends to fluctuate continuously and randomly when the object surface moves. The fluctuation of

the intensity of individual speckle is in fact noise and should not be taken into account when matching the speckle image pairs. Instead, it is the relative location of the speckles between the speckle image pairs that determines if the image pairs are correlated, and the amount of relative shifting. This explains why the normalized correlation algorithm, functioning well on the regular images by matching the image pairs pixel by pixel according to their intensity level, does not work well on the speckle image pairs.

Alternatively, a phase correlation algorithm based on the Fourier Transform is able to discard the intensity information and reply primarily on the phase information for matching the image pairs. The overall procedure using a phase correlation technique for speckle image shift detection is described below.

Suppose a pair of speckle patterns is given, corresponding to deformed and un-deformed states. The two speckle images can be represented as $f(x, y)$ for the un-deformed one and $f(x-u, y-v)$ for the deformed one, where (u,v) denotes the components of the local displacement vector which are regarded as constants here (Zhao, 2006)

In the first step, two complex spectrums of the image pair are obtained as follow,

$$F_1(\omega_1, \omega_2) = \iint f(x, y) e^{-j2\pi(x\omega_1 + y\omega_2)} dxdy \tag{2.31}$$

$$F_2(\omega_1, \omega_2) = \iint f(x-u, y-v) e^{-j2\pi(x\omega_1 + y\omega_2)} dxdy \tag{2.32}$$

A basic property of Fourier Transform yields (Bracewell, 1978),

$$F_2(\omega_1, \omega_2) = e^{-j2\pi(u\omega_1 + v\omega_2)} F_1(\omega_1, \omega_2) \tag{2.33}$$

The normalized cross-power spectrum of the two images is then calculated as

$$\frac{F_1(\omega_1, \omega_2) F_2^*(\omega_1, \omega_2)}{\left| F_1(\omega_1, \omega_2) F_2(\omega_1, \omega_2) \right|} = e^{j2\pi(u\omega_1 + v\omega_2)} \tag{2.34}$$

By applying a second-step FFT to the resulting spectrum, $F(e^{j2\pi(u\omega_1 + v\omega_2)}) = \delta(u,v)$, a pulse signal appears in the second FFT spectrum image at (u,v), which represents the

displacement vector between the image pairs. In this approach, the FFT spectrums $F_1(\omega_1, \omega_2), F_2(\omega_1, \omega_2)$ consist of both magnitude information and the phase information. After the normalization, the magnitude information is removed and only the phase information is retained.

For verification purposes, a pair of speckle images with relative shifting were cross-correlated using both the normalized correlation algorithm and the phase correlation algorithm. The resulting correlation images were very different. In the correlation image produced by the normalized correlation algorithm, as shown in Figure 2-6, the peak is suppressed by the high intensity of background noise. While for the phase correlation, as shown in Figure 2-7, the peak is very clear.

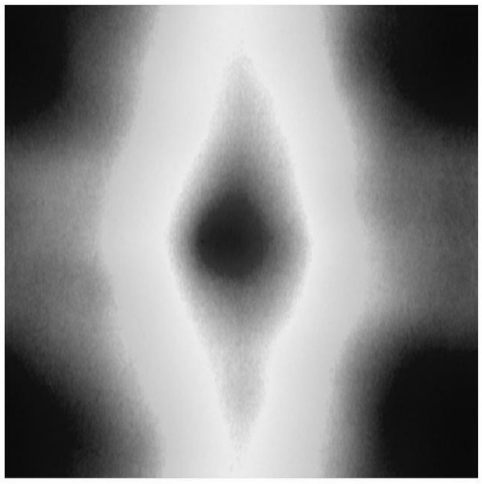

Figure 2-6 Normalized correlation results for a typical speckle image pairs

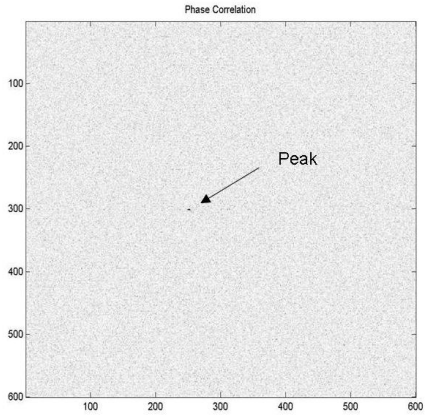

Figure 2-7 Phase correlation results for a typical speckle image pairs

Chapter 3 - Hardware design for the optical strain sensor

This chapter discusses the hardware design of the strain sensor. Multiple factors must be brought into the consideration during this design stage. The main objectives of the design are listed in the following.

- To develop a portable surface strain sensor capable of measuring surface strain. The sensor dimension should be as small as possible and the weight should be light for the portability of the sensor.
- Measurement uncertainty to be on the order of 25-50 microstrain in order to have capability similar to the Whittemore gauge whose uncertainty is about 50 microstrain.
- Nominal range of measurement should be large enough to facility easy positioning and alignment of the sensor in handheld work mode.
- The sensor is aimed for a commercial product to replace the industrial standard Whittemore gauge. Thus it should be easy to manufacture and assemble.
- The sensor is to be for use in harsh environment where various condition including extreme temperature, humid, vibration and dust pose challenge to the sensor's function. For example, one of the field application that the sensor has been applied to is the transfer length measurement of railroad cross-tie in a manufacturing plant. The temperature in the plant varies as much as 60 ºF through the year, with max temperature more than 100 ºF in the summer. The sensor must be able to withstand harsh environments and maintain high functional performance in operation.
- Minimal training required

The digital speckle photography (DSP) technique that has been reviewed in Chapter 1 was chosen to be used for the development of the optical strain sensor. DSP technique has large dynamic range, e.g. the maximum deformation or displacement that the technique can measure, which makes it more robust than other optical strain measurement techniques based on laser speckle. DSP technique generally has relatively lower resolution, which is limited by the speckle

size that typically ranges at the micrometer level. But the resolution is high enough for the concrete beam strain measurement application.

During the development of the current laser speckle strain sensor, four (4) generations of successively improved designs have been manufactured and tested. A prototype was fabricated for each design either on an optical breadboard for concept validation or in a portable form for use in field testing. For each design, improvements were made based on the knowledge learned through the testing and analysis of the prototype based on the previous generation design. The four (4) generations of designs and their prototypes are described below in chronological order of their development.

3.1 5-axis motion measurement system

An optical system capable of measuring the desired 5-axis (five degree of freedom) object movement was constructed during the early stage of the current laser speckle strain sensor development, and resulted in the author's Master thesis.(Zhao, 2006). The 5-axis motion measurement technique, employed in this optical breadboard layout was important to the strain sensor development in that the object surface during deformation is usually subjected to full 6 degrees of freedom movement. The traditional optical speckle methods, though designed to measure in-plane movement, are also sensitive to surface tilt and other rotational modes that are very likely to happen during the concrete surface strain measurement. These rotation effects will introduce severe error to the surface displacement or strain measurement if properly taken into account..

The characteristics of the previously developed 5-axis motion measurement system are described below (Zhao, 2006). The system employed the concepts of "translation-only" plane and "tilt-only" plane to separate the surface in-plane displacement and out-of-plane tilt; thereby, eliminating or greatly reducing rotation-induced error. The 5^{th} axis movement (in-plane rotation) was detected by using a polar-correlation technique. The 6^{th} axis movement (out-of-plane translation) of the specimen surface is shown both theoretically and experimentally to have no contribution to the in-plane surface strain, and is therefore not measured by the sensor.

A schematic of the 5-axis motion measurement system is shown in Figure 3-1. A prototype of this optical system was also built on breadboard, as shown Figure 3-2. Experiments were conducted to confirm that the system is able to separately and accurately resolve 5 axis motion: X, Y, tilt, yaw, and roll of the specimen, with the expected insensitivity to out-of-plane displacement (Zhao, 2006).

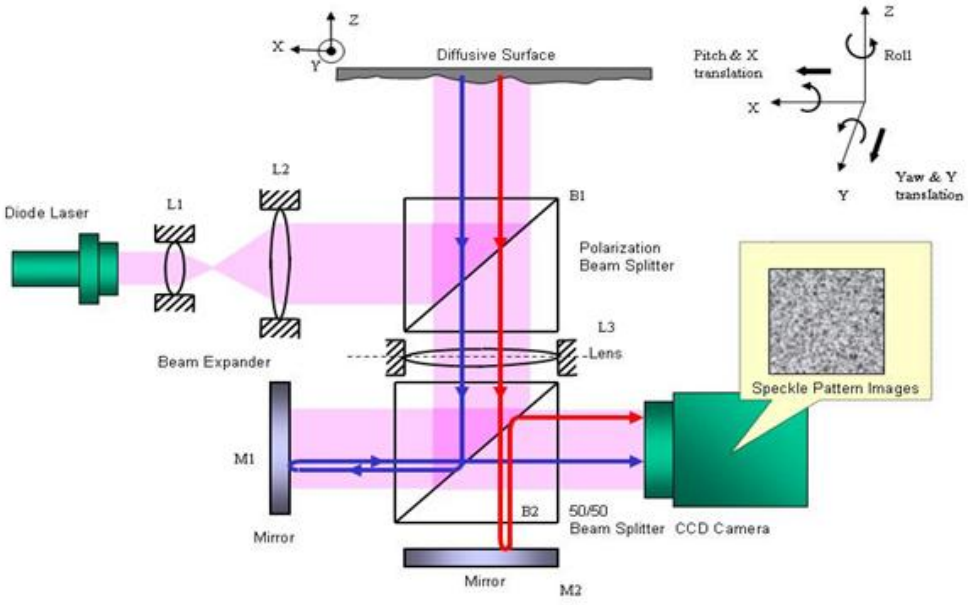

Figure 3-1 5-Axis Measurement Imaging System

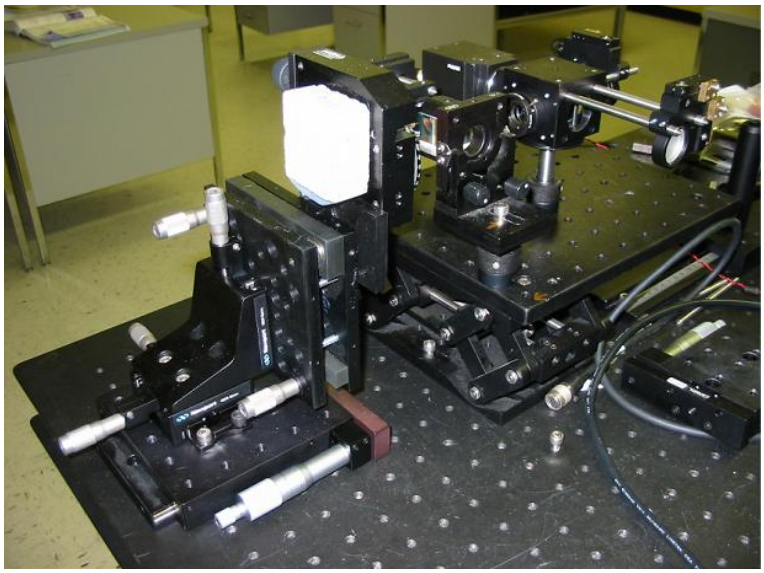

Figure 3-2 Breadboard prototype for the 5-Axis motion measurement system

3.2 Single module design

Based on the 5-axis breadboard motion measurement system, a portable laser speckle strain sensor was designed and fabricated utilizing one laser head and one camera

Since only the in-plane displacement components (*X*, *Y* displacements) are of interest in the measurement of surface strain, an optical strain sensor was built to measure the in-plane displacement components of two nearby surface points on the object surface by detecting the speckle shifts at the corresponding "translation-only" planes only. The configuration of the imaging system makes the sensor insensitive to any surface motion other than the in-plane displacement. A schematic diagram of the sensor is shown in Figure 3-3. The sensor is an integration of two identical displacement measurement systems that measure the displacements at point A and point B, respectively.

A laser is collimated by lens L1, L2 and then directed to the specimen surface at point A and point B respectively using polarization beam-splitter B1. The reflected waves from the diffusive surface are directed through the beam-splitter B1 and the lens L3. Right in front of lens L3 is a non-polarizing beam-splitter B2 that sends the reflected laser beams to Mirror M4. The light beams then go back through the beam-splitter B2 and are finally captured by the CCD camera. Mirror M4 is used to make the sensor more compact by folding (doubling) the optical path length. Since there are two laser beams, reflected from point A and point B on object surface and sent to a CCD camera, the CCD camera actually captures two speckle patterns at the same time. The analysis of the speckle images would be more complicated if the two speckle patterns overlapped each other. There are two approaches to prevent this from happening. One approach involves manually blocking one laser beam at a time and taking the speckle image twice. When the laser beam that illuminates point A is blocked, the speckle image captured by the camera is generated by point B only. Likewise when the laser beam that illuminates point B is blocked, the speckle image captured by the camera is generated by point A only. The other approach is to block half of each of the laser beams with Stop 1 and Stop 2, as shown in Figure 3-3, such that only half of the areas around point A and point B are illuminated. This results in two simultaneous side-by-side speckle patterns (Figure 3-4) on the CCD camera, generated by point A and point B, respectively.

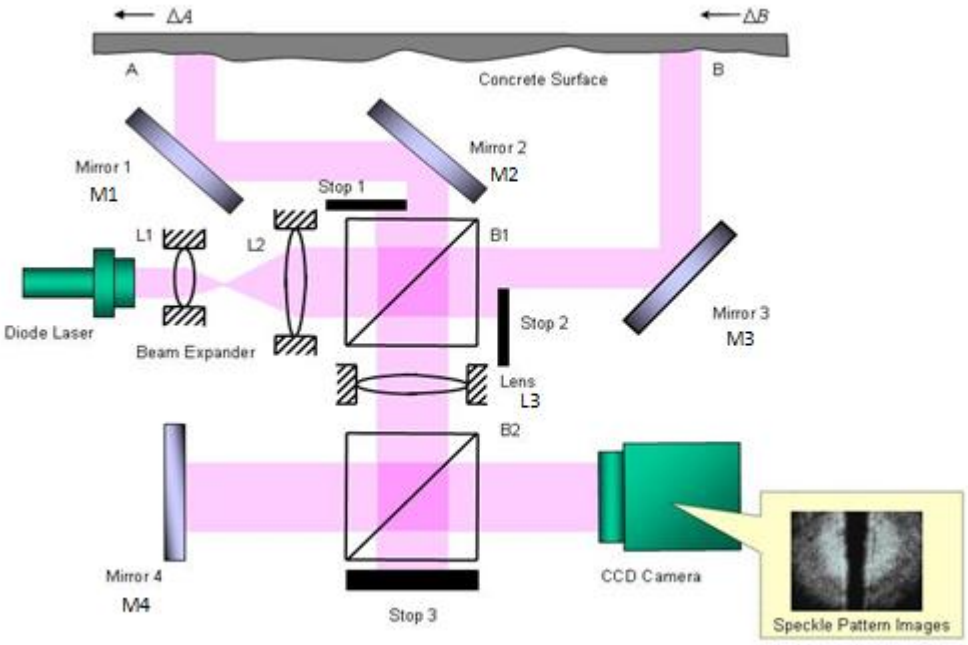

Figure 3-3 Single module design

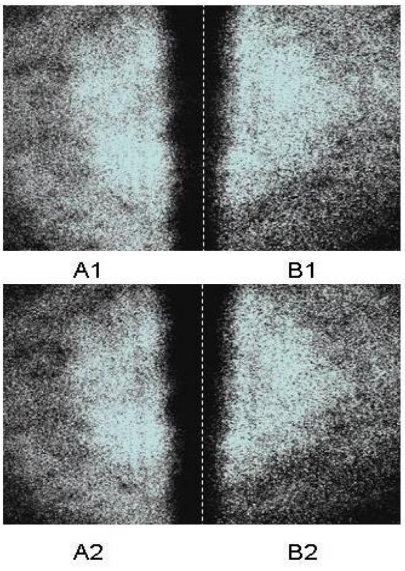

Figure 3-4 Image splitting

The prototype of single module design and its interior view (dust cover removed) are shown in Figure 3-5 and Figure 3-6 respectively. The optical system was built using the Cage System® components from Thorlabs company for rapid fabrication. The camera is a Marlin

F145B CCD camera with a resolution of 1392 by 1040 pixels. All the optics components, the camera and the laser head are mounted on a single piece of 8”x2” steel base. The sensor were enclosured in a metal box with the dimension of 11”x7”x4”. The mass of the sensor is 7 lbs.

Figure 3-5 Prototype based on single module design

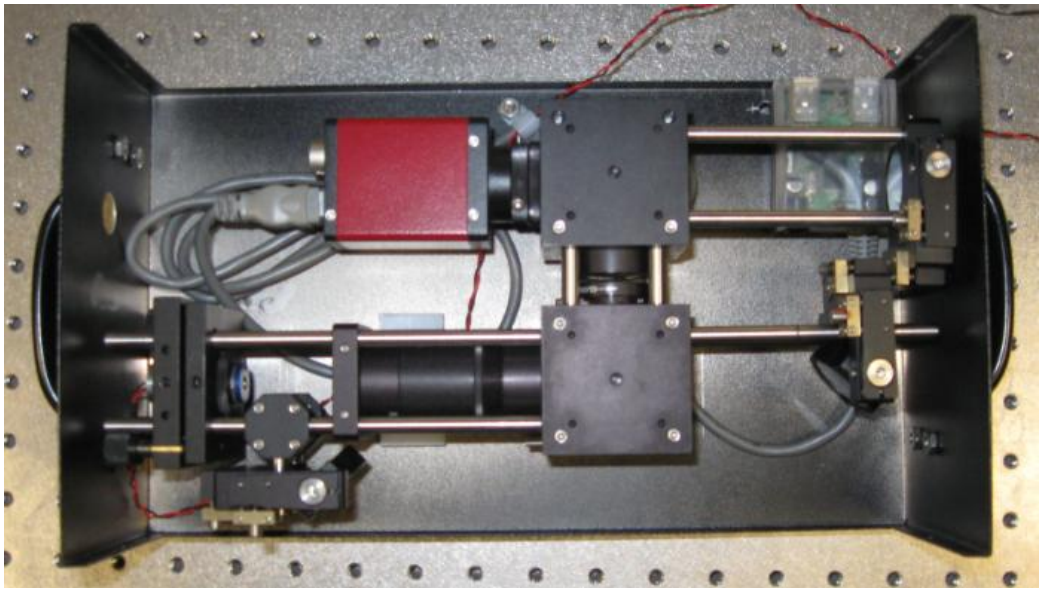

Figure 3-6 Interior view of the prototype based on the single module design

During the measurement, the optical strain sensor is first positioned onto the concrete surface before the detensioning. The CCD camera then captures a speckle image of the two side-

by-side speckle patterns as shown in Figure 3-4, which are generated by point A and point B, respectively. These two patterns are denoted as A1 and B1. The sensor is then removed from the concrete surfaces. After the detensioning, the optical sensor is positioned (mounted) back onto the surface. The camera captures another speckle image with two speckle patterns, which are denoted as A2 and B2. By applying a cross-correlation technique to the pair of speckle patterns A1 and A2 (before and after the detensioning processes), the displacement ΔA can be extracted. The displacement ΔB can be extracted from pattern B1 and pattern B2 in a similar fashion.

As shown in Figure 3-7, the axial surface strain, ε, between point A and point B can thus be determined from $\varepsilon = \frac{\Delta B - \Delta A}{L}$, where L is the gauge length 203.2 *mm* (8 inches) for the current setup.

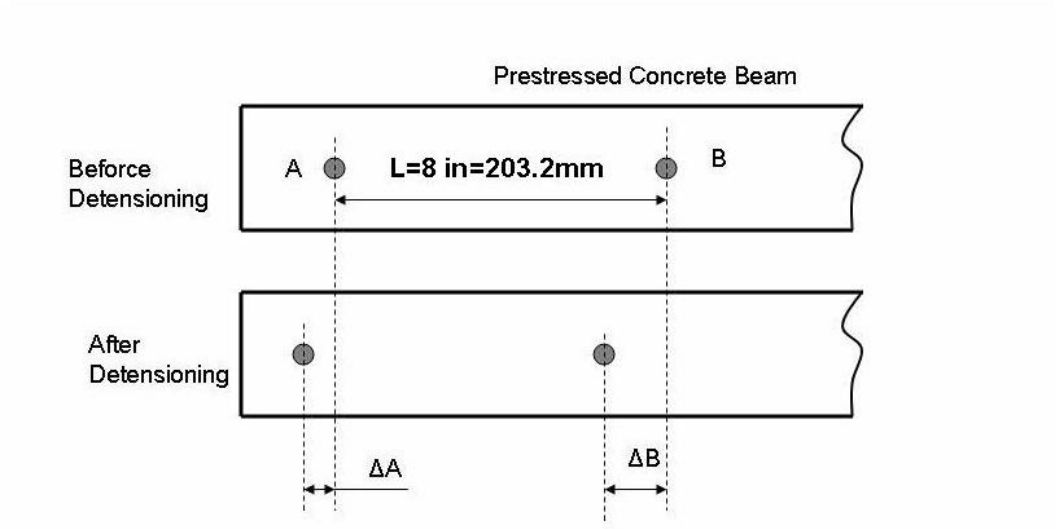

Figure 3-7 Strain Measurement

The single module strain sensor was extensively tested in a laboratory environment as well as on actual prestressed concrete beams in the field. The measurement results were compared with those obtained using traditional gauges (Whittemore gauge and the electrical resistance strain gauge) and showed good consistency. The experiments and applications are discussed in detail in Chapter 6. A provisional patent was also granted for the design.

The laser speckle strain sensor based on the single module design, although proved to be a working unit, suffered from the following drawbacks:

- Assembly

  The single module design made use of one set of optical system component to capture the images of two areas on the object surface. To achieve this, three mirrors (M1, M2, M3) in Figure 3-3 are used in the system. The laser light had to be spilt and directed to the two surface areas to be measured using these three mirrors. At the same time the three mirrors were also used to direct the reflected light from the two separate areas on the object surface onto the single camera, whose size was only 6.4mm by 4.8mm. The two-folded adjustment of the three mirrors proved to be a very difficult task.

- Gauge length

  With the single module design, the gauge length was fixed after the sensor was assembled. To change the gauge length, the whole system would have to be redesigned and rebuilt.

- Measurement range

  The single module design integrated two identical displacement measurement systems into one system by sharing the lens and camera. To prevent the images of the two surface areas from overlapping each other on the single camera, a mechanism was taken to separate the two speckle images. One of the approaches involved manually blocking one of the two laser beam at a time. This required additional manual operation by the user and significantly reduced the measurement pace. The other approach was to block half of each of the laser beams, which resulted in two side-by-side speckle patterns on the CCD camera. Each speckle pattern used only half area of the CCD chip, as shown in Figure 3-4. However, this approach causes the measurement range of the sensor be halved.

- Weight

  The prototype sensor weighed 7lbs. It makes the user fatigue quickly when the sensor was operated in manual mode and was handheld by the user.

3.3 Dual module design

In observing the drawbacks associated with the single module design, the next generation of the sensor took the form of modular design, which consisted of two identical modules that were attached to each other rigidly side by side. The new sensor detects the displacement at two points (usually 8 inches apart, but adjustable) on the specimen surface, which is converted into the surface strain by dividing the net displacement by the gauge length. The displacement measurement is based on the Digital Speckle Photography (DSP) technique. The principle of the measurement technique is as follows: A typical measurement is fulfilled by recording the speckle images before and after the object displacement or deformation. The two images are then cross-correlated and the peak position of the correlation image indicates the displacement of each ends.

A schematic of the dual module design is shown in Figure 3-8. The two individual modules are identical, except that one is a "right handed module" and the other is a mirror-arranged (or left-handed) copy of the right-handed module. Each of the modules consists of a 5mW diode laser head that emits laser light of 635 nanometers wavelength, which is then expanded by lens L1 (12.7mm focal length) and lens L2 (35mm focal length) into a collimated laser light of 10mm diameter. The expanded laser light is then directed to the specimen surface by a beam-splitter B1. The reflected waves are imaged at a magnification of unity by the lens L2 onto a CCD image sensor of 1392x1024 pixels whose output signal is then sent to a PC for data processing. The image sensor is a monochrome Lu130M CCD camera powered by 5v DC with 4 Watts power consumption. The whole optical system for individual module was rigidly mounted on single metal base to keep the relative position of the optics components fixed. The two modules were then rigidly attached together to keep the gauge length of the sensor constant.

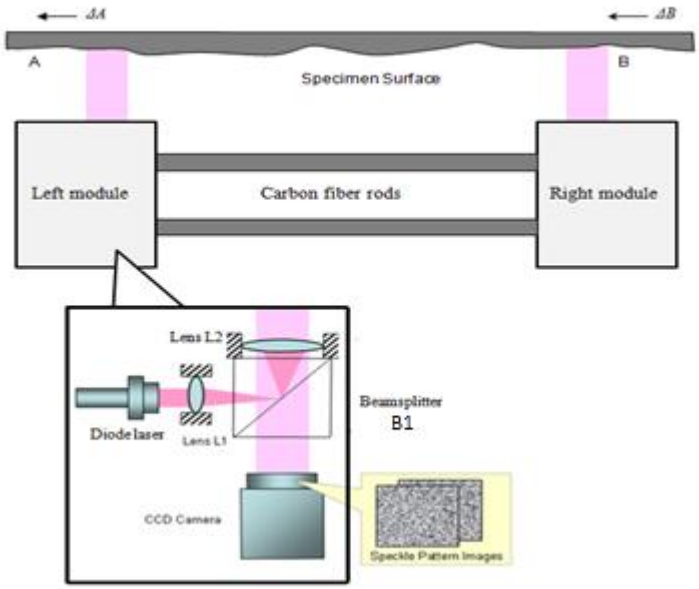

Figure 3-8 Dual module design

It is notable that the lens L2 serves two purposes in the system. It collimates the laser light and also images the reflected speckle pattern to the camera. Since the imaging system is a conjugate configuration, a double convex lens is required. However, regular convex lenses with spherical surface suffer spherical aberration, which distorts the speckle image and introduces measurement error. The lens actually used in the optical strain sensor is a triplet lens that consists of three single lenses, one convex lens and two concave lenses. The positive aberration from the convex lens and the negative aberration from the concave lens are cancelled out. This setup dramatically reduces the distortion of the imaging system.

A schematic of the dual module design with current nominal dimensions labeled is shown in Figure 3-9.

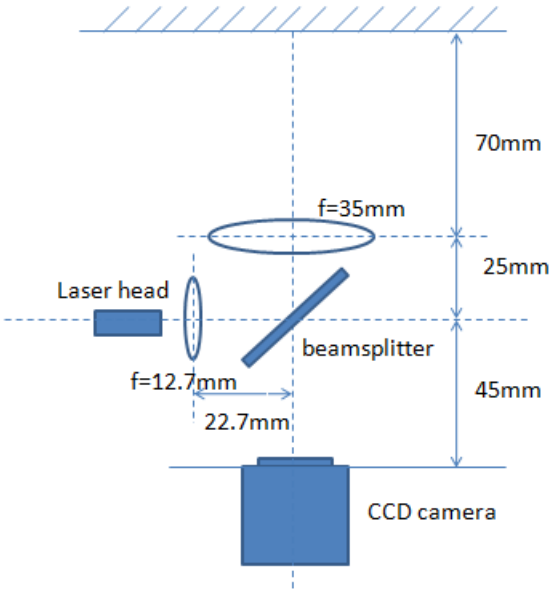

Figure 3-9 Schematic of the dual module design with dimensions labeled

Since the basic methodology of single module design and dual module design are similar ,it would appear that strain sensors based on either design should be able to measure the strain with comparable resolution. However, in terms of the practical functionality and performance, the dual module design is more preferable for the following reasonings:

- Assembly

  Unlike the single module design that requires tedious adjustment of multiple mirrors during the assembly process, the dual module design does not require any mirrors, so it is almost adjustment free.

- Gauge length

  With the dual module design the adjustment of the gauge length is very easy. All the user needs to do is to unscrew the two modules from the rods or bars that connect the two modules together, adjust the distance between the two modules to achieve the desired gauge length, and then re-tighten the screws to fix the locations of the two modules. With the auto calibration feature that will be discussed in Chapter 5, the calibration of the system parameters takes less than five minutes and can be done in the field without the need for special additional calibration equipment.

- Measurement range

  Unlike the single module design that requires mechanisms to prevent the speckle images of the two inspected area from being overlapped with each other, the dual module design is free of this problem since each of the speckle images is captured by a separate CCD camera. The measurement range is also doubled, compared to that of the single module design that adopts the splitting image approach, because the entire CCD array is devoted to measure the separate end-point displacement.

The dual module design also has its drawbacks:

- Since the dual module design consists of two sets of nearly identical optical systems, the total cost is doubled compared to the single module design.
- As an electronic component, the image captured by the CCD camera is subject to drift due to various noises. In the dual module design, the two cameras each suffer their own image drift. The sum of the independent drifts of the two speckle images from left and right modules is reflected as a distance change in the measurement, causing error in the strain reading. The single module design does not suffer from this problem due to the fact that both speckle images are captured by the same camera such that the camera drift affects both speckle images, which in turn is canceled out in the measurement results.
- In practice, the two cameras in the dual design will have a minor orientation difference no matter how well the sensor is assembled. The analysis in Chapter 5 shows that even a 0.4 degree orientation difference can cause an error comparable to the nominal resolution of the sensor if not taken into account. To deal with the problem caused by the orientation difference of the two cameras, a more complicated calibration algorithm has to be implemented.

Overall the traits of the dual module design overweigh its disadvantages. Efforts were subsequently expended on its implementation and perfection of the dual module design. Both the third and the fourth generation prototypes are fabricated based on the dual module deign. They are discussed below.

3.3.1 The third generation prototype

Figure 3-10 shows the third generation prototype that is based on dual module design. The two modules (left and right-handed) shown are attached rigidly to each other using two "L shaped" cross-section steel channels (1" flange length, 7" long) and eight ¼"-20 mounting screws. Figure 3-11 shows the interior view of an individual module. A "L shaped" bracket was used as the base for the module. The optics are mounted on one edge of the bracket and the camera are on the other edge. The module was covered with a plastic enclosure made from rapid-prototyped ABS-Plastics. The dimensions of the individual module were 5"x4"x2" and the total weight of the prototype was 5.2 lbs.

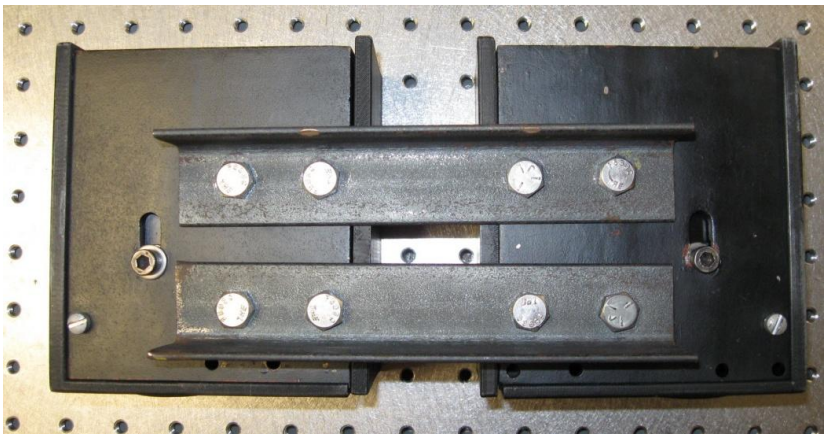

Figure 3-10 The third generation prototype based on dual module design

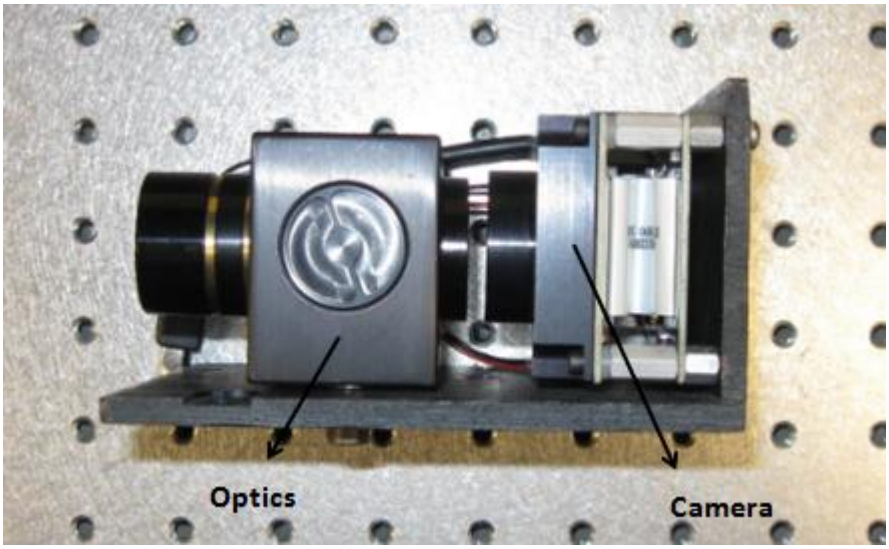

Figure 3-11 Interior view of the individual module of the third generation

This third generation prototype based on dual module design was extensively tested in laboratory environment. Severe errors were observed in the measurement of surface displacement and strain. Through investigation, it was found that the significant errors were from a thermal expansion effect primarily related to the camera heating. As an electrical device, the speckle strain sensor has an inherent thermal expansion effect, which resulted in an enormous displacement or strain. The moment the sensor is turned on, the electrical components, mainly the camera running at 4 Watts, starts to dissipate heat and causes the continuous thermal expansion on the hardware. The effect of the thermal expansion on the strain sensor is two-fold. First, there is a possible change of the sensor gauge length, and second, there is possible an accompanying change in the optical imaging system configuration.

- Change of the sensor gauge length

  Since the channel bars used in this third generation prototype that connect the two modules are steel, whose thermal expansion coefficient nominally is $7.3\ 10^{-6}\ in/in\ ^{o}F$, every degree Fahrenheit increase in temperature will cause the steel bar or the sensor gauge length to expand as much as 7.3 microstrain, which will in turn be falsely recorded by the sensor as the specimen deformation. Although it is possible to compensate for the error by recording an appropriate temperature change of the connection bar during the operation of the strain sensor, the compensation may not be accurate and may make the system far more complicated.

- Change of the optical imaging system

  In the optical imaging system, the relative positions of various components are supposed to be fixed. However, since the optics were mounted on one edge of the "L" shaped steel bracket and the camera were on the other edge, the deformation of the bracket could change the relative positions of the optics and the camera, and in turn cause measurement error by the sensor. More importantly, it is difficult to predict how much error will be introduced by the deformation of the bracket, since this will depend on the temperature distribution of the steel bracket, thus the compensation of this error could be difficult to implement in practice.

3.3.2 The fourth generation prototype

The fourth generation prototype was also based on dual module design, and was developed with multiple measures to minimize the effects of thermal expansion on the sensor strain measurement.

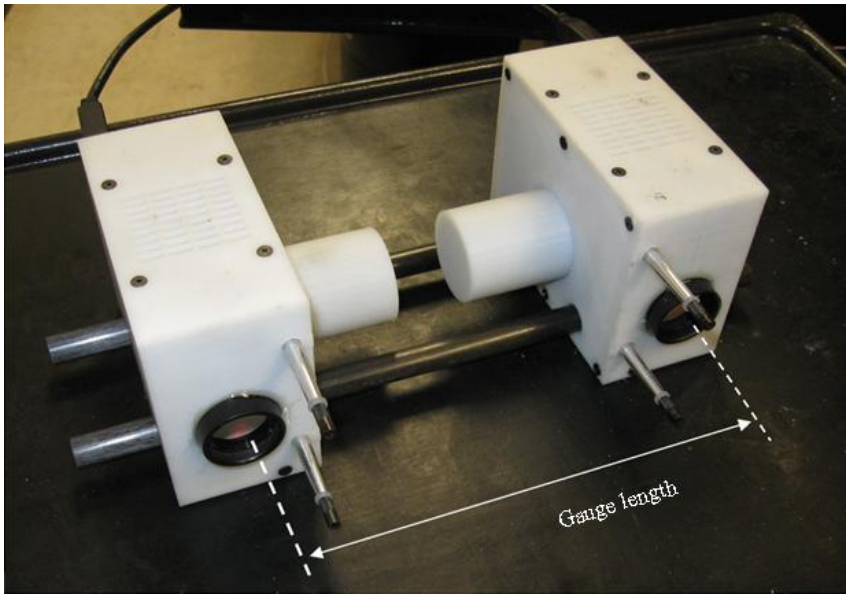

Figure 3-12 The fourth generation prototype based on dual module design

Figure 3-12 shows the fourth generation prototype. For this design, the two modules were attached rigidly to each other using two carbon fiber rods whose thermal expansion coefficient is 1/10 of that of steel. This significantly reduces the sensor gauge length change caused by temperature change. Figure 3-13 shows the interior view of an individual module. The optics and the camera's CCD chip were attached together as one piece. The whole imaging system of each individual module is mounted rigidly on an aluminum base. This prevented the relative positions of the imaging system components from change. In addition, the main heat generation component, which is the camera circuit board, was positioned far away from the rest of the imaging system. Air vent slits were made at the top of the enclosure to facility heat dissipation to outside by free convection.

The module was enclosured in a box fabricated from ABS plastic using a Rapid-prototyping system. The dimension of an individual module is 4”x3”x2” and the total weight of the prototype is 2.6 lbs.

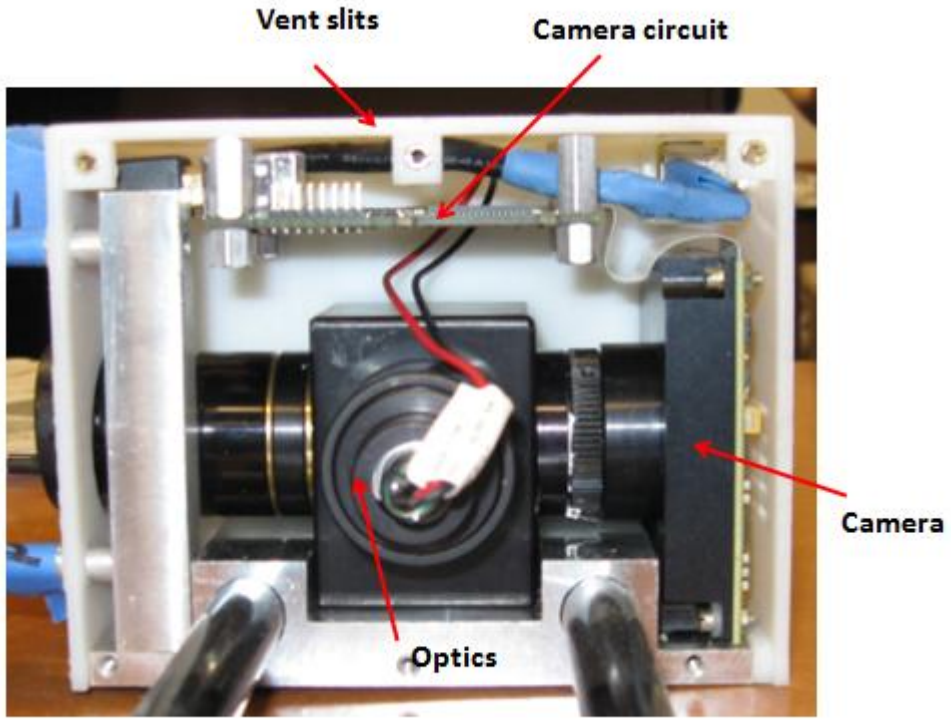

Figure 3-13 Interior view of the fourth generation prototype

An experiment was conducted to quantitatively evaluate the effect of thermal expansion on the strain measurement. This was accomplished by measuring strain on a non-deforming surface using the third generation prototype and the fourth generation prototype. Tests started from a state initially in equilibrium with the ambient temperature. Ideally both sensor prototypes should report zero since the specimen surface undergoes no deformation. However as the camera dissipates heat and the temperature of the sensor starts to climb, the effect of the thermal expansion will be reflected by the non-zero readings of both prototypes. Figure 3-14 shows the measured deflection reading from the third generation prototype in pink curve and that from the fourth generation prototype in blue curve. It can be seen that the deflection reported by the third generation prototype keeps increasing until it stabilizes at 12 microns. Considering the system’s nominal resolution of 20 microstrain (see Appendix C) with an 8” (203.2mm) gauge length which corresponds to 4 microns, the error from thermal expansion is three times of the nominal

resolution of the sensor and must be reduced to make the sensor usable in real application. In contrast, the fourth generation prototype reported less than 2 microns throughout the experiment, showing that the measures that were taken in the design of the fourth generation prototype successfully reduced the effect of the thermal expansion on the strain sensor performance.

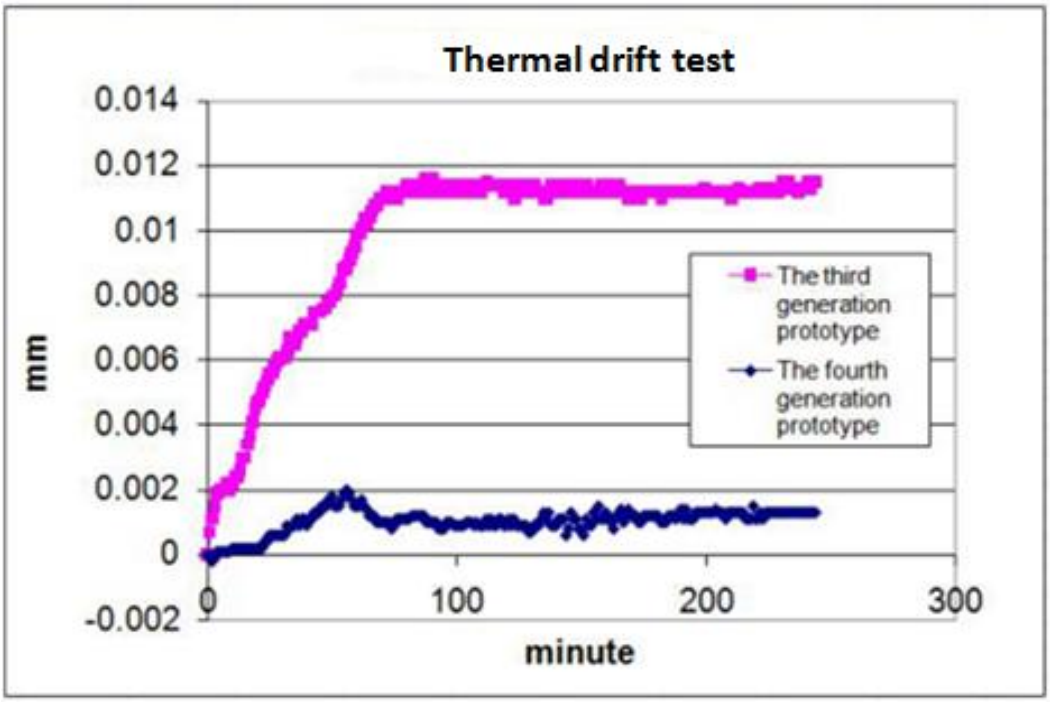

Figure 3-14 Experiment to evaluate thermal expansion effect

3.4 Components of the optics system

3.4.1 Laser Head

The laser head used in the optical strain sensor is a compact laser diode module. It consists of a laser diode circuit, collimating lens and the drive circuit, packaged in a metal or plastic housing.

In choosing the laser head for the sensor, there are several factors to consider. Ideally the laser beam intensity profile is a Gaussian shape due to several beneficial properties that come with it. A Gaussian profile beam always remains Gaussian along its path of propagation through the optical system (Hecht, 1998). Thus the propagation of Gaussian beams through an optical system can be treated almost as simply as geometric optics. However a low quality laser head

might produce a saw-tooth type of laser beam profile (Figure 3-15). It is hard to predict the behavior of a non-Gaussian shape laser beam when it goes through the lens. In addition, the inconsistency of the laser beam profile will introduce artificial noise to the speckle image captured by the camera and this interferes with repeatability of the strain measurement. Figure 3-16 shows the beam profile from the high quality laser module used in the strain sensor, whose beam profile is close to Gaussian shape.

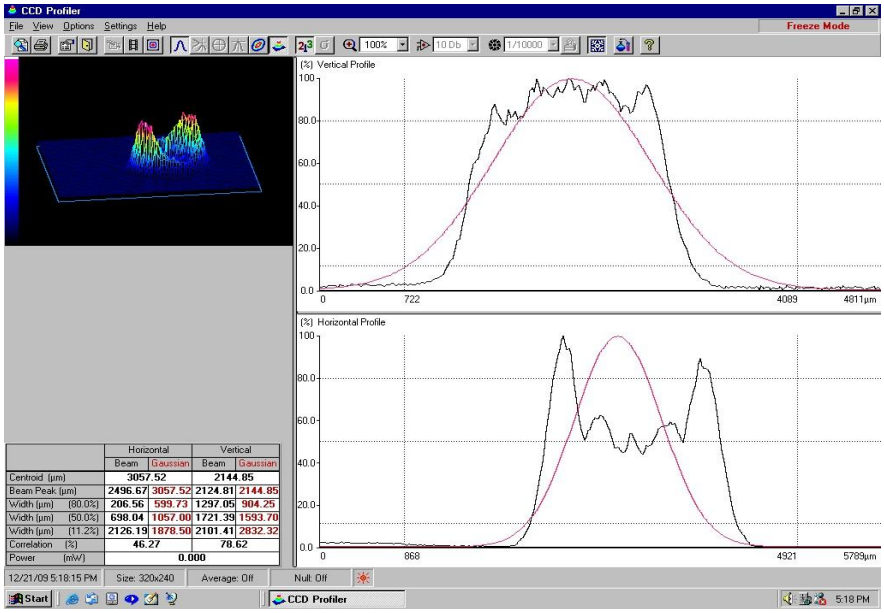

Figure 3-15 Saw-tooth laser beam profile

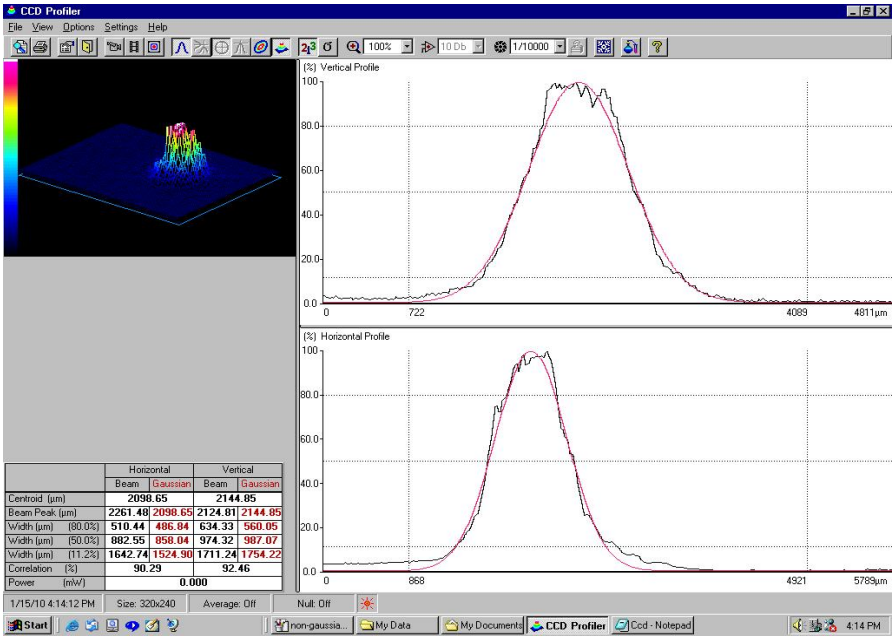

Figure 3-16 Gaussian laser beam profile

The other important issue of the laser head is the collimating lens it uses. Since the laser light emitting from the laser diode exhibits high divergence and astigmatism, a collimating lens, usually aspherical, is used to circularize the beam and remove astigmatism. Many laser heads in the market use acrylic lens because it is much easier to manufacture aspherical lens in plastic than in glass. However, since the optical sensor is supposed to be used in harsh environment where the ambient temperature can fluctuate tens of degree, the thermal properties of the collimating lens have to be taken into consideration. It is known that the thermal expansion of acrylic (315 ppm/°C) is several hundred times larger than that of the BK7 glass (0.98 ppm/°C) (Herzig, 1997). To minimize the effect of the temperature change on the sensor performance, a laser head with a glass collimating lens was preferred.

Another performance parameter of the laser module that is affected by the temperature is the beam pointing stability. Laser pointing stability, whose unit is typically $\mu rad / °C$, is a measure of how much the beam axis angle drifts over time as the temperature changes. When the laser beam drifts, the distance between the laser beams of the two modules will change too, inadvertently affecting the accuracy of the strain sensor. The laser heads used in the sensor are two "high performance diode laser modules 1112A2-0001" from Diode Laser Concept company. It is claimed by the company that the pointing stability is 10 $\mu rad / °C$. Using a laser profiler (Beamstar-V-PCI, PHIR company), an attempt was made to verify the pointing stability rating of the laser module. The laser profiler was positioned 0.7m distance from the sensor. After the sensor was turned on, the temperature inside the sensor and the laser pointing location on the laser profiler were monitored for 80 minutes. Figure 3-17 shows the laser pointing drift to be as high as 40 microns, as the temperature increased by 5 $°C$ due to the heat dissipated from the camera.

Thus the pointing stability can be calculated as $40\mu m / 0.7m / 5°C \approx 11.4 \mu rad / °C$. The result is quite close to the claimed rating of the laser head.

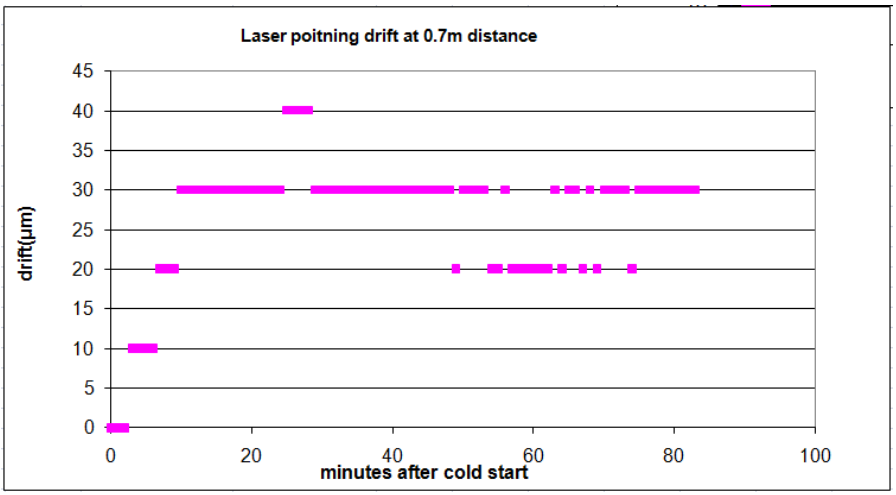

Figure 3-17 Laser pointing stability test

3.4.2 CCD Camera

Besides the compactness, low power usage and low noise, there are other critical features that must be taken into consideration with the camera selection for the optical strain sensor.

- Synchronous acquisition and global shutter

  The two cameras of the optical strain sensor must be able to take synchronous shots, otherwise any rigid motion between the sensor and the object, within the time of the two shots, will be reflected in the strain measurement and cause significant error. It is the same reason that a global shutter feature is necessary. A CCD has millions of opto-detectors, with each one corresponding to a pixel. With a global shutter, all the opte-detectors start and stop exposing at the same time, eliminating the potential error associated with surface motion during the exposure period of the camera.

- Fast image capturing speed

  The optical strain sensor is designed for both manual operation and on-track operation. For both operation configurations, it is inevitable that the sensor undergoes movement or suffers vibration during operation. A fast image capturing speed will help minimize the blur of the image.

- Adjustable shutter

  A versatile strain sensor should be able to measure strain on various material surfaces from concrete and metal, to fiber glass. In addition, the sensor should also function in different ambient light environments including daylight, indoor and night condition. The adjustable shutter feature enables the sensor to adjust the intensity of the captured image according to surface reflectivity and illumination condition.

- Expansibility

  Although the current sensor design consists of two modules, it should be possible to build a multiple module system to capture the strain in multiple locations at the same time, as suggested in Figure 3-18. Furthermore, instead of only measuring the strain in one direction, a rosette setup could be implemented using four individual modules to measure the three independent components of surface strain (Figure 3-19). The expansion of the system in this manner could require that multiple cameras be attached to one computer and capture the images at the same time.

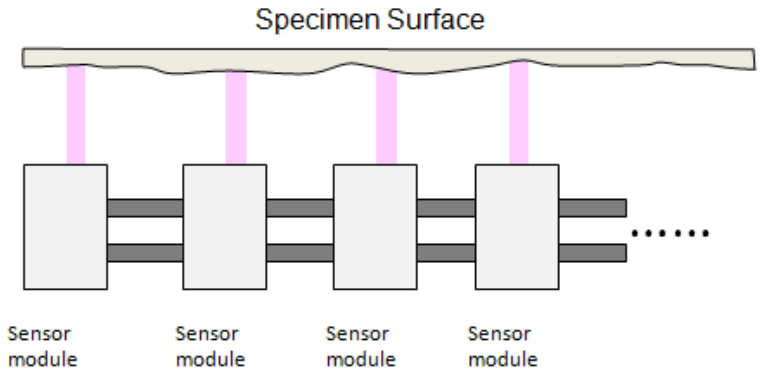

Figure 3-18 Multiple modules setup

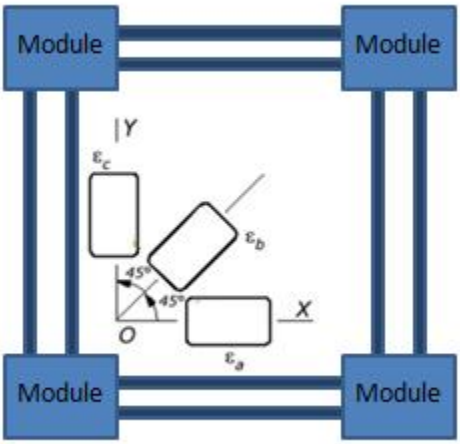

Figure 3-19 Rosette setup for two dimensional strain measurement

3.4.3 Alignment mechanism

The measurement procedure generally consists of two steps: 1. Take speckle images from the undeformed surface as an initial or baseline reading; 2. Take speckle images from the deformed object surface. Since the dynamic range of the optical strain sensor is ± 2mm, to conduct step 2 of the measurement procedure, a mechanism must be introduced to help the user align the sensor onto the position on the object surface within ± 2mm of where the initial reading takes place. If the sensor is mounted on a track, the alignment would be ensured by the track itself. However, in the case of manual operation, there have to be some markings left on the object surface to guide the alignment. This is needed to ensure correlation between the displaced image and the baseline image.

Such kind of markings must satisfy the following requirements

- Inexpensive
- Good use on concrete and metals.
- Must not fade or rub off. .

Several possible marking mechanisms were evaluated for practicality.

- Fluorescent marking

The idea is to use a fluorescent material to serve as the marker. When the marker is illuminated by an ultraviolet (UV-light) emitter that is mounted on the sensor, it would

absorbs ultraviolet light and emits visible light, signaling the user that the sensor is in alignment. This kind of marking mechanism does not leave visible markings on the object surface, which might be appealing to some applications. However, the UV-lasers are expensive. Too expensive to the point where only making an alignment point is not worth it. In addition, since there is no visible light be emitted when the alignment is not close, the user might lack the guidance to show where the target location is, or what direction to move for alignment.

- Visible marking tracked by crosshair laser light

  With this solution a crosshair laser is attached to the optical strain sensor. The object surface is marked with a cross sign using a paint marker. The user positions the sensor by aligning the crosshair beam of the laser to the cross sign on the object surface. This solution has the advantage of easy application of the marking. However, one drawback is that the user's eyes become fatigue after several minutes of watching the laser light. In addition, the crosshair laser light becomes less visible under the sunlight.

- Visible marking and supporting legs

  In this approach, the sensor is equipped with three or four supporting legs as shown in Figure 3-20. Two dots are marked on the object surface. The user positions the sensor by aligning two tips of the supporting legs with the two dots. In practice this solution was found to work quite well. It is also quite simple to implement.

Figure 3-20 Visible markings and supporting legs used as the alignment mechanism

Chapter 4 - Software development for the optical strain sensor

The software of the optical strain sensor was coded using Visual C++ for flexible hardware control and high speed computation. A user-friendly interface was developed that is described in detail in the software manual in Appendix D. This chapter mainly discusses the data processing of the raw speckle image pairs captured by the cameras of the optical sensor to extract the strain information from the object surface. The data processing for each separate camera module consists of several steps as shown in the Figure 4-1.

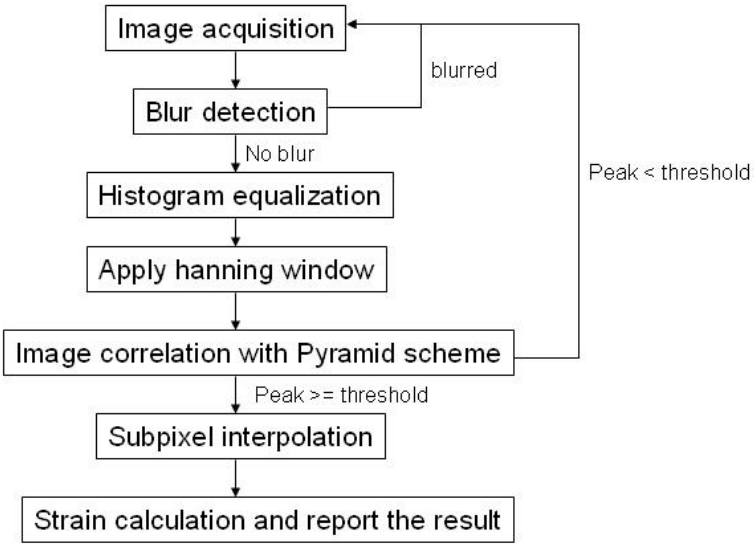

Figure 4-1 Image processing diagram

\

4.1 Preprocessing

The raw speckle image usually suffers blur, noise and imbalance of intensity. The direct application of a digital correlation algorithm at this early stage could result in loss of correlation and broad correlation peak that gives low accuracy in the prediction of image shifting from surface strain. The goal of preprocessing is to make the raw images more suitable for analysis by a digital correlation algorithm.

- Blur detection

The acquisition of an image by the CCD camera is done by accumulation of photoelectrons on the CCD chip for a certain time period, usually several milliseconds. If the sensor moves during the integration period, the captured images will suffer a blur effect. The blurred images lose most of the high frequency information and this can cause the correlation algorithm to report a fake match of the speckle image pairs. An algorithm is employed to detect blur in the captured image by transforming the image into the spatial frequency domain using a 2D Fourier transform, and calculating the ratio of the low frequency power to the high frequency power. If the ratio exceeds a predefined threshold, it means the there is significant blur effect in the image. The blurred image will then be discarded and the software will command the camera to capture another frame of the speckle pattern until a non-blurred one is obtained.

- Histogram equalization

The intensity of the image captured by the camera is usually unbalanced, i.e. the grey level of the pixel concentrates to a limited range of the full grey range 0-255. For example, the histogram of a typical raw speckle image is shown Figure 4-2 (a), in which the grey levels of the pixel concentrates to the range lower than 100. Histogram equalization increases the dynamic range of the grey level by making the histogram a uniform profile. The histogram of the same speckle image after being equalized is shown in Figure 4-2 (b).

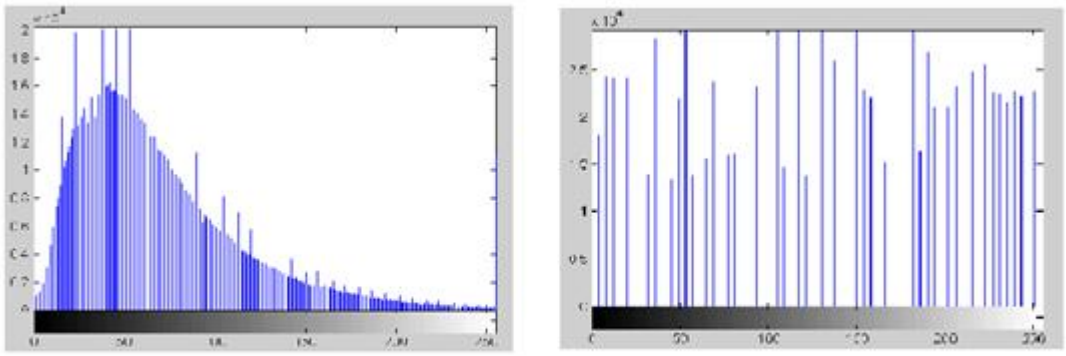

(a) Histogram of a typical speckle image (b) Histogram after equalization

Figure 4-2 Histogram equalization

- Reduction of FFT spectral leakage using hanning window

The phase correlation technique relies heavily on the Fourier transform to transform the image to the frequency domain. However, Fourier transform inherently is supposed to be applied to infinite periodic signals instead of the finite non-periodic signals like a digitalized image. When the Fourier transform of a finite non-periodic signal is computed, the resulted complex spectrum suffers from artifacts. Figure 4-3 shows a speckle image and its frequency spectrum. It shows a horizontal line and a vertical line across the frequency spectrum. The two artifact lines are from the abrupt intensity change at the vertical boundary and horizontal boundary respectively of the speckle image. This phenomenon is also called spectral leakage. These artifacts will cause the software to report a false positive matching of the speckle image pairs if it is not removed. These artifacts can be reduced by elementwise multiplication of the original image by a window that tapers the intensity value at the image boundary to zero. Many types of windows have been proposed to reduce the effect of spectral leakage. Their performances vary depending on if the signal is random or sinusoidal. For a random signal like speckle, hanning window has been shown to provide better frequency resolution than other windows. (Harris, 1978).

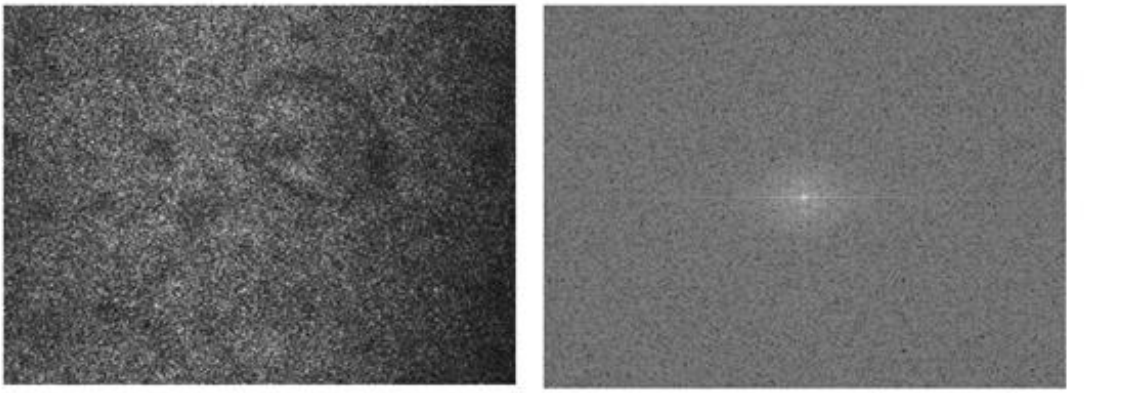

(a) a typical speckle image (b) Complex spectrum of the speckle image

Figure 4-3 A typical speckle image and its frequency spectrum

The hanning window is defined as

$$hann(x) = 0.5\left(1-\cos(2\pi\frac{x}{M})\right) \qquad 0 \le x \le M \qquad (4.1)$$

where M is the window size.

A 2D hanning window is defined as

$$hann(x,y) = 0.25\left(1-\cos(2\pi\frac{x}{M})\right)\left(1-\cos(2\pi\frac{y}{N})\right) \qquad 0 \le x \le M, 0 \le y \le N \qquad (4.2)$$

where M,N are the 2d window size.

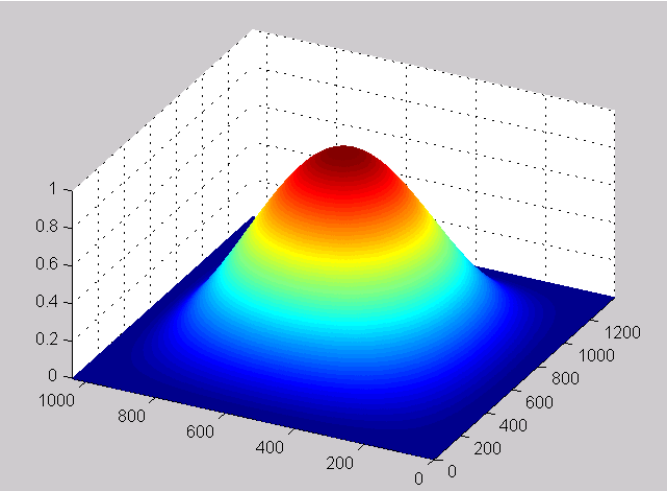

Figure 4-4 Hanning window

Figure 4-4 shows the profile of the hanning window, which is applied to the raw speckle image before it is transformed to the frequency domain. The filtered speckle image, whose boundary abruption is greatly tapered, and the Fourier transform pattern of the filtered speckle image are shown in Figure 4-5. It is notable that the artifacts are not visible any more.

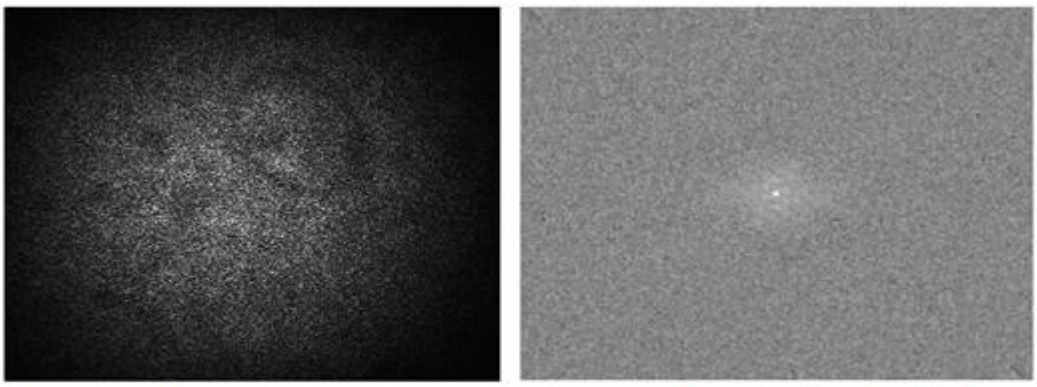

(a) Filtered speckle image using hanning window

(b) Complex spectrum of the filtered speckle image

Figure 4-5 Filtered speckle image and its frequency spectrum

4.2 Digital correlation procedure

The theory of digital correlation has been described in Chapter 3. This section will focus on how it is implemented.

- Pyramid scheme

The correlation procedure is very computationally expensive. Since most of the calculation cost is on the Fourier Transform, the software makes use of FFTW(http://www.fftw.org/), a free C subroutine library from MIT that is known for its speed and performance. However, even with FFTW, it takes about 2 seconds to compute the correlation on an image pairs of 1392x1040 pixels using a P4 computer. To speed up the correlation procedure between the image pairs, a pyramid scheme is employed in the optical strain software.

The two images that are to be correlated are both scaled down to half size n time, creating two image trees with each consisting of n+1 images, where n is the downsampling depth, as shown in Figure 4-6.

The downsampling technique is implemented by convolving the image with a two dimensional Gaussian filter, defined as

$$f(x,y) = \frac{1}{2\pi\sigma^2} e^{\frac{-(x^2+y^2)}{2\sigma^2}} \tag{4.3}$$

because it provides better performance for the downsampling task compared to other types of filters (Shapiro, 2001).

The images of the same image tree are similar to each other but with different size and resolution. The parent image is twice the size and higher resolution of the child image. The idea of the pyramid is that the lower resolution image pairs can be correlated first, in order to estimate the possible start positions for the correlation computation for their parent image pairs. The parent image pairs can then be correlated in a small area around the estimated start position to find the actual displacement. The procedure is described as follows:

Suppose the original image size is M by N, and the image trees have n levels. The image pairs at the bottom of the tree have the size of M/n by N/n pixels and the correlation between

them gives the relative displacement (u_n, v_n). Since there is a 2:1 parent-child relations between the pixels at the level k-1 image and level k image in the image trees, a pixel displacement in level k corresponds to a two pixel displacement in level k-1. Thus, by multiplying the relative pixel displacement (u_n, v_n) at level n by two, the relative displacement between the image pairs at the n-1 level can be estimated to be $(2u_n, 2v_n)$. When conducting the correlation on the image pairs of level n-1, the two images are compared over the small area of M/n by N/n size with relative position displacement $(2u_n, 2v_n)$ and produce the new relative displacement (u_{n-1}, v_{n-1}). The operation is repeated upward along the image tree till the root of the image tree is reached, where the correlation between the two small areas of M/n by N/n size gives relative displacement (u_0, v_0), which is also the relative displacement between the original image pairs.

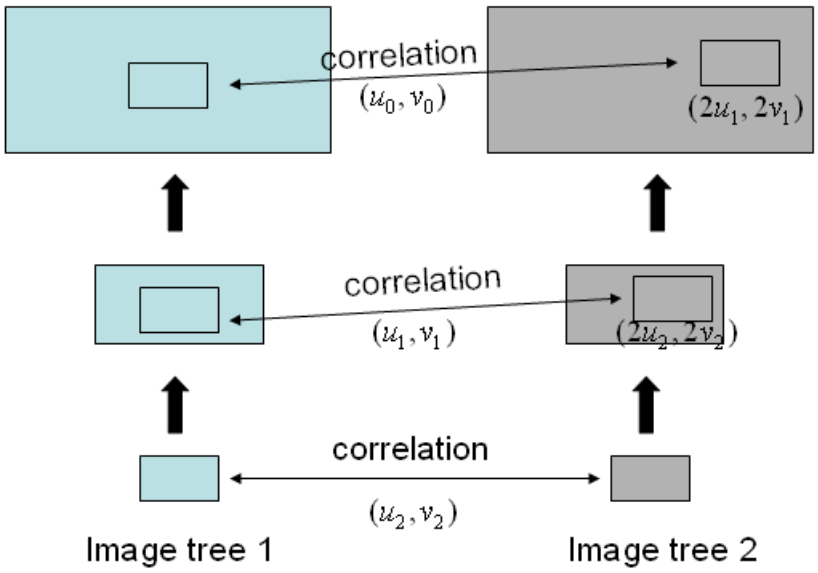

Figure 4-6 Pyramid scheme

- Subimage scheme

Given image pairs I1 (initial image) and I2 (post-deformation image), instead of correlating the two full images, a small patch of I2, usually at the center of the image, is used as a template. The software slides the template from the top left to the bottom right of the image I1,

trying to find the best match. The reason that the correlation is conducted using multiple subimage pairs instead of the full image pairs is due to the fact that correlation on small size images are more robust to image rotation. Correlation inherently is suitable for tracking the translation of the image but not the rotation. (Weixin Zhao, 2004). For a large image, the disruption of the image rotation on the correlation is more severe because a small rotation can cause large translations on the image boundary. For a small size image, the effect of image rotation is less severe. However too small template will consist of limited size of speckle pattern and this makes it hard for the searching process to identify a match. In the software, a template of 256x256 size was used, which provided robustness against the image rotation and enough resolution. The detailed procedure is described below:

The captured reference (baseline) image I1 is split into many sub-window areas of 256 pixels by 256 pixels size, denoted as Refblock_i, $0 \le i \le N-1$, where i is the block index and N is the total subimage number. A sub-window of 256 pixels by 256 pixels size is also extracted from the center area in the after-deformation image I2, denoted as Defblock. Since the sizes of the subimages are small, it can be assumed that there is no change within the sub-image, and the shift between the sub-image pairs is uniform at every point. Thus, using the phase correlation procedure described in Chapter 3, The N subimages Refblock_i and the subimage Defblock produce n peaks and n displacement vector, which are denoted as p_i and $(u,v)_i$. The sub window pair with the maximum peak indicates the best match and is used further to extract the subpixel displacement information.

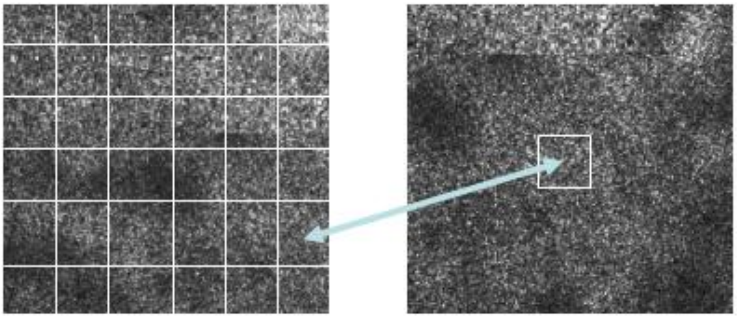

Figure 4-7 Sub-image scheme

4.3 Sub-pixel interpolation

The displacement vector of the correlation has an integer pixel resolution, with an uncertainty of ± 1/2 pixel. Two approaches have been identified to achieve sub-pixel resolution for image correlation process.

One possible approach is to upsample both images, then conduct the correlation on the upsampled image pairs. For example, to achieve 1/20 pixel subpixel resolution for the correlation on two sub-images of 256x256 pixels, both sub-images have to be upsampled to 20 times larger images with the size of 5120x5120 pixel. The correlation computation required on the image pairs of 5120x5120 is enormous and very time consuming.

The other approach is to compute the correlation on the image pairs without being upsampled and then interpolate in the region near the peak location to extract the peak location in sub-pixel resolution. At first, it may look like try to extract unmeasured information. However, the interpolation procedure can be justified by the reasoning that the correlation image is generated by matching thousands of individual speckles in the image pairs. Each pair of speckle image element gives an integer pixel displacement. The actual peak location is determined by averaging the large quantity of displacement vectors provided by these speckle pair matching. Thus, the information that is used to extract the sub-pixel location of the peak is already embedded in the correlation image.

There are many interpolation methods available to extract sub-pixel peak location, including parabolic peak fitting, Gaussian peak fitting, etc. These peak fitting methods only use the neighboring points' information for the interpolation and suffer from the 'peak-locking' effect; i.e. the sub-pixel peak detected tends to be close to the integer pixel location (Sung, 2004). A more advanced interpolation, called zero padding fitting, is used in the image analysis for the optical strain sensor software. First, the correlation image is transformed to the frequency domain by means of a Fourier transform. Suppose the Fourier transform pattern of the correlation image has a size of 256 by 256 pixels. To achieve 1/20 pixel peak location resolution, zero-valued pixels are appended to the high frequency end so that we have a Fourier pattern of 20*256 by 20*256 pixel as shown in Figure 4-8. After padding zeroes in the high frequency area, there is no change in the real and imaginary parts of the Fourier spectrum, nor in the phase spectrum. The only change is in the densified spatial sampling frequency. If an inverse Fourier

transform is applied to the zero-padded spectrum pattern, the result will be an interpolated correlation image with 20 times higher resolution than the original correlation image.

However, the inverse Fourier transform of the full zero padded pattern calculates the interpolation value at every location, while we are only interested in the upsampled information in the proximity of the peak. Furthermore, computation of the inverse Fourier transform of the full zero padded pattern is not practical due to the extremely large size of the padded pattern. Alternatively, the software calculates the upsampled information around the peak area only by employing a matrix implementation of the inverted Digital Fourier Transform.

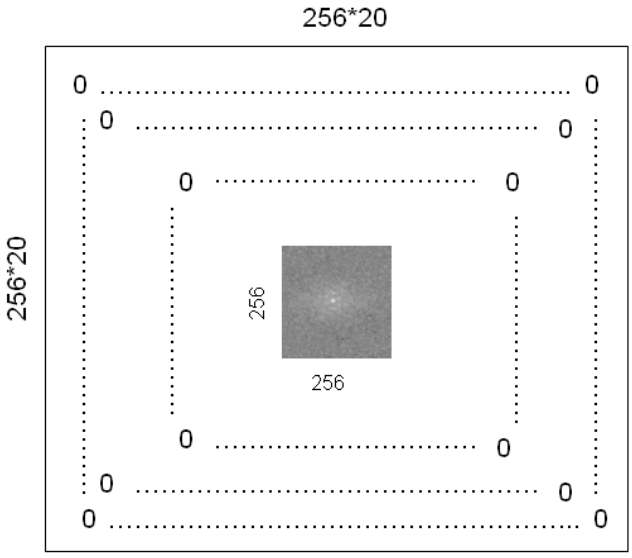

Figure 4-8 Zero padding interpolation

The Digital Fourier Transform is defined as, (Deng, 2008)

$$x(k_1,k_2)=\sum_{i_1=0}^{N-1}\sum_{i_2=0}^{N-1}X(i_1,i_2)\bullet w^{k_1i_1+k_2i_2},k_1,k_2=0,1,...,N-1 \tag{4.4}$$

where $w=e^{j2\pi/N}$.

If $X(i_1,i_2)$ is the zero padded spectrum pattern, then $x(k_1,k_2)$ represent the interpolated correlation image matrix that is being calculated.

The matrix form of Equation (4.4) can be written as

$$x_{N\times N}=W_{N\times N}X_{N\times N}W_{N\times N} \tag{4.5}$$

where $X_{N\times N}$ is the matrix form of the zero padded spectrum pattern; $x_{N\times N}$ is matrix form of the interpolated correlation image matrix that we are trying to obtain; and $W_{N\times N}$ is a N by N matrix whose (k,i) entry is $w = e^{j2\pi ki/N}$,i.e.

$$W_{N\times N} = \begin{bmatrix} 1 & 1 & 1 & \dots & 1 \\ 1 & w & w^2 & \dots & w^{N-1} \\ 1 & w^2 & w^4 & \dots & w^{2(N-1)} \\ \vdots & \vdots & \vdots & & \vdots \\ 1 & w^{N-1} & w^{2(N-1)} & \dots & w^{(N-1)(N-1)} \end{bmatrix} \tag{4.6}$$

Using the matrix form of the Fourier transform implementation, the value of any single point on the interpolation image can be calculated. For example, the value of the entry (i,k) in the interpolation image is calculated by

$$x(i,k) = W_{\text{ith row}} X_{N\times N} W_{\text{kth column}} \tag{4.7}$$

Thus the area near the peak location can be interpolated using Equation (4.7), to yield the desired peak location to sub-pixel resolution. It is notable that the zero padding interpolation method makes use of the information from all the pixels value in the correlation image; thus it is more accurate and suffers no 'peak locking' error problem.

4.4 Refreshing reference

It is possible to have the camera take multiple speckle images as the object continuously undergoes displacement, and then use an incremental method to increase the measurement range. Initially the first speckle image would serve as a reference (baseline) image, and every newly taken image would be correlated with it to extract the object surface motion information. As the object surface displaces further from the initial position, the correlation coefficient decreases due to the de-correlation effect that happens when the two images share less similarity. Before the correlation coefficient drops to a predefined threshold indicating significant de-correlation, the reference image would be replaced by the newest speckle image. Following this procedure, it should be possible to recover a well-defined correlation peak. Further speckle displacement

could then be determined by adding up the speckle displacements before the replacement of the reference pattern. Theoretically, the measurement range is indefinite as long as every pair of consecutive speckle images does not exceed the threshold of significant de-correlation.

Chapter 5 - Calibration

This chapter discusses measurement error sources associated with the laser speckle strain sensor, including distortion of the lens, misalignment between the initial baseline reading and the second reading and misalignment between the two modules of the sensor. Their effects on the strain measurement accuracy of the sensor are investigated. Two calibration methods are proposed to correct these errors using the homography projection technique, the mathematical instrument that describes the relationship between the physical scene and the image captured by the camera.

5.1 Measurement error sources of the laser speckle strain sensor

5.1.1 Distortion due to the lens

No lens is perfect. There are several kinds of aberrations associated with lens. The most common one is spherical aberration. Many simple lenses are made into the spherical profile for lower manufacturing cost. There do exist “parabolic” lenses which have a more mathematically ideal profile with minimum aberration, but they are is expensive and the lens selection is limited. Spherical aberration causes the parallel light rays distant from the lens axis to be focused in a slightly different place than the light rays close to the axis. When using a spherical lens for imaging an object surface to the camera plane, the images obtained exhibit radial distortion, as shown in Figure 5-1. The light beams farther from the lens axis bend more than the beams close to the lens axis. Thus the distortion increases from 0 at the center of the image to higher level at the edge of the image.

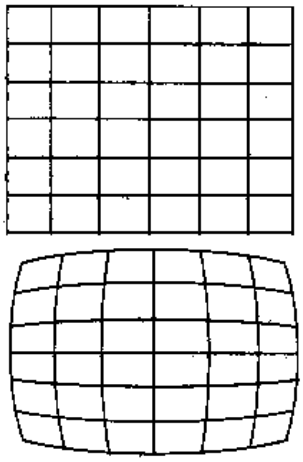

Figure 5-1 Camera image distortion

Obviously the image distortion introduces measurement error to the strain sensor since the image shift is not linear to the surface movement if the image is distorted. To reduce this effect and keep the cost low at the same time, triplet lenses were chosen as the imaging lenses of the sensor. The triplets lenses consists of one concave lens and two convex lenses, whose aberration effect cancels out, producing an almost aberration-free image.

To evaluate the scale of the error that is caused by the image distortion, an experiment was conducted which is described:

Image pairs (initial baseline reading and post-movement reading) were taken by the camera using the triplet lens as the imaging lens. The object surface under observation undergoes primarily only linear motion. Thus, the pixel shift of the image pairs at any location of the images should be identical if without image distortion. The pixel shifts were calculated at 3 regions in each of 5 image pairs. One of the image pairs are shown in Figure 5-2.

The pixel shifts of these 3 regions are listed in Table 5-1. It is shown that maximum standard deviation of the pixel displacement among the 5 image pairs is 0.06 pixel, corresponding to 1.4 microstrain for the 8 inches gauge length configuration. Thus it can be concluded that the image distortion has an insignificant effect on the measurement of the optical strain sensor. Observing this, the distortion effect is neglected in the camera calibration model used in the later analysis associated with this chapter.

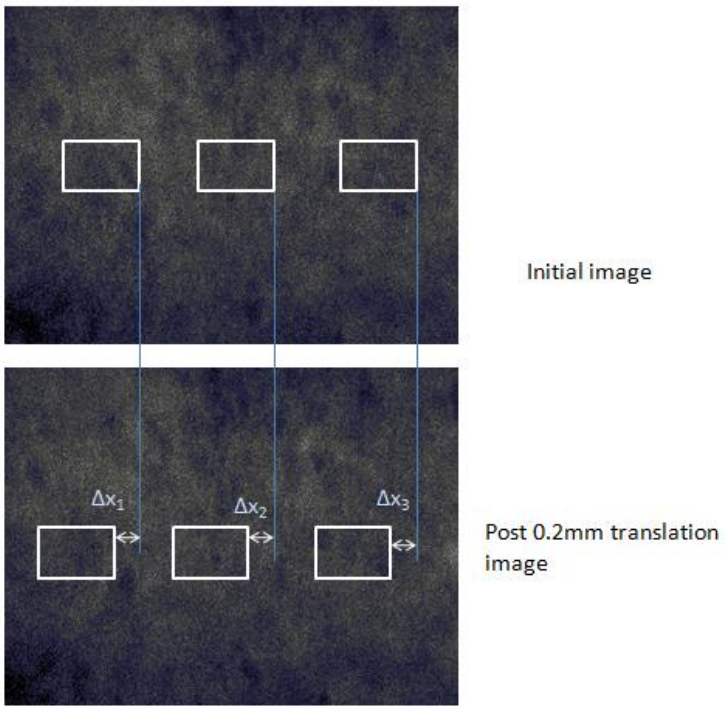

Figure 5-2 Image pairs for the camera distortion experiment

Table 5-1 Data of the camera distortion experiment

object displacement(mm)	0.20	0.20	0.20	0.20	0.20
Δx_1(pixel)	5.92	5.96	5.96	5.92	5.96
Δx_2(pixel)	5.96	6.00	5.96	6.00	5.92
Δx_3(pixel)	6.04	5.96	5.92	5.92	5.96
standard deviation=	.06	.02	.02	.05	.02

5.1.2 Error due to misalignment

As shown in Figure 3-5, the surface strain, ε, between point A and point B was measured by $\varepsilon = \frac{\Delta B - \Delta A}{L}$, where L is the gauge length 203.2 *mm* (8 inches) for the current setup and ΔA, ΔB are the surface displacements at point A and point B. The strain calculation scheme described above is suitable for the ideal situation that the sensor is aligned perfectly. However, in the real situation, significant errors could occur, either due to the sensor misalignment between before and after deformation readings, or due to the misalignment between the two cameras in the sensor.

5.1.2.1 Misalignment between the initial reading and the second reading

During the operation of the sensor, when taking the second reading, it is inevitable that the sensor will be misaligned to some extent with respect to the sensor position during the initial reading. This is mainly represented by a rotation about Z-axis (the axis perpendicular to the object surface), as shown in Figure 5-3.

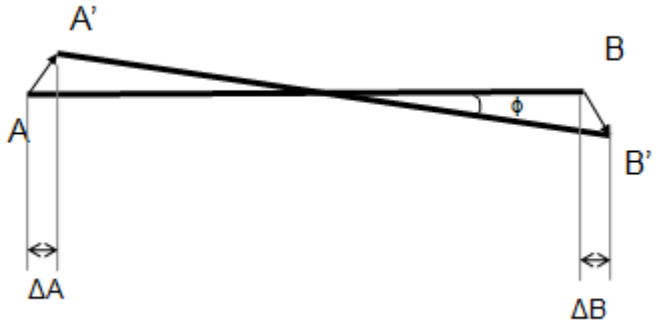

Figure 5-3 Misalignment between the initial reading and the second reading

Suppose point A and point B represent the measurement locations for the two modules of the sensor for during initial reading. Assume the specimen surface does not undergo any deformation and assume the sensor is misaligned by an angle of ϕ relative to the initial reading

setup. When taking the second reading, the measurement locations of the two modules of the sensor will move to point A' and point B'. The sensor will report a non-zero strain reading $\varepsilon = \frac{\Delta B - \Delta A}{L} = \frac{L(1-\cos\phi)}{L} = 1-\cos\phi$, which is actually an error introduced by the misalignment of the sensor between the initial reading and the second reading. The error is essentially independent of the gauge length and primarily dependent on the misalignment angle.

Table 5-2 shows the measurement error caused by the misalignment angle from angle 0.1 degree to 1 degree. It is shown that at a misalignment angle of 0.4 degree, the error is 24.34 microstrain, or about the same order as the nominal resolution of the strain sensor. At a mislaignment angle of 1 degree, the error increases to 152 microstrain. Thus the effect of the rotation with respect to Z-axis should not be overlooked and must be controlled or corrected.

Table 5-2 Error caused by the sensor misalignment

Misalignment angle (degree)	Error caused by misalignment (microstrain)
0.1	1.52
0.2	6.08
0.3	13.69
0.4	24.34
0.5	38.03
0.6	54.77
0.7	74.55
0.8	97.37
0.9	123.24
1.0	152.15

5.1.2.2 Misalignment between the two modules of the sensor

The modular design of the sensor provides the advantages of easy fabrication and flexible gauge length adjustment, but an important issue must be taken care during the calibration. Since the sensor consists of two cameras, ideally the x and y axis of the two cameras' coordinate systems should be parallel with each other and have no orientation difference. It is important because the distance change (or strain) can be calculated only when all the displacement vectors

are with respect to the same coordinate system. However in practice, the orientation of the two cameras in the two modules can hardly perfectly parallel due to the nature of the assembling of the device. The actual relationship between the two cameras coordinate is shown in Figure 5-4. Even if it is possible to conduct the installation of the cameras carefully and achieve a minimum orientation difference between the two coordinate systems, considering the fact that a 0.4 degree misalignment angle introduces as much as 24 microstrain error as described in the previous analysis, the coordinate orientation difference between the two cameras of the sensor causes about the same order of error that should not be overlooked. Therefore, to be able to calculate the displacement change or the strain accurately, the orientation difference between the two camera coordinate systems must be taken care of, in other word, the surface displacements detected by the two cameras must be converted into the same coordinate.

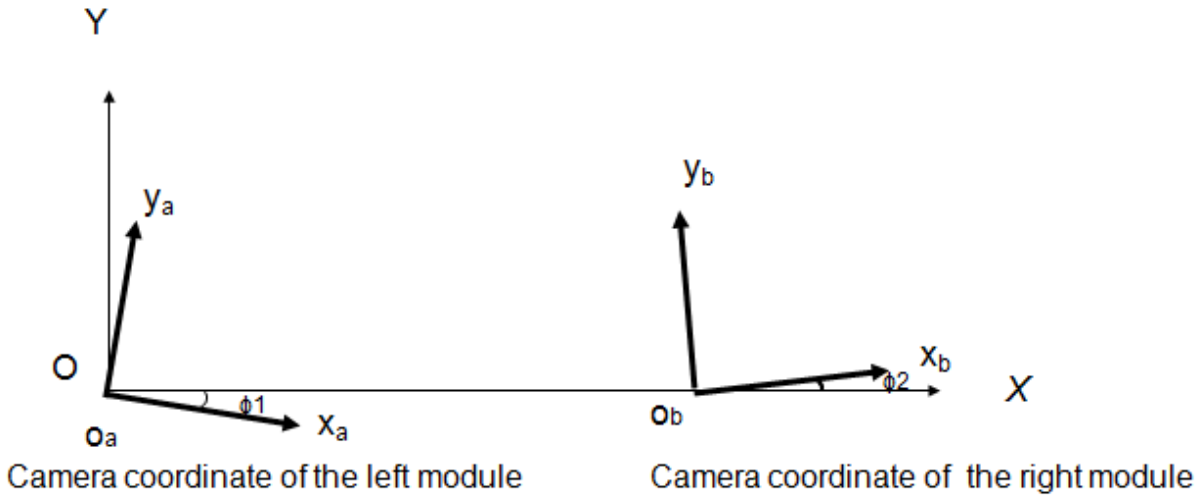

Figure 5-4 Misalignment between the two modules of the sensor

5.2 Homography projection

To correct the misalignment errors that were discussed above, various information related to the camera orientation must be collected during the calibration procedure. For this purpose, the homography projection technique is used.

For an image of the object surface that is taken by the camera, the pose of the object relative to the camera coordinate system can be described using rotation and translation matrix.

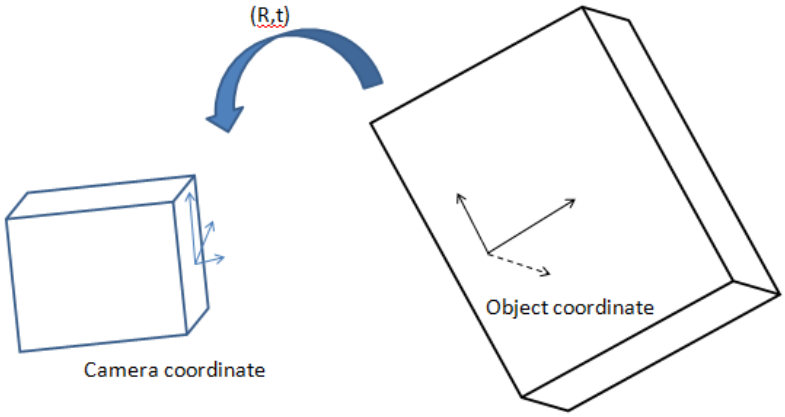

Figure 5-5 Transformation from object coordinates to camera coordinates

A rotation of a vector is equivalent to giving the vector a new description in a different coordinate system, which is implemented by multiplying the vector by a square matrix of the appropriate size. A two dimensional rotation of angle α is represented as a multiplication of the vector by a 3x3 matrix as shown in Equation (4.8). Rotation in the three dimensional space is equivalent to three two-dimensional rotations on the X,Y,Z axes respectively. Rotating on the X,Y,Z axis respectively with angles α, β, ϕ is given by the product of the three matrices $R_x(\alpha)$, $R_y(\beta), R_z(\phi)$:

$$R_x(\alpha) = \begin{pmatrix} 1 & 0 & 0 \\ 0 & \cos(\alpha) & \sin(\alpha) \\ 0 & -\sin(\alpha) & \cos(\alpha) \end{pmatrix} \tag{4.8}$$

$$R_y(\beta) = \begin{pmatrix} \cos(\beta) & 0 & -\sin(\beta) \\ 0 & 1 & 0 \\ \sin(\beta) & 0 & \cos(\beta) \end{pmatrix} \tag{4.9}$$

$$R_z(\phi) = \begin{pmatrix} \cos(\phi) & -\sin(\phi) & 0 \\ \sin(\phi) & \cos(\phi) & 0 \\ 0 & 0 & 1 \end{pmatrix} \tag{4.10}$$

And

$$R = R_x(\alpha)R_y(\beta)R_z(\phi) \tag{4.11}$$

The translation vector is the offset from the origin of the object coordinate to the origin of the camera coordinate system,that is,

$$t = O_{object} - O_{camera} \tag{4.12}$$

Given a point $Q(X,Y,Z)$ in the object coordinate system, its coordinate $q(x,y,z)$ in the camera coordinate can be expressed as $q(x,y,z) = RQ(X,Y,Z) + t$.

Homography is a special case of the coordinates transformation (Faugeras, 1993). It is used to describe the projection from a two-dimentional surface (object surface) to another two-dimentional surface(Camera surface) as shown in Figure 5-6.

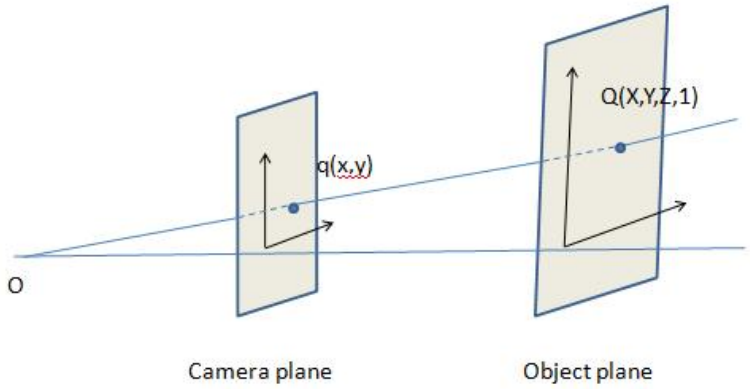

Figure 5-6 Homography Projection from objection coordinate to camera coordinate

In the homography projection model, the homnogeneous coordinates are defined as

$$Q = \begin{bmatrix} X \\ Y \\ Z \\ 1 \end{bmatrix} \qquad q = \begin{bmatrix} x \\ y \\ 1 \end{bmatrix} \tag{4.13}$$

where Q is a point in the object coordinate and q is the projection point of Q on the image plane. Their relationship can be expressed as

$$\begin{bmatrix} x \\ y \\ 1 \end{bmatrix} = M \begin{bmatrix} R & t \end{bmatrix} \begin{bmatrix} X \\ Y \\ Z \\ 1 \end{bmatrix} = M \begin{bmatrix} R_x(\alpha)R_y(\beta)R_z(\phi) & t \end{bmatrix} \begin{bmatrix} X \\ Y \\ Z \\ 1 \end{bmatrix} \tag{4.14}$$

where M is the magnification factor.

Since the camera plane is at the imaging plane, the image shift is not sensitive to the object tilt (rotation about the x-axis) and yaw(rotation about the y-axis), the rotation angles about the x-axis and the y-axis of the object surface do not change the projection matrix between the object coordinate and the camera coordinate. Therefore, we can assume the β and ϕ are zero and Equation (4.14) becomes,

$$\begin{bmatrix} x \\ y \\ 1 \end{bmatrix} = M \begin{bmatrix} \cos(\phi) & -\sin(\phi) & 0 & t_x \\ \sin(\phi) & \cos(\phi) & 0 & t_y \\ 0 & 0 & 1 & t_z \end{bmatrix} \begin{bmatrix} X \\ Y \\ Z \\ 1 \end{bmatrix} \tag{4.15}$$

Since the out-of-plane movement of the object surface is very small, we can assume that the entry Z of the object position vector Q is zero. Furthermore, we are only interested in the relative movement of the objection surface point Q, instead of its absolute projection position on the camera plane, the translation entry t_x, t_y can also be assumed to be zero. Equation (4.15) can then be simplified to be

$$\begin{bmatrix} x \\ y \end{bmatrix} = M \begin{bmatrix} \cos(\phi) & -\sin(\phi) \\ \sin(\phi) & \cos(\phi) \end{bmatrix} \begin{bmatrix} X \\ Y \end{bmatrix} \tag{4.16}$$

or,

$$\begin{bmatrix} x \\ y \end{bmatrix} = \begin{bmatrix} M\cos(\phi) & -M\sin(\phi) \\ M\sin(\phi) & M\cos(\phi) \end{bmatrix} \begin{bmatrix} X \\ Y \end{bmatrix} \tag{4.17}$$

5.3 Two calibration methods for the strain sensor

In this section two calibration methods are proposed to correct the misalignment errors that are discussed in Section 5.1. The first method translates the displacement vectors from the two different camera coordinates to the same coordinate systems by using the rotation matrix described in section 5.3. The calibration setup is shown in Figure 5-7.

The sensor is mounted on a traverse stage that does horizontal movement. The displacement is accurately measured by a dial gauge. A piece of specimen, for example a piece of concrete block, is kept stationary in front of the sensor so that both observation points of the two cameras are on the specimen surface. Furthermore, throughout the experiment, the specimen is not subjected to any load. This ensures that the surfaces seen by the two cameras always displace at the same direction by an equal distance.

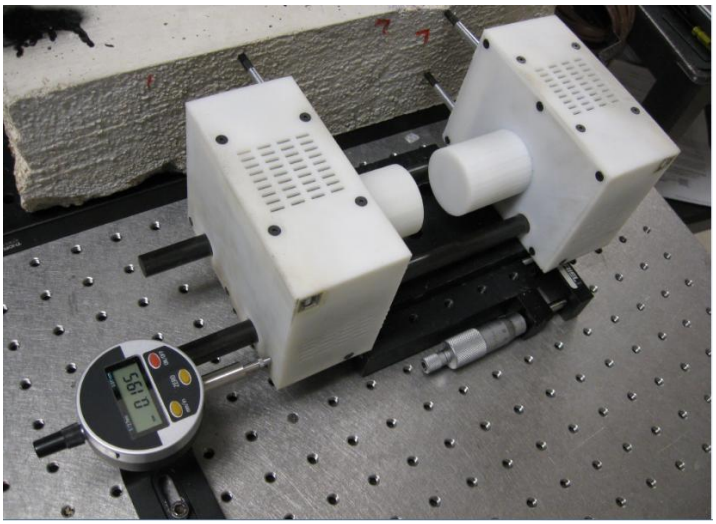

Figure 5-7 Setup of the first calibration method

The next step is to displace the traverse stage from 0 to 1mm with increments of 0.1mm. At every increment, the images are recorded by both camera and are then analyzed by the cross-correlation algorithm described in Chapter 4. The displacement of the traverse stage and the corresponding image shift of the cameras in the unit of pixel are shown in the Table 5-3. Since there is always an angle between the x-axis of the camera coordinate system and the transverse stage displacement direction, the speckle image taken by the camera has both x and y component. At the last row of the tables, the average incremental displacements of the speckle image corresponding to 0.1 mm surface displacement are calculated.

Table 5-3 Calibration data from camera A and camera B

Camera A Surface movement(mm)	Cumulative x1 displacement (pixel)	Cumulative y1 displacement (pixel)	Incremental x1 displacement (pixel)	Incremental y1 displacement (pixel)
0	0	0		
0.1	-23.08	0.12	-23.08	0.12
0.2	-45.72	0.60	-22.64	0.48
0.3	-68.16	0.84	-22.44	0.24
0.4	-90.72	1.00	-22.56	0.16
0.5	-112.44	1.16	-21.72	0.16
0.6	-134.84	1.48	-22.40	0.32
0.7	-157.00	1.60	-22.16	0.12
0.8	-179.56	1.80	-22.56	0.20
0.9	-201.20	1.96	-21.64	0.16
1.0	-223.24	2.04	-22.04	0.08
		Average=	-22.324	0.204

Camera B Surface movement(mm)	Cumulative x2 displacement (pixel)	Cumulative x2 displacement (pixel)	Incremental x2 displacement (pixel)	Incremental x2 displacement (pixel)
0	0	0		
0.1	-23.12	-0.40	-23.12	-0.40
0.2	-45.92	-0.88	-22.80	-0.48
0.3	-68.20	-0.96	-22.28	-0.08
0.4	-90.16	-1.00	-21.96	-0.04
0.5	-112.56	-1.24	-22.40	-0.24
0.6	-134.88	-1.48	-22.32	-0.24
0.7	-157.36	-1.52	-22.48	-0.04
0.8	-179.76	-1.60	-22.40	-0.08
0.9	-202.28	-1.84	-22.52	-0.24
1.0	-224.56	-2.06	-22.28	-0.22
		Average=	-22.456	-0.206

By Equation (4.17), we have

$$\begin{bmatrix} x_1 \\ y_1 \end{bmatrix} = \begin{bmatrix} M_1\cos(\phi_1) & -M_1\sin(\phi_1) \\ M_1\sin(\phi_1) & M_1\cos(\phi_1) \end{bmatrix} \begin{bmatrix} X_1 \\ Y_1 \end{bmatrix} \tag{4.18}$$

and

$$\begin{bmatrix} x_2 \\ y_2 \end{bmatrix} = \begin{bmatrix} M_2\cos(\phi_2) & -M_2\sin(\phi_2) \\ M_2\sin(\phi_2) & M_2\cos(\phi_2) \end{bmatrix} \begin{bmatrix} X_2 \\ Y_2 \end{bmatrix} \tag{4.19}$$

Alternatively, Equation (4.18) and Equation (4.19) can be written as,

$$\begin{bmatrix} X_1 \\ Y_1 \end{bmatrix} = \begin{bmatrix} \alpha_1 & -\beta_1 \\ \beta_1 & \alpha_1 \end{bmatrix} \begin{bmatrix} x_1 \\ y_1 \end{bmatrix} \tag{4.20}$$

and

$$\begin{bmatrix} X_2 \\ Y_2 \end{bmatrix} = \begin{bmatrix} \alpha_2 & -\beta_2 \\ \beta_2 & \alpha_2 \end{bmatrix} \begin{bmatrix} x_2 \\ y_2 \end{bmatrix} \tag{4.21}$$

Using the data in Table 5-3,

$$\begin{bmatrix} 0.1 \\ 0 \end{bmatrix} = \begin{bmatrix} \alpha_1 & -\beta_1 \\ \beta_1 & \alpha_1 \end{bmatrix} \begin{bmatrix} -22.324 \\ 0.204 \end{bmatrix} \tag{4.22}$$

and

$$\begin{bmatrix} 0.1 \\ 0 \end{bmatrix} = \begin{bmatrix} \alpha_2 & -\beta_2 \\ \beta_2 & \alpha_2 \end{bmatrix} \begin{bmatrix} -22.456 \\ -0.206 \end{bmatrix} \tag{4.23}$$

solving Equation (4.22) and Equation (4.23), we obtain the value of parameters $\alpha_1, \beta_1, \alpha_2, \beta_2$

Thus the displacement vectors (x_1, y_1) and (x_2, y_2) detected by the two cameras can be converted to the displacement vectors (X_1, Y_1) and (X_2, Y_2) on the object plane by using Equation (4.20) and Equation (4.21). As shown in Figure 5-8, since the vectors (X_1, Y_1) and (X_2, Y_2) are with respect to the same coordinate, the surface strain can be readily calculated by

$$\varepsilon = \frac{\left|\overrightarrow{pq}\right| - \left|\overrightarrow{O_a O_b}\right|}{\left|\overrightarrow{O_a O_b}\right|} = \frac{\sqrt{(L + X_2 - X_1)^2 + (Y_2 - Y_1)^2} - L}{L} \tag{4.24}$$

where $\left|\overrightarrow{O_a O_b}\right| = L$ is the distance between the two observation points on the object surface, which is also defined as the gauge length of the sensor.

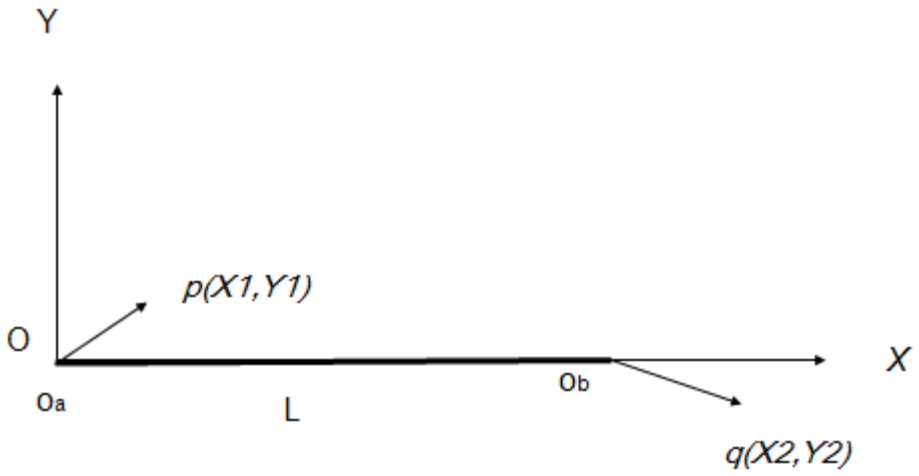

Figure 5-8 Strain calculation with orientation difference of the two camera coordinate systems

The drawback of this method is that it is time consuming and requires addition equipments (a traverse system and the dial gauge). The calibration can usually be only done in the lab. Considering the fact that every time when the user needs to adjust the gauge length, it is necessary unattach and reattach the two modules, causing the orientation difference of the two cameras change. Therefore the sensor must be recalibrated every time when the gauge length is adjusted, which is not convenient for the user. In fact, most commercial strain sensors require specific equipment for calibration. For example the Messphysk company's laser speckle extensometer ME53-33 incorporates a calibration system into the sensor system as shown in Figure 5-9, which enables the end users to calibrate the sensor by themselves (ME-53 Laser speckle extensometer manual). However it makes the system bulky, and the calibration procedure is still time-consuming.

Figure 5-9 Messphysk company's laser speckle extensometer ME53-33

A new calibration method, called Auto Calibration, is proposed. It does not require any specific equipment and can be done very fast by the end user.

Suppose the coordinate system *OXY* in Figure 5-8 is an arbitrary coordinate system attached to the sensor. Now the orientation differences of the two camera coordinates with respect to this arbitrary coordinate are ϕ_1 and ϕ_2, whose values are unknown. Assume that camera A detects a displacement vector (x_1, y_1) between the reference image and the post-deformation image. Similarly, suppose camera B detects a displacement vector of (x_2, y_2). Note that x_1, y_1, x_2, y_2 are in the unit of pixels. The displacement vectors (x_1, y_1) and (x_2, y_2) can be converted to the displacement vectors in physical unit with respect to the arbitrary coordinate system *OXY* using Equations (4.20) and Equation (4.21), as described below.

Expanding Equation (4.20) and Equation (4.21) into the algebra form, yield,

$$\begin{cases} X_1 = \alpha_1 x_1 - \beta_1 y_1 \\ Y_1 = \beta_1 x_1 + \alpha_1 y_1 \\ X_2 = \alpha_2 x_2 - \beta_2 y_2 \\ Y_2 = \beta_2 x_2 + \alpha_2 y_2 \end{cases} \tag{4.25}$$

The distance change of the two observation spots on the object surface can be expressed as

$$\begin{aligned}\Delta_d &= \left|\overrightarrow{pq}\right| - \left|\overrightarrow{O_a O_b}\right| \\ &= \sqrt{(L + X_2 - X_1)^2 + (Y_2 - Y_1)^2} - L \\ &= (L + X_2 - X_1)\sqrt{1 + \left(\frac{Y_2 - Y_1}{L + X_2 - X_1}\right)^2} - L \\ &= (L + X_2 - X_1)\left[1 + \frac{1}{2}\left(\frac{Y_2 - Y_1}{L + X_2 - X_1}\right)^2\right] - L\end{aligned} \tag{4.26}$$

Now, by Taylor expansion,

$$\Delta_d = (L + X_2 - X_1) + \frac{1}{2}\frac{(Y_2 - Y_1)^2}{(L + X_2 - X_1)} - L \tag{4.27}$$

Since $\frac{(Y_2 - Y_1)^2}{(L + X_2 - X_1)} \approx \frac{(Y_2 - Y_1)^2}{L}$

$$\Delta_d = X_2 - X_1 + \frac{(Y_2 - Y_1)^2}{2L} \tag{4.28}$$

Expanding this equation by using the equation system (4.25), will result in be a very complicated expression, and the unknown variables will be difficult to determine. Observing that $(X_2 - X_1)$ and $(Y_2 - Y_1)$ are of the same scale and $|Y_2 - Y_1| \ll L$, $\left|\frac{(Y_2 - Y_1)^2}{2L}\right| \ll |X_2 - X_1|$, yield

$$\Delta_d \approx X_2 - X_1 \tag{4.29}$$

Therefore, $\frac{(Y_2 - X_1)^2}{2L}$, which is the second order term in Equation (4.28), is temporarily ignored and will be calculated later.

Thus by equation system (4.25)

$$\Delta_d \approx -\alpha_1 x_1 + \beta_1 y_1 + \alpha_2 x_2 - \beta_2 y_2 \tag{4.30}$$

To determine the distance change by the image motion detected by the two cameras, the four unknown parameters $\alpha_1, \beta_1, \alpha_2, \beta_2$ must be determined. This can be done by the following procedure:

1. Position the sensor on a flat specimen surface such that each camera observes a point on the surface. The specimen surface should not have any deformation throughout the experiment.
2. Take the reference or baseline images
3. Remove the sensor and then put it back. Try to align the sensor to the position where the reference images are taken.
4. Take the images and calculate their relative displacement with respect to the reference image using the cross-correlation method described in Chapter 4. The results are two displacement vectors (x_1, y_1) and (x_2, y_2) in units of pixels.
5. Repeat step 3 and step 4 for N times. N is recommended to be larger than 10 for enough a sample size. The demo experiment results are shown in Table 5-4.

Table 5-4 Experimental data of the Auto Calibration method demonstration

	Image displacement of camera A		Image displacement of camera B	
Reading #	x1(pixel)	y1(pixel)	x2(pixel)	y2(pixel)
1	-31.08	-63.16	-31.96	23.92
2	2.68	-39.20	2.52	-5.00
3	-85.12	-134.80	-87.00	-185.68
4	29.00	-32.92	28.08	-65.36
5	-66.72	-19.16	-66.20	-106.04
6	19.08	-58.28	17.20	-134.84
7	-14.04	-125.92	-15.88	-36.36
8	-37.92	-128.44	-39.08	26.96
9	-87.04	-44.16	-87.60	-24.00
10	215.84	-97.44	213.92	38.24
11	18.00	-110.40	18.36	153.08
12	46.88	-86.72	45.88	-5.96
13	-42.04	-55.92	-42.32	-45.96
14	-63.72	-139.00	-64.88	7.00

The N displacement vectors obtained by the above procedure are denoted as $[x_{11} \quad y_{11} \quad x_{21} \quad y_{21}], [x_{12} \quad y_{12} \quad x_{22} \quad y_{22}] \ldots, [x_{1N} \quad y_{1N} \quad x_{2N} \quad y_{2N}]$.

Since throughout the experiment, the specimen surface is free of deformation, the relative distance change Δ_d are all zero for all the N observations. Therefore by Equation (4.30) we have

$$\begin{bmatrix} x_{11} & y_{11} & x_{21} & y_{21} \\ x_{12} & y_{12} & x_{22} & y_{22} \\ \vdots & \vdots & \vdots & \vdots \\ x_{1N} & y_{1N} & x_{2N} & y_{2N} \end{bmatrix} \begin{bmatrix} -\alpha_1 \\ \beta_1 \\ \alpha_2 \\ -\beta_2 \end{bmatrix} = 0 \tag{4.31}$$

Denoting $A = \begin{bmatrix} X_{11} & Y_{11} & X_{21} & Y_{21} \\ X_{12} & Y_{12} & X_{22} & Y_{22} \\ \vdots & \vdots & \vdots & \vdots \\ X_{1N} & Y_{1N} & X_{2N} & Y_{2N} \end{bmatrix}$ and $h = \begin{bmatrix} -\alpha_1 \\ \beta_1 \\ \alpha_2 \\ -\beta_2 \end{bmatrix}$

gives,

$$Ah = 0 \tag{4.32}$$

The trivial solution of the homogenous system of linear equations (4.32) is zero, which is useless. And since the row number N is larger than the column number 4, there is no exact non-zero solution. Instead, the approach is to find the least square solution for the homogenous system of linear equations. That is, to find h that minimize $|Ah|$ subject to $|h| = 1$.

Using Singular Value Decomposition (SVD), matrix *A* can be written in the form:

$$A = U \sum V^T = \sum_{i=0}^{4} \sigma_i u_i v_i^T \tag{4.33}$$

The "right singular vector" of the matrix *A* corresponding to the smallest σ_i is the solution h, whose entries are the value of the four parameters $\alpha_1, \beta_1, \alpha_2, \beta_2$.

Now given the image displacements (x_1, y_1) and (x_2, y_2) that are detected by the two camera of the sensor, we can calculate the distance change between the two observed points on the object surface using Equation (4.28) and Equation (4.25).

$$\begin{aligned} \Delta_d &= X_2 - X_1 + \frac{(Y_2 - Y_1)^2}{2L} \\ &= -\alpha_1 x_1 + \beta_1 y_1 + \alpha_2 x_2 - \beta_2 y_2 + \frac{(\beta_2 x_2 + \alpha_2 y_2 - \beta_1 x_1 - \alpha_1 y_1)^2}{2L} \end{aligned} \tag{4.34}$$

And the surface strain can be then calculated by $\varepsilon = \frac{\Delta_d}{L}$.

The calibration method described above makes the sensor very flexible and easy to use. The calibration procedure does not require any additional equipment except a flat surface, thus it can be done in the field or even when the sensor is mounted on the rail system. The computation for solving the 4 parameters $\alpha_1, \beta_1, \alpha_2, \beta_2$ has been incorporated into the current software and most of the time that the procedure takes is to collect the N displacement vectors, which needs less than 1 minutes. This is significant less than the time required by the previous method, which usually takes a couple of hours. With the Auto Calibration method, the adjustment of the gauge length becomes a trivial issue. All the user needs to do is to unattach the two modules, reattach the two modules with the desired gauge length, and take less than 1 minute to calibrate the parameters.

Chapter 6 - Validation and application of the laser speckle strain sensor

The purpose this chapter is to demonstrate that the new developed optical strain sensor is a general strain measurement device that can be readily used not only in the laboratory, but also in the harsh environment of the prestressed concrete industry. Furthermore, it requires with minimum surface preparation.

A series of laboratory setups were fabricated and used to conduct direct comparisons with various conventional measurement techniques, including Whittemore gauge and the electrical resistance strain sensor. These experiments were conducted both indoors (laboratory), and outdoors (field) in order to validate the ability of the optical strain sensor to measure concrete surface strain with high resolution and consistency. After the validation, the sensor was further applied to the real field measurement for the diagnostic testing of prestressed concrete members and, in particular, prestressed railroad cross-ties.

6.1 Validation using a two concrete block system

Shown in Figure 6-1 is the manual motion system used for verifying the performance of the optical strain sensor in a concrete surface measurement. Two small pieces of concrete block were positioned side by side with approximately 8 inches apart. The concrete block shown on the left was attached to a manual traverse system whose displacement was measured by a digital dial gauge of resolution of 0.001mm (Shars 303-3506). The concrete block on the right was held stationary.

The system was used to create a relative linear displacement between the two concrete blocks by displacing the concrete block on the left while the concrete block on the right remained stationary. The relative displacement between the two concrete blocks was increased from 0mm to 2mm, with 0.1mm increments, and was measured by both the digital dial gauge and the laser speckle strain sensor. The results are shown in Figure 6-2. The readings by the two devices (optical strain sensor and dial gauge) have excellent agreement. The differences between the two

sensor's readings are below 4 microns over the entire measurement range, as shown in Figure 6-3.

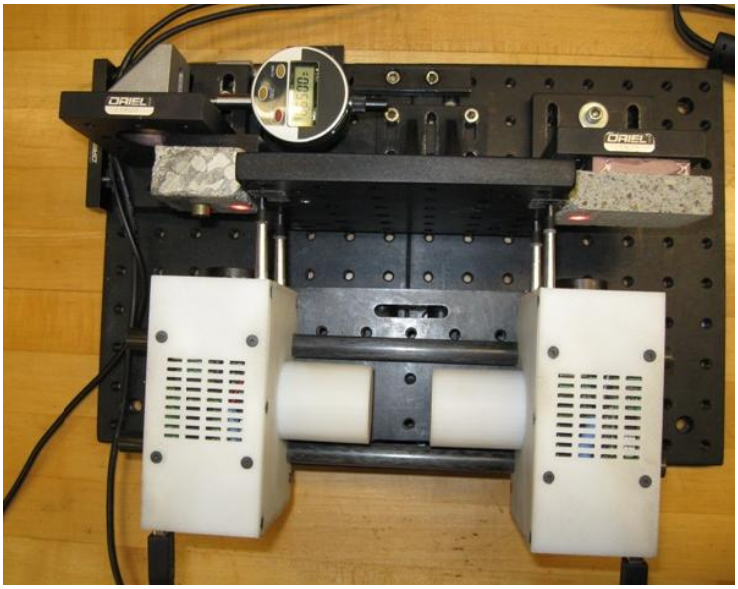

Figure 6-1 A two concrete block system

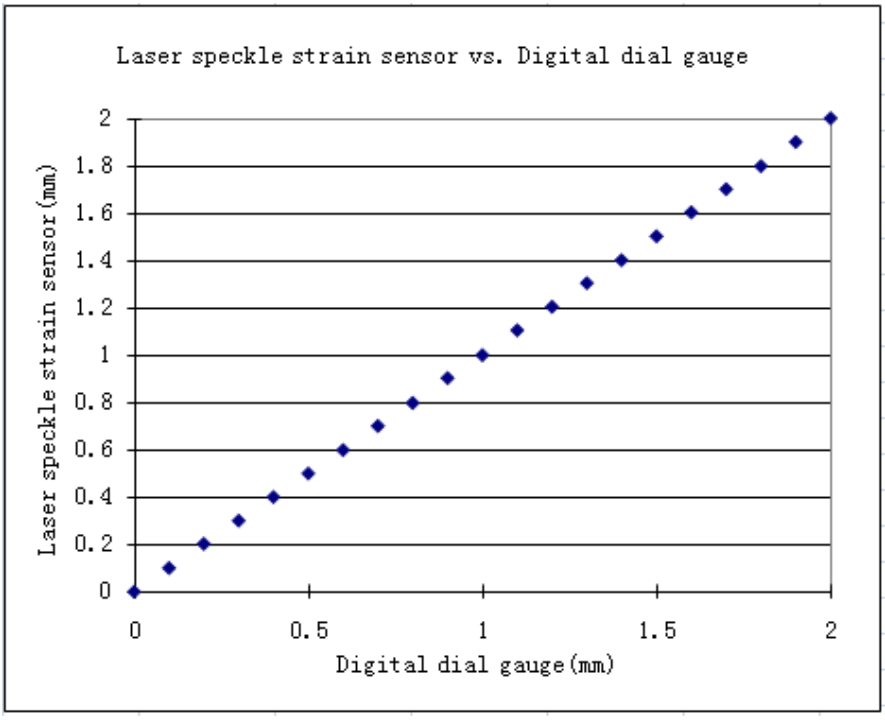

Figure 6-2 Comparison of laser speckle strain sensor and Digital dial gauge

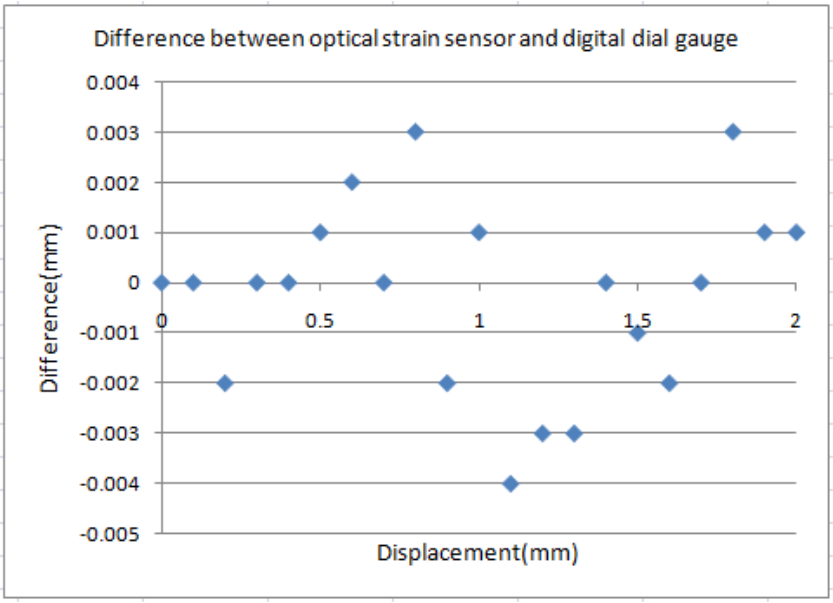

Figure 6-3 Difference between optical strain sensor and digital dial gauge measurements

6.2 Comparison with a Whittemore gauge during compressed concrete beam strain measurement

An experiment was conducted to measure the surface strain of a small concrete beam under different compressional loads by using both the optical strain sensor (the second generation prototype) and the Whittemore gauge for direct comparison.

A concrete beam of length 300mm and 90mm by 90mm square cross-section was mounted on the compression test setup as shown in Figure 6-4. The concrete beam was loaded with two different compressional loads at 2,000*lbs* and 4,000*lbs*. At each load level, the deflections between two fixed points mounted on the beam surface was measured by the Whittemore gauge. The laser speckle strain sensor was also used in handheld mode to measure the surface deformation at the same time for comparison purposes.

The results from the optical strain sensor and the Whittemore gauge are both shown in Figure 6-5. It can be seen that the readings by the two sensors have excellent agreement with differences between the results below 6 microns. The repeatability of the 5 measurements shown using the laser speckle strain sensor at the same load level are excellent too.

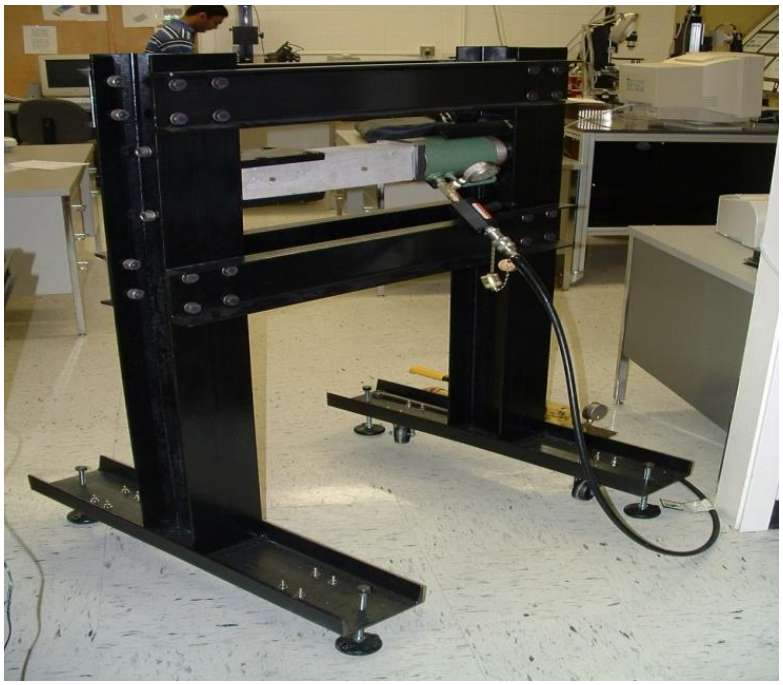

Figure 6-4 A concrete beam under compression

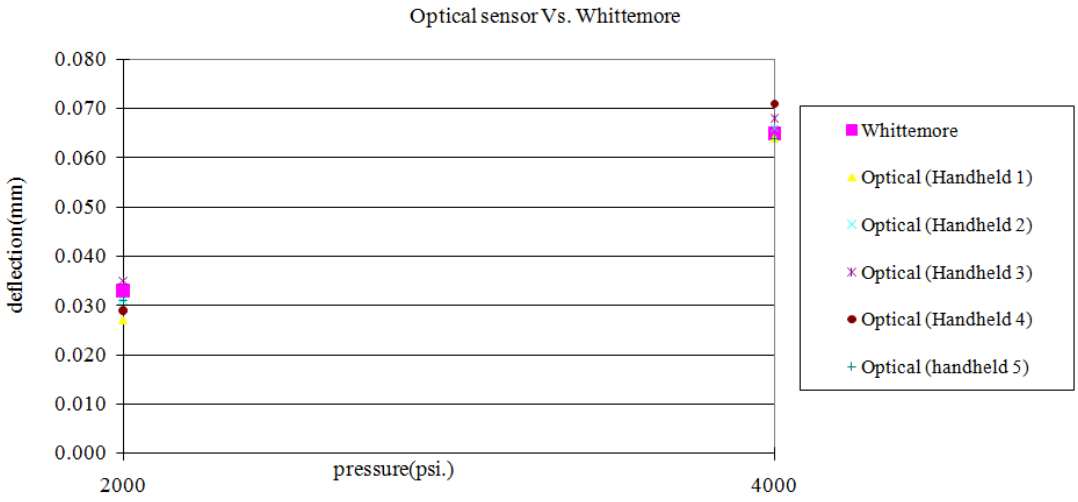

Figure 6-5 Surface deflection measurement obtained by Whittemore gauge and laser speckle strain sensor

6.3 Comparison with an electrical resistance strain gauge during compressed concrete beam strain measurement

An experiment was conducted to measure the surface strain of a concrete beam under different compressional loads by using the optical strain sensor (the second generation prototype), and using the electrical resistance strain gauge (ESG) for direct comparison.

An experimental setup used was that shown in Figure 6-6. A concrete beam of length 300mm and 90mm by 90mm square cross-section was mounted on the compression test setup, and the optical strain sensor was positioned alongside the tested concrete beam. The beam was loaded with compressional loads ranging from 3,000*lbs* to 21,000*lbs* in 2,000*lbs* increments. This setup was successfully used to assist in isolating the longitudinal (axial) strain component from the other distortions that are inherently present due to varying degrees of bending and torsion,

At each load level, the strain between two fixed points on the beam surface was measured by the optical strain sensor. An electrical resistance strain sensor was also used to measure the surface strain at the same time for comparison purposes.

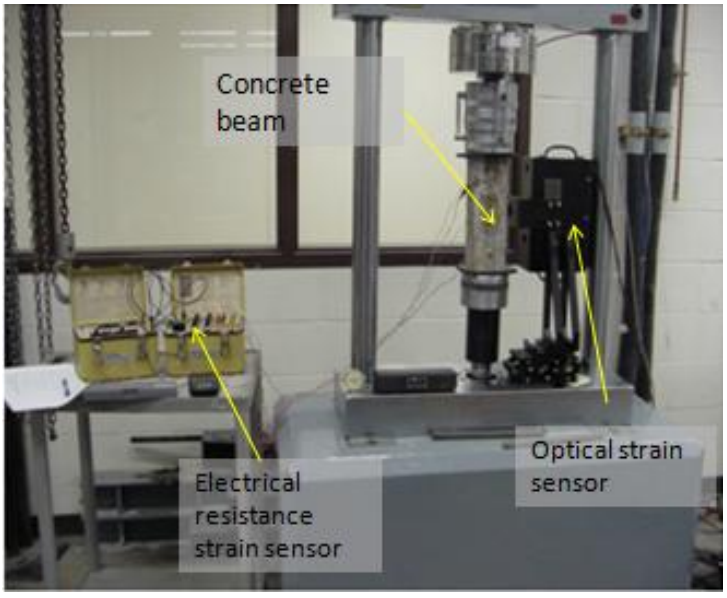

Figure 6-6 Experiment setup of the comparison of laser speckle strain sensor and electrical resistance strain gauge (ESG) sensor

The results from the optical strain sensor and the electrical resistance strain gauge are shown in Figure 6-7 and the differences between these two different sensor measurements are shown in Figure 6-8. It can be seen that the readings by the two sensors have excellent agreement, with differences between the results falling below 6 microstrain.

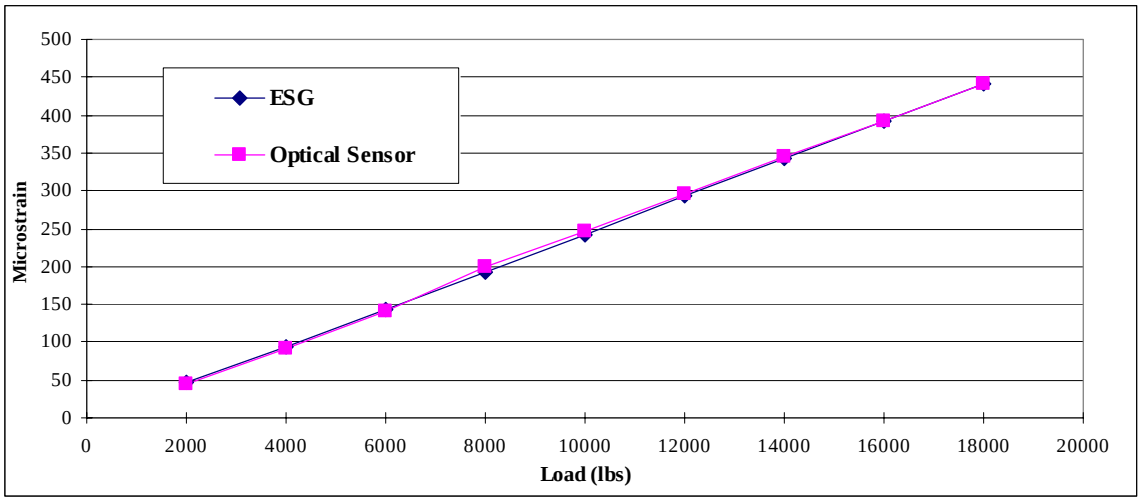

Figure 6-7 Measurement results of surface strain

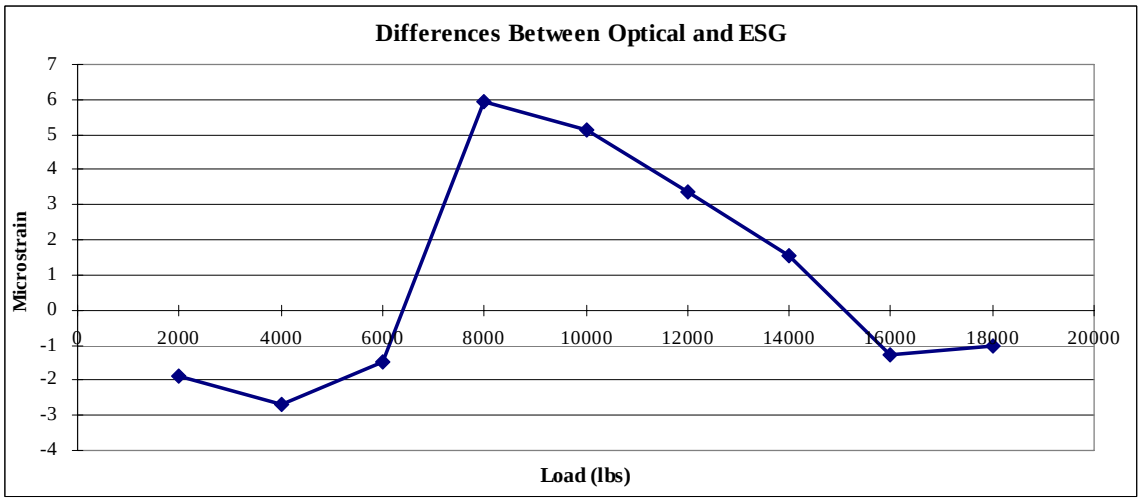

Figure 6-8 Difference of the measurements between optical strain sensor and electrical resistance strain sensor

6.4 Application of the optical strain sensor to a prestressed concrete member

Currently prestressed concrete is widely used in civil engineering infrastructure, especially in applications that require extra length, like bridges, skyscrapers, foundations, pipes and piles, pavements, and water tanks, due to its great advantage over traditional concrete in

sustaining tension (Naaman, 1982). Prestressed concrete is manufactured by casting around already tensioned steel strands. After the casting process is complete and the concrete has hardened, a detensioning procedure is undertaken by cutting the strands at both ends of the concrete beam to release the tension. The shrinking strands grip the concrete and keep it in a compressed state. The tension force that the concrete beam will experience during service will be offset by this pre-established compression; thus producing a minimum chance of crack as long as loads are such that the concrete remains in compression state (Naaman, 1982).

Typically, the transfer length, defined as the distance required to transfer the fully effective prestress force in the reinforcing-strand to the concrete, is used to evaluate the quality and performance of concrete members. The method that is most commonly used by industry for the transfer length measurement is accomplished manually using a Whittemore gauge that has been discussed in Section 1.2.1. To measure the transfer length, "points" are typically mounted using epoxy onto the concrete beam, as shown in Figure 6-9. The Whittemore gauge is used to measure the distance change between the points, which in turn gives the surface strain profile of the concrete beam. A typical strain profile is a curve that varies approximately linearly from zero at the member end to a constant value at a distance from the end of the beam. This distance is equal to the transfer length.

Figure 6-9 Metal points bonded onto the concrete surface

To evaluate the optical strain sensor's ability to measure transfer length, several pretensioned concrete members were fabricated using different concrete mixtures, and the strain

profile was measured on one side of each member, using both the traditional Whittemore gage and the non-contact laser speckle method.

6.4.1 Surface strain measurement using the second generation prototype

The laser speckle strain sensor used in this experiment was the second generation prototype based on single module design that has been discussed in Chapter 3. The mixtures used in this experiment corresponded to SCC mixtures that were part of another prestressed concrete study and previously reported (Peterman, 2007). The pretensioned members were each 9'-6" long with a trapezoidal cross-section as shown in Figure 6-10. Surface strain measurements for the trapezoidal specimens were obtained using both the standard (Whittemore) technique and the laser speckle (optical) technique.

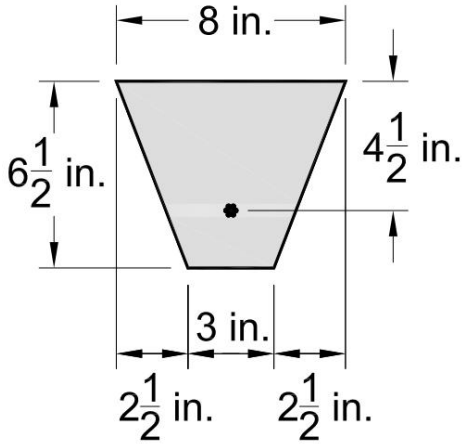

Figure 6-10 Cross-section of the pretensioned concrete member

In order to facilitate the laser speckle measurements, an aluminum rail was mounted to the side of the member as shown in Figure 6-11. The rail was attached to the members using small ¼-inch-diameter inserts that were cast into the sides of the pre-tensioned concrete members. Because of the insensitivity of the sensor to undesirable degrees of freedom, no high precision traverse setup was required, and simple visual manual positioning was adequate. This is very important for the measurement of prestress concrete strain in the field. Since the laser speckle method utilizes the concrete surface characteristics to measure displacements, the surface strains can be quickly determined without the time-consuming process of adhering gage points to the concrete surface.

In addition to using the laser speckle strain sensor, “gage points” were also bonded to the concrete beam surface in order to provide a direct comparison between the two methods of strain measurement.

Figure 6-11 Experiment setup for transfer length measurement of prestressed concrete member using the second generation prototype

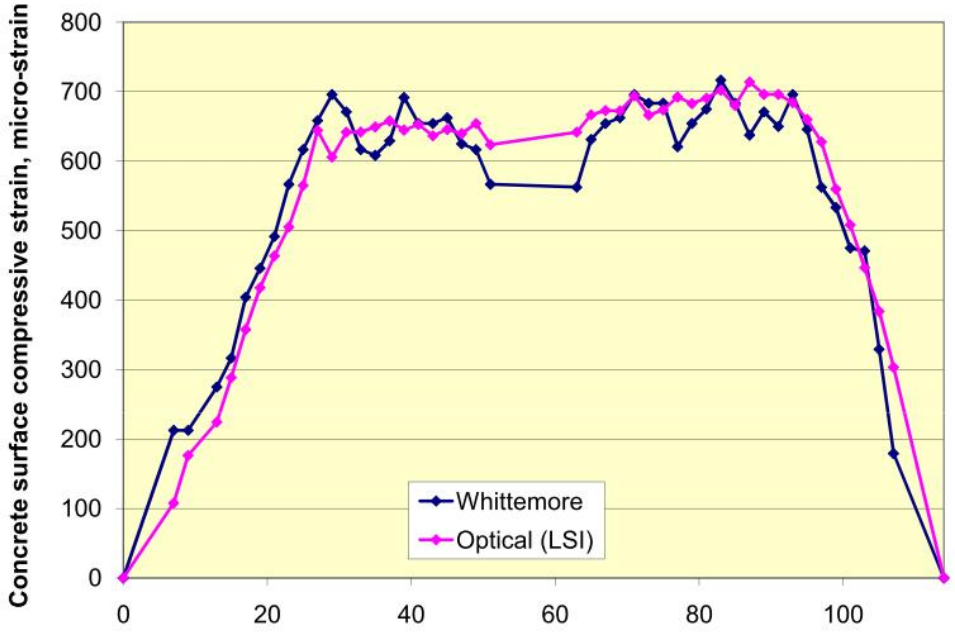

Figure 6-12 Comparison of strain measurements immediately after de-tensioning of a pre-tensioned specimen

The results from this beam test are shown in Figure 6-12. It can be seen that the laser speckle strain sensor results in much smoother data with less scatter than that generated from the existing surface strain measurement technique using the Wittemore gauge. The laser speckle technique has been validated on members cast in both indoor and outdoor operations.

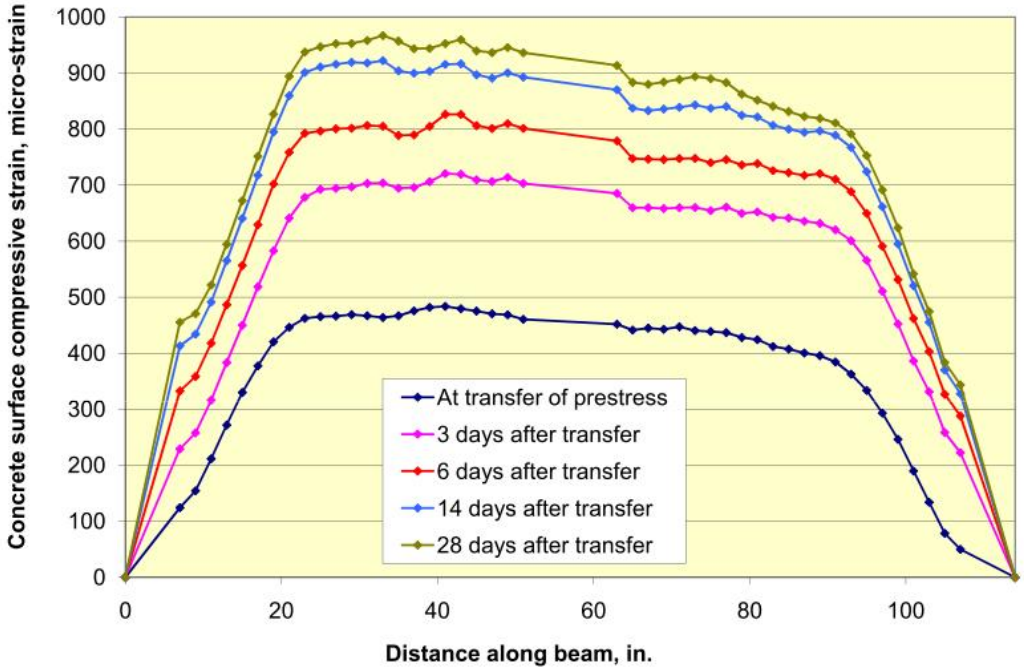

Figure 6-13 Optical surface-strain measurements during the first 28-days after de-tensioning

The surface strain of the prestressed concrete member was further monitored for 28 days after the detensioning. This is to investigate the capability of the laser-speckle for long term strain measurement. As shown in Figure 6-13, the laser speckle method works very well during the first month after de-tensioning. Note in this figure that the peak strains vary along the length of the member, producing an asymmetric shape. This was due to a slight horizontal eccentricity of the strand in the small trapezoidal cross-section, which produced bi-axial bending in the member.

6.4.2 Surface strain measurement using the fourth generation prototype

A prestressed concrete beam strain measurement experiment that is similar to that described in section 6.2.1 was conducted using the fourth generation prototype of the laser speckle strain sensor. The fourth generation prototype, as discussed in Chapter 3, is based on the same laser speckle technology as the second generation prototype, but has different hardware design (dual module design vs. single module design) and is more accurate and flexible.

The pretensioned members were each 9'-6" long with a rectangular cross-section as shown in Figure 6-14. In order to facilitate the laser-speckle measurements, three small ¼-inch-diameter inserts were cast into the pre-tensioned concrete members to allow an aluminum rail to sit on the top of the member surface. The sensor was then installed on the rail and was able to traverse freely on it.

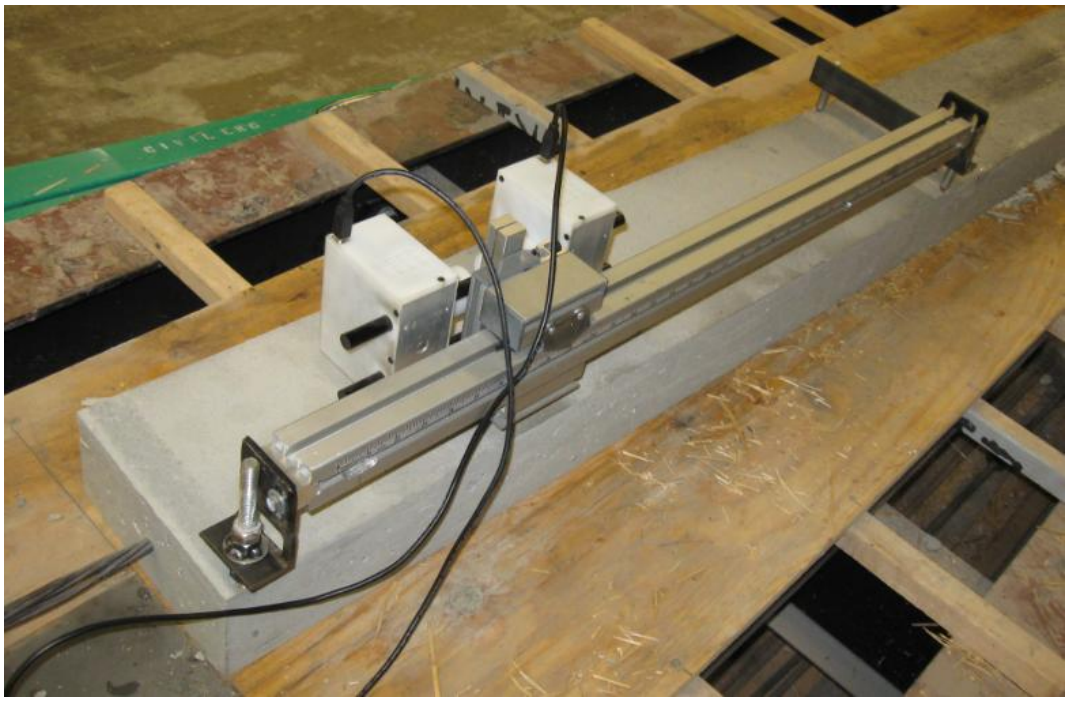

Figure 6-14 Experiment setup for the transfer length measurement of prestress concrete member using fourth generation prototype

Surface strain measurements were obtained using the fourth generation laser speckle strain device. The results from this beam test are shown graphically in Figure 6-15. It is clear

that the Laser Speckle Strain sensor results show scatter below 10 microstrain, much less than that of the similar experiment described in Section 6.4.1 in which the second generation laser speckle strain device was used. This is realized because of several improvements in the design of the fourth prototype over the previous versions, including the dual module design, less sensitivity to thermal expansion effect and better camera hardware, as discussed in Chapter 3.

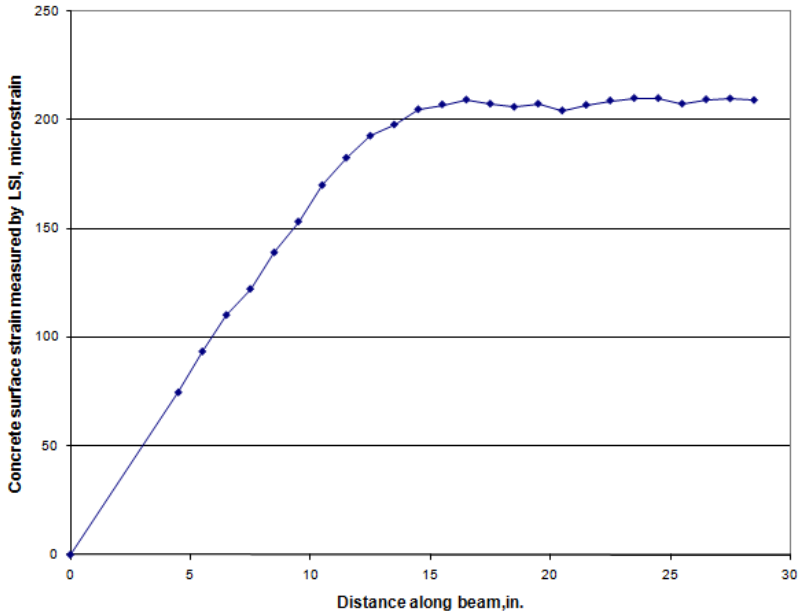

Figure 6-15 Concrete surface strain measurements immediately after de-tensioning of a pre-tensioned specimen using laser speckle strain sensor

6.5 Transfer length measurement of prestressed railroad cross-tie

Prestressed concrete railroad cross-ties are becoming increasingly popular in the United States, and are an essential component for high speed railway lines. Currently, the production of the prestress concrete rail cross-ties is a highly automatic process in the USA. For instance, in the CXT concrete cross-tie production plant in Grand Island, NE, the production of the cross-tie involves pouring concrete mix on a grid of strands of 386 feet length that are tensioned at 300 thousand lbs force in a heated bed. The headed bed expedites the curing process of the concrete mix that typically takes days to a period as short as 8 hours. After the concrete mix is cured, the

386 feet long prestressed beam goes through a saw cut machine continuously and is cut into 8'-6" long cross-ties. The plant is capable of producing several thousand cross-ties each day. In order for these prestress concrete ties to function adequately over their expected service life, the prestressing force must be fully introduced into the railroad tie at a location well before the rail load is applied. Once again, the length required to transfer the prestressing force into the concrete cross-tie member is the "Transfer Length". However, currently the concrete rail cross-tie industry does not conduct transfer length measurements except occasionally for research purposes. This due to the fact that there does not exist a transfer length measurement method that is robust enough for the harsh environment of the plant and capable of keeping up with the working speed of the production line.

To evaluate the feasibility of the in-plant transfer length measurements using the laser speckle strain sensor, two trips have been made to the CXT concrete cross-tie production plant in Grand Island, NE. One trip was on October 22nd in 2010, and the other trip was on February 8th in 2011.

In order to facilitate the laser-speckle measurements, three small ¼-inch-diameter inserts were cast into each of the cross-tie immediately after the pouring of the concrete mix. The inserts allow an aluminum rail to sit on the top of the member surface conveniently. The sensor was that was installed on the rail was able to traverse freely on it, as shown in Figure 6-16.

Figure 6-16 Laser speckle strain sensor mounted on a rail at CXT concrete cross-tie plant

Before the detensioning of the cross-tie, initial laser speckle readings were taken every 0.5 inch for the first 10 points, counting from the end of the tie, and every 1 inch thereafter along the beam; by traversing the laser speckle strain sensor on the rail manually. A total of 70 data points were obtained for each tie, with 35 data points for either side.

After the cross-tie was detesioned (i.e., the tensioned reinforcing strands were cut and prestressing force was transferred to the concrete member), post-dententioning readings were taken. The two sets of readings were compared, correspondingly, to extract the strain information at each location, which in turn was used to plot the strain profile of the cross-tie for the "transfer length" determination.

The application of the laser speckle strain sensor to the cross-tie transfer length measurement was not successful in our first trip to CXT concrete cross-tie production plant. The software failed to find correlation between the corresponding speckle image pairs. Thus it could not extract the surface strain information along the cross-ties. This was due to a de-correlation effect that was caused by the dramatic physical change of the cross-tie surface when the ties went through the saw-cutting machine. Here the cross-tie surface undergoes severe abrasions including washing, scrubbing, wiping and vacuuming, as shown in Figure 6-17. The change of the concrete surface's microscopic profile causes significant de-correlation to the speckle image pairs. To reduce the de-correlation effect, microscopic reflective particles were bonded to the cross-ties to serve as artificial speckle before the initial readings were taken, as shown in Figure 6-18. The particles were much less vulnerable to the severe abrasions than the concrete surface itself and helped keep the correlation that was critical for the laser speckle strain sensor to be functional in the this extreme situation.

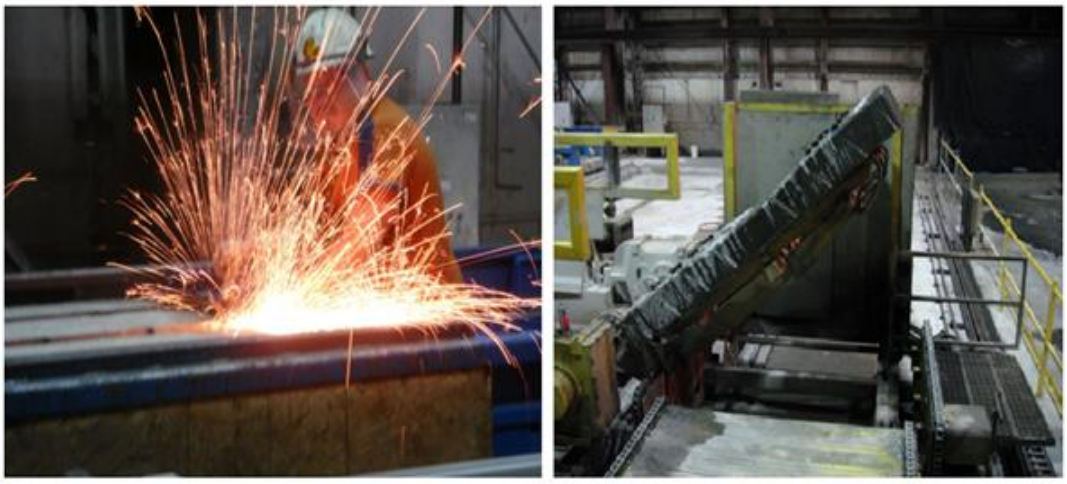

(a) Cutting

(b) Washing, scrubbing, wiping and vacuuming on the tie surface

Figure 6-17 Severe abrasions to the cross-tie surface at the saw-cutting machine

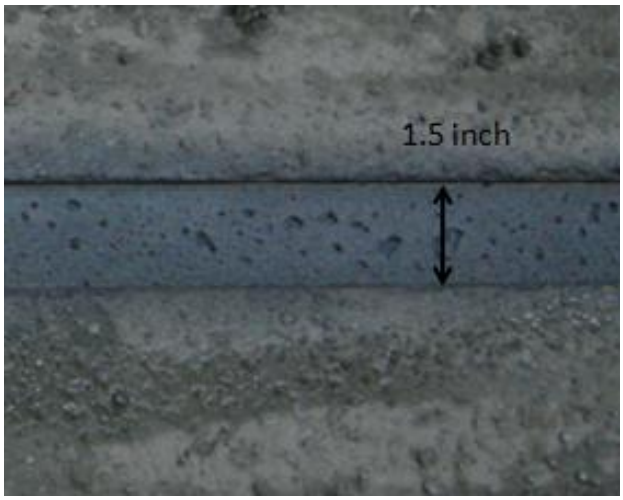

Figure 6-18 Cross-tie surface bonded with microscopic reflective particles

With the microscopic particles applied to the surface of the cross-tie, the laser speckle strain sensor was able to find the correlation between the corresponding speckle image pairs and extract the surface strain information of the cross-ties. The total time for measuring each tie was about 3 minutes. This was made possible because no high precision traverse setup was required and simple visual manual positioning was adequate. The results from the in-plant cross-tie measurement are shown in Figure 6-19,6-20,6-21. To evaluate the capability of the laser speckle strain sensor to monitor the long-term surface strain trend, another set of readings were taken for

each cross-tie ten days after the pouring. It can be seen in that the laser speckle strain sensor has successful extracted the surface strain information both for short term and long term effect.

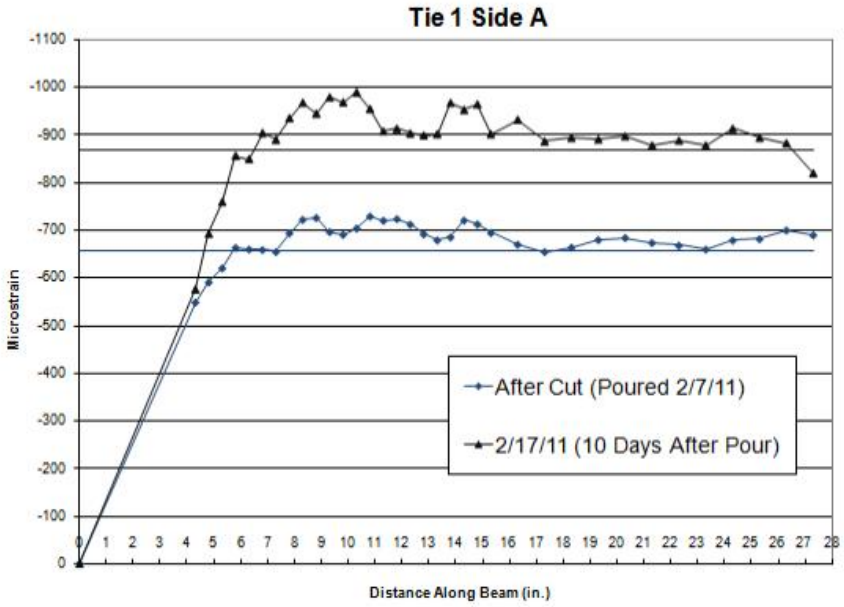

Figure 6-19 Cross-tie surface strain measurement (Tie 1 Side A)

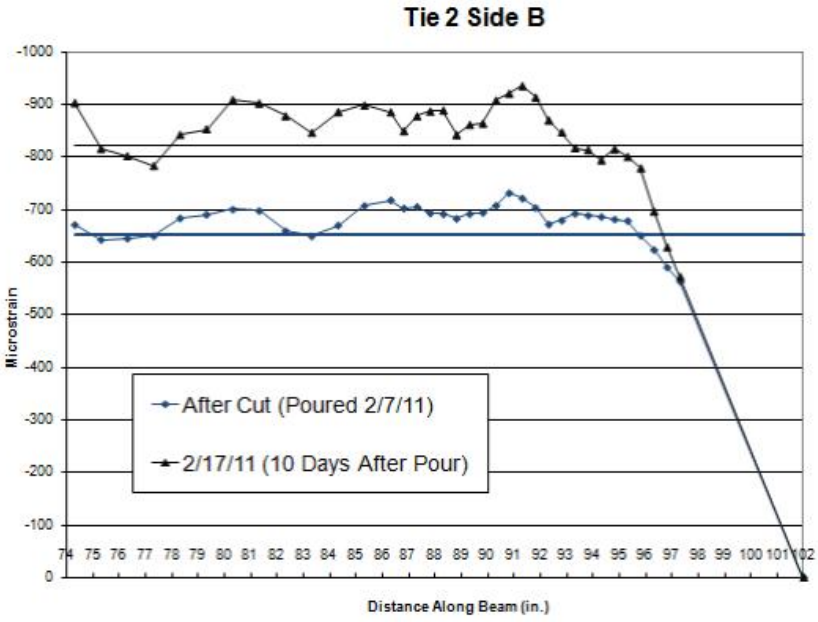

Figure 6-20 Cross-tie surface strain measurement (Tie 2 Side B)

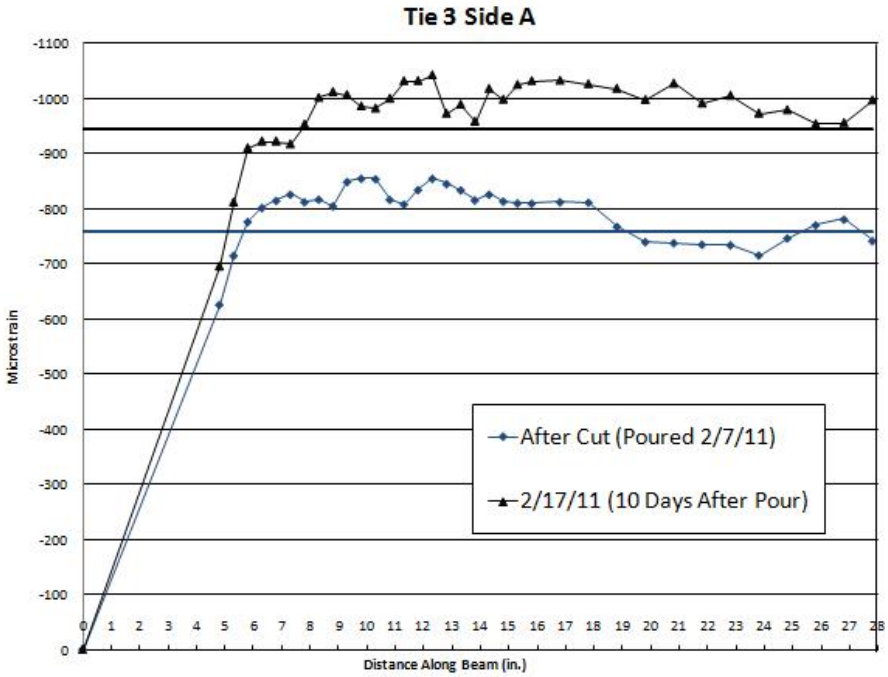

Figure 6-21 Cross-tie surface strain measurement (Tie 3 Side A)

Chapter 7 - Conclusion

This dissertation presented the development of a general non-contact surface strain measurement technique based on the laser speckle principle that is able to rapidly and accurately determine concrete surface strains. The characteristics and behavior of the speckle were investigated. The relationship between the multi-degree of motion of the subject surface and the induced motion of the speckle pattern was also addressed. Based on the laser speckle measurement technique, four (4) generations of designs have been made. A prototype was fabricated for each design either on an optical breadboard for concept validation, or in a portable form for field test operation. For each generation design, improvement was made based on the knowledge learned through the test of the previous generation prototype. The fourth generation prototype, incorporating a unique modular design concept and unique self-calibration function, exhibits several preferable features such as flexible adjustment of the gauge length, easy expansion to rosette 2D strain measurement and high accuracy.

Extensive testing has been conducted in the laboratory environment for validation of the sensor's capability for concrete surface strain measurement. The experimental results from the laboratory testing have shown that the measurement precision of this new laser speckle strain measurement technique can easily achieve 20 microstrain. Furthermore, the laser speckle strain sensor was applied to the transfer length measurement of typical prestressed concrete beams for both short term and long term monitoring. The measurement of transfer length by the sensor was unprecedented since it appears that it was the first time that laser speckle technique was applied to prestressed concrete inspection, and particularly for use in transfer length measurement. In the following field application of the laser speckle strain sensor in the CXT rail cross-tie plant, the technique reached 50 microstrain resolution, comparable to what could be obtained using mechanical gauge technology. It was also demonstrated that the technique was able to withstand extremely harsh manufacturing environment.

The accuracy and robustness of the device presents great potential for various civil engineering applications, such as crack propagation monitoring and bridge health monitoring. It can also be used to measure the surface strain of materials other than concrete. These include any materials with rough surface, such as steel, aluminum and fiber glass.

The sensor has shown its capability of rapidly obtaining the surface strain profile for the transfer length determination. The procedure has the potential to be further expedited by mounting the sensor on an automatic traverse instead of manually moving it. In contrast to the conventional transfer length measurement methods that interrupt the daily casting and de-tensioning sequence, the automation of the transfer length measurement could be incorporated into the manufacturing production line for prestressed concrete member, such as the railroad cross-tie application, thus bringing the real-time online diagnostics and monitoring of the prestressed concrete production into reality.

References

A. L. Window, G. S. (1982). *Strain gauge technology.* London ; New York: Applied Science.

A.A. Mufti, J. N. (2008). Health monitoring of structures & related education and training needs of civil engineers. *Bridge Maintenance, Safety Management, Health Monitoring and Informatics - IABMAS '08: Proceedings of the Fourth International IABMAS Conference,* (pp. 33-39). Seoul, Korea.

Bracewell, R. N. (1978). *The Fourier Transform and Its Applications.* New York: McGraw-Hill.

Brinson, M. E. (1984). Resistance-foil strain-gage technology as applied to composite materials . *Experimental Mechanics, Vol 26* , 153-154.

C. Joenathan, B. F. (1998). Speckle interferometry with temporal phase evaluation for measuring large object deformation. *Applied Optics* , Applied Optics.

Ceravolo, A. D. (2005). Monitoring and Response of CFRP Prestressed Concrete Bridge . *Sensing Issues in Civil Structural Health Monitoring* , 85-94.

D.A.Gregory. (1976). Basic physical principles of defocused speckle photography: a tilt topology inspection technique. *Optics and Laser Technology* , Vol. 8 .

Dainty, J. C. (1975). *Laser speckle and related phenomena.* New York: Springer-Verlag Berlin Heidelberg.

Deng, L. e. (2008). Efficient image reconstruction using partial 2D Fourier transform. *Proceedings of the IEEE Workshop on Signal Processing Systems* (pp. 49 - 54). Washington, D.C. Metro Area, USA: SiPS.

Eduard Schenuit, R. B. (2008). Optical strain measurement on small specimens based on laser speckles. *Materials Science Forum* , 237-242.

Faber, M. H., & Stewartb, M. G. (2003). Risk assessment for civil engineering facilities: critical overview and discussion. *Reliability Engineering & System Safety* , 173-184 .

Faugeras, O. (1993). *Three-Dimensional Computer Vision.* The MIT Press.

Fuhr, P. (2000). Measuring with Light Part 2: Fiber-Optic Sensing-From Theory to Practice. *Sensors* .

Goodman, J. W. (1996). *Introduction to Fourier Optics.* New York: McGraw-Hill Science.

Harris, F. J. (1978). On the use of windows for harmonic analysis with the discrete Fourier transform. *Proceedings of the IEEE, Vol. 66 No.1* , 51-83.

Hecht, E. (1998). In *Optics, Third Edition.* Addison Wesley Longman, Inc.

Helena (Huiqing) Jin, W.-Y. L. (2006). Strain Measurement of Microsamples Using Laser Interferometry. *International Mechanical Engineering Congress and Exposition* (pp. 563-567). Chicago, Illinois, USA : ASME.

Herzig, H. P. (1997). *Micro-optics Elements Systems and Applications.* Taylor Francis Books Ltd.

Hong-Nan Li, G.-D. Z.-S. (2007). Strain transfer analysis of embedded fiber Bragg grating sensor under nonaxial stress. *Optical Engineering* .

http://mathworld.wolfram.com/BesselFunctionoftheFirstKind.html. (n.d.).

L.X. Yang, R. W. (1999). Strain and stress analysis by means of a novel sensor: MicroStar. *International Workshop on Video-Controlled Materials Testing.* Nancy, France.

Malo, K. B. (2008). Planar Strain Measurements on Wood Specimens . *Experimental Mechanics, vol 49* , 575-586.

ME-53 Laser speckle extensometer manual. (n.d.). Retrieved from http://www.messphysik.com/index.php?id=16&L=1

Merzbacher, A. D. (1996). Fiber optic sensors in concrete structures: a review. *Smart Materials and Structures* .

MTS LX laser extensometer. (2009). Retrieved from http://www.mts.com/ucm/groups/public/documents/library/dev_003699.pdf

Mufti, A. A. (2003). Integrated sensing of civil and innovative FRP structures. *Progress in Structural Engineering and Materials, vol5* , 115–126.

MUSPRATT, M. A. (1969). STRAIN MEASUREMENT IN REINFORCED CONCRETE SLABS. *Strain* , 152–156.

Naaman, A. E. (1982). *Prestressed concrete analysis and design: fundamentals.* New York: McGraw-Hill.

Neild, S. A. (2005). Development of a Vibrating Wire Strain Gauge for Measuring Small Strains in Concrete Beams. *Strain* , 3–9.

Peterman, R. (2007). The Effects of As-Cast Depth and Concrete Fluidity on Strand Bond. *PCI Journal* , 72-101.

R.Wegner, A. (1999). The miniaturization of speckle interferometry for rapid strain analysis. *Proceedings of SPIE, v. 3824,* (pp. 30-36). Munich, Germany.

S C Liu, K. P. (1995). Civil infrastructure systems research: hazard mitigation and intelligent material systems. *Smart material structure* , 169-174.

Samala, P. R., Su, M., & etc. (2005). Strain measurement of a mouse bone by 3D-electronic speckle pattern interferometry. *Annual SPIE Optics and Phootonics Symposium, Proceeding of SPIE* (pp. 58800C1-9). San Diego, CA: SPIE.

Shapiro, L. G. (2001). *Computer Vision.* Prentence Hall.

Sung, B. J. (2004). Sub-pixel image interpolations for PIV. *Proceedings of 2004 Korea-Japan Joint Seminar* . POSTECH, Korea.

Weixin Zhao, B. T. (2004). A novel optical technique for measuring 5-axis surface movement. *Two- and Three-Dimensional Vision Systems for Inspection, Control, and Metrology II, Proceedings Vol. 5606* (pp. 66-73). SPIE.

Zhao, W. (2006). A novel optical technique for measuring 5-axis surface movement, M.S. thesis. *Kansas State University, Kansas* .

Appendix A - Hardware Components List (the fourth generation prototype)

Part name	Manufacturer or retailer	part#
15mm Dia. Unmounted Linear Glass Polarizing Filter	Edmund optics	NT54-925
C-MOUNT 15MM THIN LENS MT.	Edmund optics	NT54-616
C-Mount Plate Beamsplitter 50R/50T VIS	Edmund optics	NT49-685
C-MOUNT 12.5MM THICK LENS MT	Edmund optics	NT54-623
C-MOUNT 12.5MM THIN LENS MT	Edmund optics	NT55-246
C-MOUNT 20MM THICK LENS MT.	Edmund optics	NT54-626
Plano-Convex Lens 12.7 x 12.7 VIS 0 Coating	Edmund optics	NT62-561
TECHSPEC® High Efficiency Anti-Reflection Coated Windows	Edmund optics	NT48-924
C-Mount Double Male Rotating Barrel	Edmund optics	NT53-865
Triplets lens	Rolyn optics	23.0600
Mono CCD camera	Lumenera Corp	Lu130M
High Performance Laser Module	Diode Laser Concept	1112A2-0001

Appendix B - Specifications and SolidWorks model of the laser speckle strain sensor (the fourth generation prototype)

- Resolution: 20 microstrain
- Positioning tolerance: ± 2mm
- Response time: 0.2 second
- Transfer length measurement time for a typical 10 feet prestressed concrete member: 3 minutes
- Mass: 2.6 lbs (2 modules combined)
- Dimensions: 4”x3”x2” (one module)

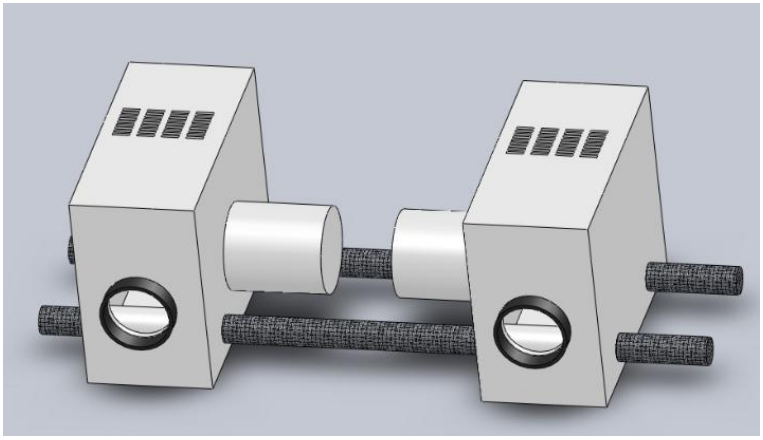

Figure B-1 3D SolidWorks model of the fourth generation prototype

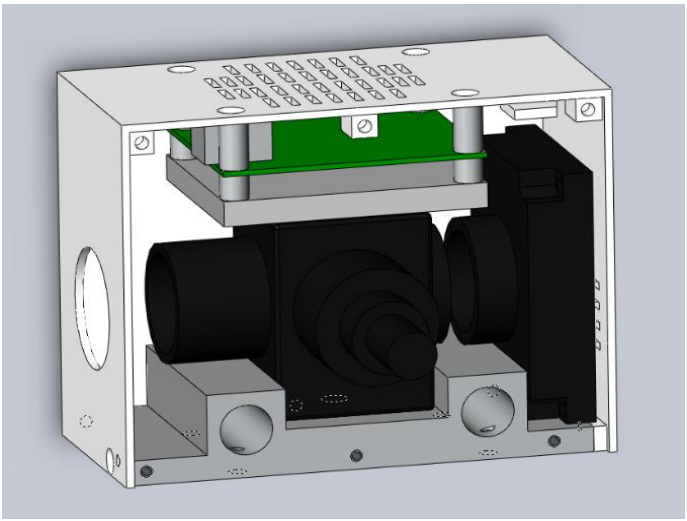

Figure B-2 3D SolidWorks model of an individual model with interior view

Appendix C - Uncertainty Analysis

This section evaluates the uncertainty of the strain measurement by the laser speckle strain sensor. The optical strain sensor measures the surface strain by detecting the in-plane displacements ΔA and ΔB of the two nearby surface points A and B, as discussed in Section 3.1, and the surface strain, ε, between point A and point B is determined by the equation $\varepsilon = \frac{E}{L}$, where $E = \Delta B - \Delta A$ is the relative deflection between point A and point B and L is the gauge length of 203.2 *mm* (8 inches) for the current setup. The uncertainty comes from three sources: (1) uncertainty of surface displacement measurement, (2) uncertainty of digital dial gauge used to calibrate the optical sensor and (3) uncertainty of gauge length L measurement. The three uncertainties are estimated individually below, and the total (or combined) uncertainty is obtained by using error propagation methods.

The manual motion system as shown in Figure 6-1 was used to estimate the uncertainty of the surface displacement measurement of the optical sensor. The concrete block on the right was stationary. The concrete block on the left was attached to a manual traverse system, whose displacement was indicated by a digital dial gauge of resolution of 0.001mm (Shars 303-3506). The displacement of the concrete block was also measured by the laser speckle strain sensor. The experiment was conducted by displacing the concrete block from 0mm to 1.000mm with increments of 0.100mm. The data is listed in Table C-1 and plotted in Figure C-1. The residual plot is shown in Figure B-2, which shows the deviation of the measured displacement from the laser speckle strain sensor as a function of the displacement (mm) measured by the digital dial gauge.

Table C-1 Experiment data for uncertainty analysis

Dial gauge(mm)	Laser speckle sensor(mm)	Deviation(mm)
0.000	0.000	0.000
0.100	0.100	0.000
0.200	0.202	0.002
0.300	0.300	0.000
0.400	0.400	0.000
0.500	0.499	-0.001
0.600	0.598	-0.002
0.700	0.700	0.000
0.800	0.797	-0.003
0.900	0.902	0.002
1.000	0.999	-0.001

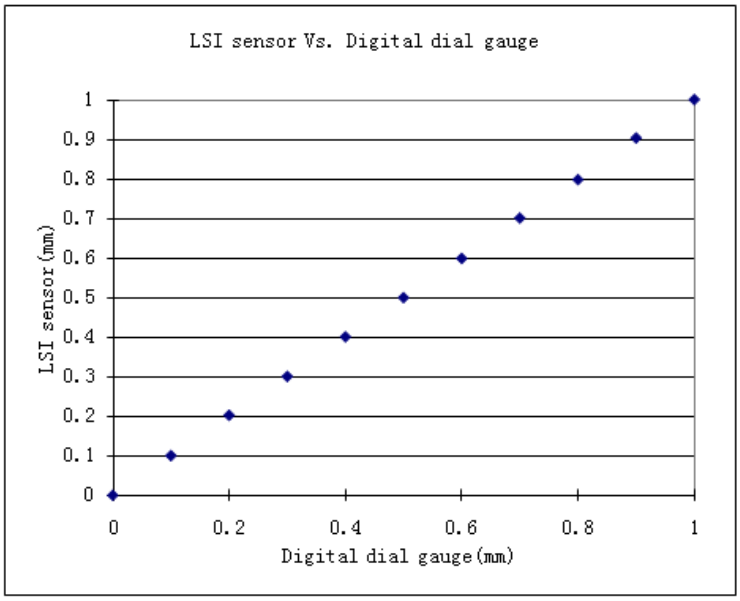

Figure C-1 Uncertainty analysis experiment data

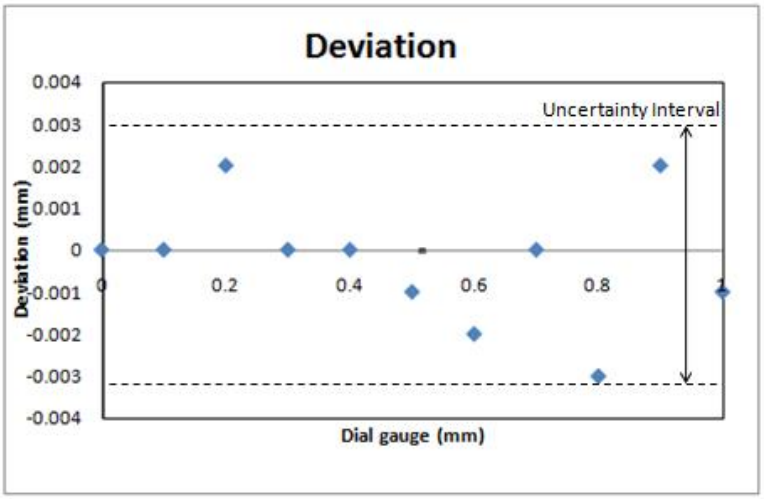

Figure C-2 Deviation between optical sensor and digital dial gauge

Figure C-2 also shows the uncertainty band covering all the residual points to within about ± 0.003 mm, which is denoted as $u_{Displacement} = \pm 0.003mm$. The uncertainty of the digital dial gauge is $u_{gauge} = \pm 0.001mm$. Using the propagation of errors method, assuming these errors are independent, the total uncertainty of the deflection measurement is given as,

$$u_E = \sqrt{u_{displacement}^2 + u_{displacement}^2 + u_{gauge}^2} = \sqrt{0.003^2 + 0.003^2 + 0.001^2} = 0.004mm$$

Since the strain is calculated by $\varepsilon = \frac{E}{L}$, the uncertainty of the strain measurement is

$$u_\varepsilon = \sqrt{\left[\left(\frac{\partial \varepsilon}{\partial E}\right)u_E\right]^2 + \left[\left(\frac{\partial \varepsilon}{\partial L}\right)u_L\right]^2} = \sqrt{\left(\frac{u_E}{L}\right)^2 + \left(u_L \cdot \frac{E}{L^2}\right)^2}$$

Since the surface strain of the prestressed concrete beam is usually less than 1000 microstrain. This means that the deflection E between two surface points 8" apart is less than 0.2mm. Substituting $E = 0.2mm$, $L = 203.2mm$, and assuming the uncertainty of measuring the gauge length is $u_L = 1mm$,

$$u_\varepsilon == \sqrt{\left(\frac{0.004}{203.2}\right)^2 + \left(1 \cdot \frac{0.2}{203.2^2}\right)^2} = \pm 20 microstrain$$

Thus the estimated uncertainty of the optical strain sensor is about ± 20 microstrain.

Appendix D - Strain Sensor User's Manual

D.1 Introduction

D.1.1 Background Information of the Optical Strain Sensor

The Optical Strain Sensor utilizes the principle of speckle correlation to measure the subject surface strain. The major components of the system are two identical modules rigidly attached side by side by steel channels. Each of the modules emits a laser beam to the subject surface, and the reflected speckle images are captured by the cameras in the sensor. The system automatically analyzes the speckle images that are taken before and after the surface deformation to extract the strain information, and present the results to the user in real time. The sensor can operates either in hand-held or stationary state depending on the application.

D.1.2 Laser Safety

The Laser Head emits visible red light beams. The laser intensity is low and can not damage human skin. However, looking directly into the laser beam can cause injury.

- Laser medium: Diode
- Radiant Power: <5 milliwatt
- Wavelength: 632.8 nanometers

D.1.3 System and Power Requirement

- 120V/60HZ AC or 5V DC
- Windows 2000 or Windows XP
- 450 MHz Pentium III or higher

- 512 MB RAM
- USB 2.0 Port

D.1.4 System Limitation

- Dynamic range: 2mm
- Scanning rate: 5hz
- Maximum ambient temperature: 130˚F

D. 2 Installation

D.2.1 Components Checklist

- Sensor body
- USB Hub and power adapter
- USB cables

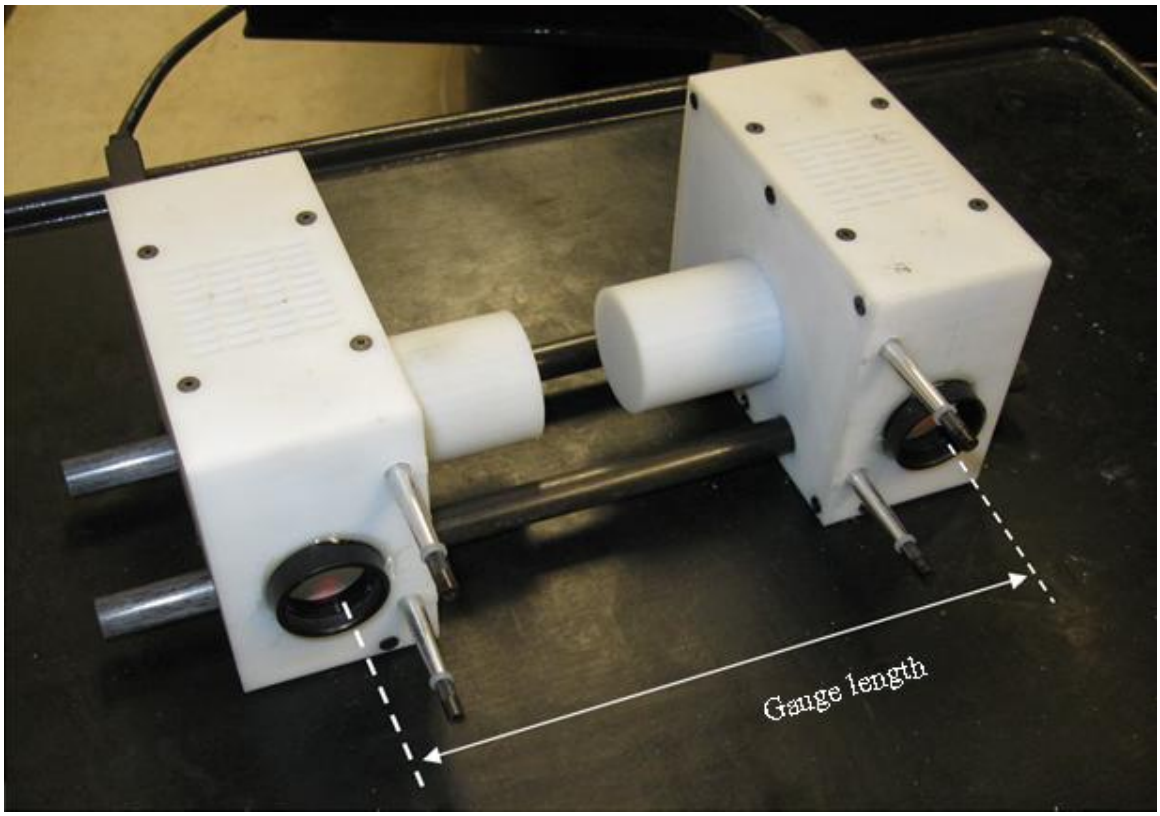

Figure D-1 Sensor body

D.2.2 Hardware Assembly

1. Cable connection

Connect the two USB cables to the two USB sockets of the sensor. The match of the USB cable and the socket is random. The connection diagram is shown in Figure 2.

Important: Do NOT plug the unconnected USB cable to the computer before installing the software.

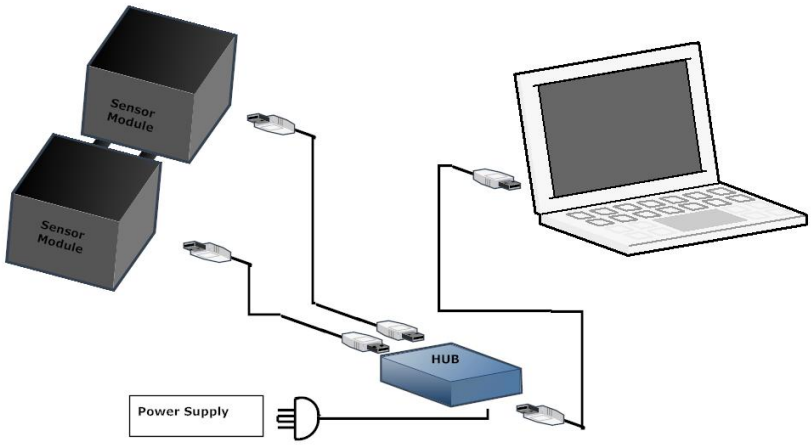

Figure D-2 Cable Connection Diagram

2. Gauge length adjustment

The gauge length of the strain sensor is equal to the distance of the two illuminated points.

The default gauge length of the strain sensor is 8 inches. The user can adjust the gauge length to meet the requirement of various applications. To change the gauge length, unscrew the 8 set screws at the bottom of the sensor, slide the sensor modules along the carbon fiber rods till the desired gauge length is achieved, tighten the 8 set screws to lock the gauge length.

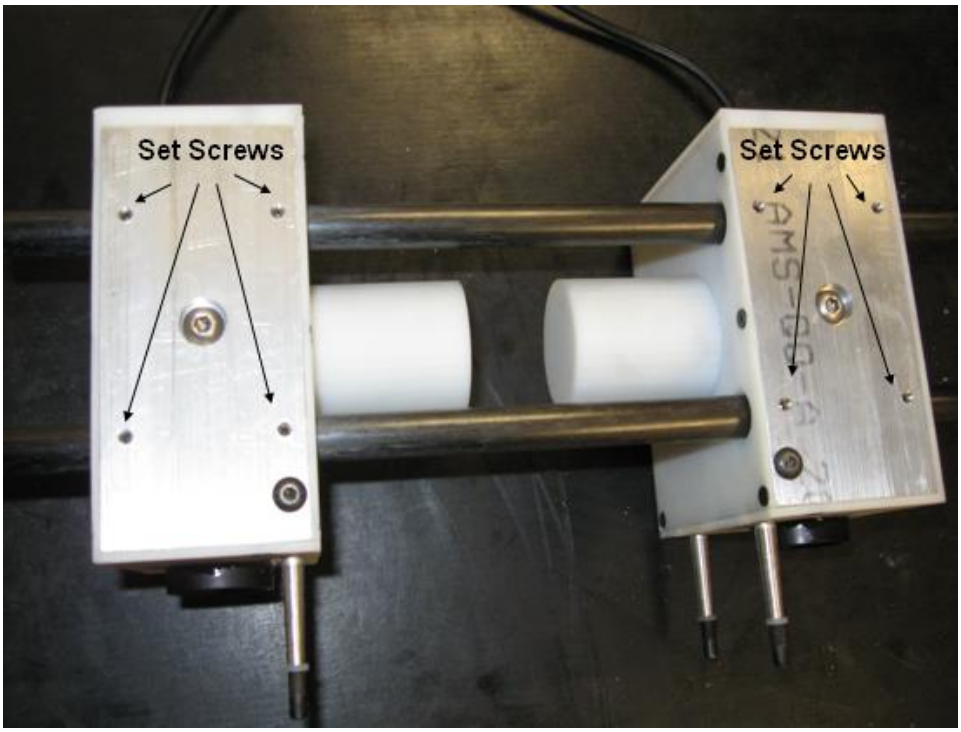

Figure D-3 Adjust gauge length

D.2.3 Installing the Software

1. Close all application software that is running and then insert the Installation CD into your CD/DVD-ROM drive.
2. Double-click on “setup.exe”.
3. Follow the onscreen prompts to install the software drivers and user application.
4. After the software has been installed, plug the power cable of the USB hub to the power supply and plug the unconnected USB cable into a free USB 2.0 High-Speed port on the computer.
5. The Window’s New Hardware Wizard will pop-up two “Lumenera Unconfigured Device” dialogs. Select “Install the software automatically” from the options that are presented to you and click Next. A warning may appear notifying you that the drivers have not been digitally signed by Microsoft. Click Continue Anyway to continue with the driver installation. Then click Finish to install the drivers. You must have administrator privileges to finish the above task.
6. Restart your computer.
7. Run the “Strain” application software from your Start\All Programs\Optical Strain Sensor menu to start the program.

D.3 Software Operation and Making Measurement

The "**Strain"** application is a program that incorporates a user-friendly interface to help users make strain measurement with the sensor, as well as manage the measurement data from multiple projects or subjects. The software's main screen is divided into 3 sections: **Camera Control, Measurement Settings and Measurement**

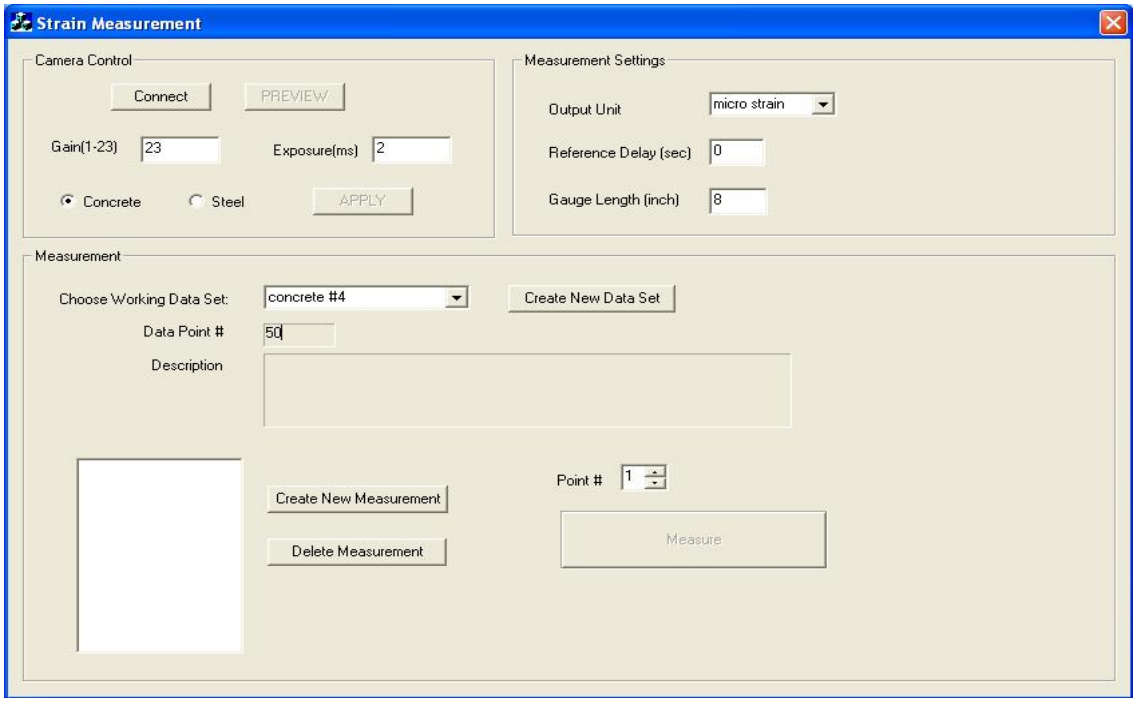

Figure D-4 Strain Application Main Window

D.3.1 Camera Control

Before measuring with the sensor, the user must configure parameters for the camera in the sensor, so that the camera can capture valid speckle images for the analysis.

The "**Connect**" button is used to initialize the strain sensor and prepare the communication between the strain sensor module and the computer.

The “**Preview**” button is used to let user see the images being captured in real- time. The two images that pop up are captured by the two modules respectively. If the images are either too dark or too bright, the user can use the controls (**Gain** and **Exposure**) that are described next to adjust accordingly. Stopping the preview can be achieved by clicking the same button.

The “**Gain**” textbox is used to set the gain value for the cameras in the strain sensor. The range of the accepted gain value is 1 to 23 in integer.

The “**Exposure**” textbox is used to set the time between the start of image capture and

the data read-out for a snapshot. The unit of the value is millisecond. If the sensor can’t obtain bright enough speckle image with the maximum available gain value, the user can increase the brightness further by increasing the Exposure time.

The “**Concrete**” radio button is used to load predefined camera settings for the subject with concrete surface.

The “**Steel**” radio button is used to load predefined camera settings for the subject with steel surface.

The “**Apply**” button is used to apply the gain value and exposure time set by the user to the strain sensor.

D.3.2 Measurement Settings

In this section, the user can configure the output unit, delay time for the initial reading, gauge length and the desired accuracy.

The “**Output Unit**” dropdown listbox is used to choose the unit of the output. The available options include “mm”, “inch”, and “micro strain”. If “mm” or “inch” is selected, the measurement output is the absolute distance change of the two illuminated points on the subject surface. If “micro strain” is selected, the output is the strain that is obtained by dividing the measured distance change by the “**Gauge Length**”.

The “**Reference Delay**” textbox is used to set the delay time during which the user can position the sensor appropriately for the initial readings. The purpose of this item will be discussed in detail in Section 3.3 of this manual.

The "**Gauge Length**" textbox is used to set the gauge length of the sensor, i.e. the distance between the two illuminated points on the subject surface.

D.3.3 Measurement

This section consists of the controls that are used to manage the application profile and conduct the measurement.

1. Clicking "**Create New Data Set**" will pop up a dialog (Figure 5) that allows the user to define new data set. There are three input fields in the dialog: "**Data Set Name**", "**Data Point Number**" and "**Description**". Alternatively the user can choose the existed data set from the dropdown list. The information of the data set created or chosen will be displayed in the "**Data Point #**" and "**Description**" textboxes in the main screen of the software.

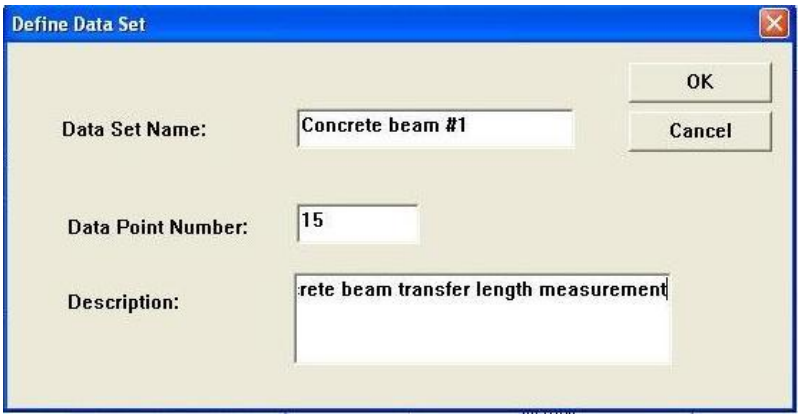

Figure C-5 Data Set Definition Dialog

2. Clicking "**Create New Measurement**" button will pop up a dialog (Figure 6) where the user can input the name of the new measurement. For example, a concrete beam might need to be inspected several times during a month. Before starting each round of the inspection, a new measurement needs to be created.

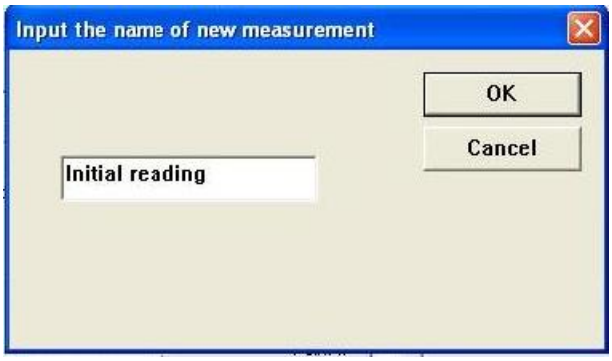

Figure D-6 Define the Name of New Measurement

3. Position the sensor on the subject surface where the user desires to make strain measurement, as shown in Figure 7. Mark a half circle around the edges of the top contact points.

Figure D-7 Making Measurement

4. Click the “Measure” button to start making the readings.

For the initial readings, the programs will wait a period before making the actual reading. The duration of the waiting time is defined in the “**Reference Delay**” in “M**easurement Settings”** section. During this period, the user can align the sensor to the marks that the user

makes in Step 3. When the delay time is over, the initial reading will be made and the sound of “ding” is played.

For the readings other than the initial readings, try to align the sensor to the same marks while the program continuously scans the subject surface. Wiggle the sensor to facilitate the scanning process. When the program detects a correlation, the measurement will be made automatically. A “ding” sound will be played and the measurement result will be displayed on the screen.

After the measurement on the current point is made, the spin button **“Point #**” will increment automatically, proceeding to the measurement of the next point. Repeat step 4.

Appendix E - Source code

Strain.cpp

```
#include "stdafx.h"
#include "Strain.h"
#include "StrainDlg.h"

#ifdef _DEBUG
#define new DEBUG_NEW
#undef THIS_FILE
static char THIS_FILE[] = __FILE__;
#endif


BEGIN_MESSAGE_MAP(CStrainApp, CWinApp)
	//{{AFX_MSG_MAP(CStrainApp)
	//}}AFX_MSG
	ON_COMMAND(ID_HELP, CWinApp::OnHelp)
END_MESSAGE_MAP()
CStrainApp::CStrainApp()
{
}
CStrainApp theApp;
BOOL CStrainApp::InitInstance()
{
	AfxEnableControlContainer();
	// Standard initialization
#ifdef _AFXDLL
	Enable3dControls();			// Call this when using MFC in a shared DLL
#else
	Enable3dControlsStatic(); // Call this when linking to MFC statically
#endif
	CStrainDlg dlg;
	m_pMainWnd = &dlg;
```

```
	int nResponse = dlg.DoModal();
	if (nResponse == IDOK)
	{
	}
	else if (nResponse == IDCANCEL)
	{
	}
	// Since the dialog has been closed, return FALSE so that we exit the
	//  application, rather than start the application's message pump.
	return FALSE;
}
```

StrainDlg.h

```
#if !defined(AFX_STRAINDLG_H__235F11AA_4538_4BD7_88AA_66E784050B55__INCLUDED_)
#define AFX_STRAINDLG_H__235F11AA_4538_4BD7_88AA_66E784050B55__INCLUDED_

#if _MSC_VER > 1000
#pragma once
#endif // _MSC_VER > 1000

#include "lucamapi.h"
#include "lucamsci.h"
#include "SnapPreviewDlg.h"
#include <stdio.h>
#include <stdlib.h>
#include "cv.h"
#include "highgui.h"
#include "fftw3.h"
#include "math.h"
#include <iostream>
#include <windows.h>
#include <mmsystem.h>
#include <direct.h>
#include <io.h>
#include <afxtempl.h>
#include "UIDialog.h"
```

```
#pragma comment(lib,"Winmm.lib")
#define CAMNUM 2

#define bs 384
#define cutoff 60
#define MatchTempType CV_TM_CCOEFF_NORMED

class CStrainDlg : public CDialog
{
// Construction
public:
BOOL CalibrationReadingSpeckle(double *subxL,double *subyL,double *subxR,double *subyR);
BOOL TakeInitialReading();
void MultipleMinLoc( IplImage *image, CvPoint location[]);
void MultipleMaxLoc( IplImage *image, CvPoint location[] );
void MinLoc( IplImage *image, double &min, CvPoint &location );
void MaxLoc( IplImage *image, double &max, CvPoint &location );
BOOL Blurcheck(IplImage *img1, IplImage *img2);
BOOL oldsensor;
void AdaptiveHist(IplImage *input, IplImage *output);
void PreProcess(IplImage *input, IplImage *output);
void Subpixel(IplImage *in, double *x, double *y, int factor);
void ShowImage(IplImage *img);

void filterproduct(IplImage* img, CvMat* filter,IplImage* productimg);
void      INTfilter(IplImage* img, CvMat* filter,IplImage* productimg, int shiftx,int shifty);
void converttofloat(IplImage* img, CvMat* filter,IplImage* productimg, int shiftx,int shifty);

BOOL Measure();
CString measurementname;
CString datasetname;
CStdioFile File;
int datapointnumber;
CStrainDlg(CWnd* pParent = NULL);         // standard constructor
CSnapPreviewDlg *m_dlgSnap;
```

```
// Dialog Data
//{{AFX_DATA(CStrainDlg)
enum { IDD = IDD_STRAIN_DIALOG };
CStatic   m_refname;
CColorListBox    m_measurementlist;
CButton m_CalibrateIntensity;
CSpinButtonCtrl  m_Spin;
CButton m_cbRound;
CStatic   m_path;
CButton m_cbLock;
CButton m_cbApply;
float      m_exposure;
float   m_exposureA;
float   m_exposureB;
float      m_gain;
CButton m_cbConnect;
CButton m_cbPreview;
CButton m_cbMeasure;
int                m_round;
CString  m_DataSetList;
int                m_accuracy;
int                m_delay;
double   m_gl;
int                m_surfacetype;
BOOL    m_invert;
int                m_configurationtype;
int                m_duration;
//}}AFX_DATA

// ClassWizard generated virtual function overrides
//{{AFX_VIRTUAL(CStrainDlg)
protected:
virtual void DoDataExchange(CDataExchange* pDX);          // DDX/DDV support
virtual void PostNcDestroy();
//}}AFX_VIRTUAL

// Implementation
```

```
protected:
int ref_index;
void CreateLargeHanning(int M,int N,CvMat* filter);
void phase_correlation_block(fftwf_complex *fft1, fftwf_complex *fft2, IplImage *poc);
double thresholdhalf;
double THRESHOLD;
double concrete_threshold1,concrete_threshold2,steel_threshold1,steel_threshold2;
int start_x,start_y;
float deflection;
CWinThread *pThread;
void fftwcopy(fftwf_complex* source ,fftwf_complex* target , int size);
BOOL m_bStop;
void cvShiftDFT(CvArr * src_arr, CvArr * dst_arr );
int height,half_height;
int width,half_width;
fftwf_plan ifft_res;
fftwf_plan fft_img2;
fftwf_plan fft_img1;
fftwf_plan ifft_res_halfsize;
fftwf_plan fft_img2_halfsize;
fftwf_plan fft_img1_halfsize;
fftwf_complex *res_fft;
fftwf_complex *img2_fft;
fftwf_complex *img1_fft;
fftwf_complex  *res;
fftwf_complex  *img2;
fftwf_complex *img1;
double p1,p2,p3,p4;
double g1,g2,g3,g4,g5;
double gbb1,gbb2,gbb3,gbb4,gbb5;
fftwf_complex *res_fft_half;
fftwf_complex *img2_fft_half;
fftwf_complex *img1_fft_half,*img1_fft_halfL,*img1_fft_halfR;
float *res_half;
float *img2_half;
float *img1_half;
void phase_correlation( IplImage *ref, IplImage *tpl, IplImage *poc );
```

```
void phase_correlation_halfsize( IplImage *ref, IplImage *tpl, IplImage *poc );
void upsampling(CvArr* in, int factor, int roff, int coff,CvArr* out,int N );
CString m_strPath;
LUCAM_SNAPSHOT lsSettings;
BOOL m_bLocked;
void CleanUp();
HICON m_hIcon;
BOOL CreateHanning(int M, int N,CvMat* filter,BOOL flag, int d);
CvMat* hanningfilter;
CvMat* blockfilter;
HANDLE hCameras[CAMNUM];
LUCAM_SNAPSHOT *pParams[CAMNUM];  // Array of ptrs to the param struct
LUCAM_SNAPSHOT params[CAMNUM];
UCHAR *ppFrames[CAMNUM];  // Array of pointers to frames;
UCHAR *pAllFrames;
BYTE *pBmpBuffer;
HANDLE hSynchronousSnapshots;
HANDLE m_hCameraA,m_hCameraB;
BOOL m_bConnected;
BOOL m_bPreviewing;
BOOL m_bSnapping;
LUCAM_FRAME_FORMAT m_lffFormat;
CFileFind f;
CString cRefFilenameL,cRefFilenameR;
float m_fFrameRate;
clock_t m_tStartTime;
clock_t m_tEndTime;
clock_t dElapsed;

// Generated message map functions
//{{AFX_MSG(CStrainDlg)
virtual BOOL OnInitDialog();
afx_msg void OnPaint();
afx_msg HCURSOR OnQueryDragIcon();
afx_msg void OnButtonConnect();
afx_msg void OnButtonPreview();
afx_msg void OnClose();
```

```
afx_msg void OnButtonApply();
afx_msg void OnButtonSetfolder();
afx_msg void OnButtonMeasure();
afx_msg void OnButtonLock();
afx_msg void OnButtonStop();
afx_msg void OnCreateDataSet();
afx_msg void OnEditchangeDataSetList();
afx_msg void OnSelchangeDataSetList();
afx_msg void OnNewMeasurement();
afx_msg void OnDeleteMeasurement();
afx_msg void OnSelchangeMeasurementList();
afx_msg void OnConcrete();
afx_msg void OnSteel();
afx_msg void OnOpendatafile();
afx_msg void OnCalibrateIntensity();
afx_msg void OnSetreference();
afx_msg void OnCalibration();
//}}AFX_MSG
DECLARE_MESSAGE_MAP()

private:
void UpdateMeasurementList();
CString defaultfolder;
CMessageDialog MessageDlg;
};

#endif // !defined(AFX_STRAINDLG_H__235F11AA_4538_4BD7_88AA_66E784050B55__INCLUDED_)
```

StrainDlg.cpp

```
#include "stdafx.h"
#include "Strain.h"
#include "StrainDlg.h"

#ifdef _DEBUG
#define new DEBUG_NEW
```

```
#undef THIS_FILE
static char THIS_FILE[] = __FILE__;
#endif

CStrainDlg::CStrainDlg(CWnd* pParent /*=NULL*/)
: CDialog(CStrainDlg::IDD, pParent)
{
//{{AFX_DATA_INIT(CStrainDlg)
m_exposure = 1.0f;
m_gain = 23.0f;
m_round = -1;
m_DataSetList = _T("");
m_accuracy = -1;
m_delay = 0;
m_gl = 0.0;
m_duration=3;
m_surfacetype = 0;
m_invert = FALSE;
m_configurationtype=0;
m_pointnumber = 0;
m_configurationtype = -1;
m_duration = 0;
//}}AFX_DATA_INIT
m_hIcon = AfxGetApp()->LoadIcon(IDR_MAINFRAME);
}

void CStrainDlg::DoDataExchange(CDataExchange* pDX)
{
CDialog::DoDataExchange(pDX);
//{{AFX_DATA_MAP(CStrainDlg)
DDX_Control(pDX, IDC_REFNAME, m_refname);
DDX_Control(pDX, IDC_MeasurementList, m_measurementlist);
DDX_Control(pDX, IDC_CalibrateIntensity, m_CalibrateIntensity);
DDX_Control(pDX, IDC_SPIN, m_Spin);
DDX_Control(pDX, IDC_ROUND1, m_cbRound);
DDX_Control(pDX, IDC_PATH, m_path);
DDX_Control(pDX, IDC_LOCK, m_cbLock);
DDX_Control(pDX, IDC_APPLY, m_cbApply);
```

```
DDX_Text(pDX, IDC_EXPOSURE, m_exposure);
DDX_Text(pDX, IDC_GAIN, m_gain);
DDX_Control(pDX, IDC_CONNECT, m_cbConnect);
DDX_Control(pDX, IDC_PREVIEW, m_cbPreview);
DDX_Control(pDX, IDC_MEASURE, m_cbMeasure);
DDX_Radio(pDX, IDC_ROUND1, m_round);
DDX_CBString(pDX, IDC_DataSetList, m_DataSetList);
DDX_Radio(pDX, IDC_ACCURACY, m_accuracy);
DDX_Text(pDX, IDC_DELAY, m_delay);
DDX_Text(pDX, IDC_GL, m_gl);
DDX_Radio(pDX, IDC_Speckle, m_surfacetype);
DDX_Check(pDX, IDC_INVERT, m_invert);
DDX_Radio(pDX, IDC_NORMCONFIG, m_configurationtype);
DDX_Text(pDX, IDC_POINTNUMBER, m_pointnumber);
DDX_Text(pDX, IDC_Duration, m_duration);
//}}AFX_DATA_MAP
}

BEGIN_MESSAGE_MAP(CStrainDlg, CDialog)
//{{AFX_MSG_MAP(CStrainDlg)
ON_WM_PAINT()
ON_WM_QUERYDRAGICON()
ON_BN_CLICKED(IDC_CONNECT, OnButtonConnect)
ON_BN_CLICKED(IDC_PREVIEW, OnButtonPreview)
ON_WM_CLOSE()
ON_BN_CLICKED(IDC_APPLY, OnButtonApply)
ON_BN_CLICKED(IDC_SETFOLDER, OnButtonSetfolder)
ON_BN_CLICKED(IDC_MEASURE, OnButtonMeasure)
ON_BN_CLICKED(IDC_LOCK, OnButtonLock)
ON_BN_CLICKED(IDC_STOP, OnButtonStop)
ON_BN_CLICKED(IDC_CreateDataSet, OnCreateDataSet)
ON_CBN_EDITCHANGE(IDC_DataSetList, OnEditchangeDataSetList)
ON_CBN_SELCHANGE(IDC_DataSetList, OnSelchangeDataSetList)
ON_BN_CLICKED(IDC_BUTTON2, OnNewMeasurement)
ON_BN_CLICKED(IDC_DeleteMeasurement, OnDeleteMeasurement)
ON_LBN_SELCHANGE(IDC_MeasurementList, OnSelchangeMeasurementList)
ON_BN_CLICKED(IDC_Concrete, OnConcrete)
ON_BN_CLICKED(IDC_STEEL, OnSteel)
```

```
ON_BN_CLICKED(IDC_OPENDATAFILE, OnOpendatafile)
ON_BN_CLICKED(IDC_CalibrateIntensity, OnCalibrateIntensity)
ON_BN_CLICKED(IDC_SETREFERENCE, OnSetreference)
ON_BN_CLICKED(IDC_Calibration, OnCalibration)
//}}AFX_MSG_MAP
END_MESSAGE_MAP()

/////////////////////////////////////////////////////////////////////////////
// CStrainDlg message handlers

BOOL CStrainDlg::OnInitDialog()
{
CDialog::OnInitDialog();



m_surfacetype=0;
m_configurationtype=0;

SetIcon(m_hIcon, TRUE);
SetIcon(m_hIcon, FALSE);

CButton* pRB = (CButton*) GetDlgItem(IDC_ACCURACY);
pRB->SetWindowText("5 ¦ÌStrain");
pRB = (CButton*) GetDlgItem(IDC_ACCURACY2);
pRB->SetWindowText("10 ¦ÌStrain");
pRB = (CButton*) GetDlgItem(IDC_ACCURACY3);
pRB->SetWindowText("25 ¦ÌStrain");
pRB->SetCheck(BST_CHECKED);
CButton* pCBmode = (CButton*) GetDlgItem(IDC_HANDHOLD);
pCBmode->SetCheck(BST_CHECKED);
pRB = (CButton*) GetDlgItem(IDC_Concrete);
pRB->SetCheck(BST_CHECKED);
CStrainDlg::OnConcrete();

CComboBox* pCBunit = (CComboBox*) GetDlgItem(IDC_UNIT);
pCBunit->SetCurSel(1);
m_gl=7.125;
m_duration=3;
```

```
CEdit* pEgl = (CEdit*) GetDlgItem(IDC_GL);
pEgl->SetWindowText("8");
m_bStop=0;
m_Spin.SetRange(1, 50);
m_Spin.SetPos(1);

m_hCameraA = NULL;
m_hCameraB = NULL;
m_bConnected = FALSE;
m_bPreviewing = FALSE;
m_bSnapping = FALSE;
m_cbPreview.EnableWindow(FALSE);
m_cbMeasure.EnableWindow(FALSE);
m_CalibrateIntensity.EnableWindow(FALSE);
m_cbApply.EnableWindow(FALSE);
m_cbLock.EnableWindow(FALSE);
TCHAR szDirectory[MAX_PATH] = "";
GetCurrentDirectory(sizeof(szDirectory) - 1, szDirectory);
m_strPath=szDirectory;
m_path.SetWindowText(szDirectory);
m_dlgSnap = new CSnapPreviewDlg;
m_dlgSnap->Create(IDD_DIALOG_SNAP_PREVIEW);
defaultfolder="C:\\Program Files\\Strain\\Data";
if (_access(defaultfolder,0)==-1)
{
CreateDirectory(defaultfolder, 0);
}
SetCurrentDirectory(defaultfolder);
CComboBox* pCB = (CComboBox*) GetDlgItem(IDC_DataSetList
);
CStringArray folders;
CFileFind finder;
BOOL bWorking = finder.FindFile(defaultfolder+"\\*.*");
while (bWorking)
{
bWorking = finder.FindNextFile();
if (finder.IsDirectory() && !finder.IsDots())
```

```
folders.Add(finder.GetFilePath());
}
// now cycle through the array
for (int i=0; i<folders.GetSize(); i++)
{

pCB->InsertString(-1, folders[i].Right(folders[i].GetLength()-defaultfolder.GetLength()-1));
}
int nCount = pCB->GetCount();
if (nCount > 0)
{
pCB->SetCurSel(nCount-1);
OnSelchangeDataSetList();
}
UpdateData(FALSE);
return TRUE;  // return TRUE  unless you set the focus to a control
}
void CStrainDlg::OnPaint()
{
if (IsIconic())
{
CPaintDC dc(this); // device context for painting
SendMessage(WM_ICONERASEBKGND, (WPARAM) dc.GetSafeHdc(), 0);
// Center icon in client rectangle
int cxIcon = GetSystemMetrics(SM_CXICON);
int cyIcon = GetSystemMetrics(SM_CYICON);
CRect rect;
GetClientRect(&rect);
int x = (rect.Width() - cxIcon + 1) / 2;
int y = (rect.Height() - cyIcon + 1) / 2;
// Draw the icon
dc.DrawIcon(x, y, m_hIcon);
}
else
{
CDialog::OnPaint();
}
```

```
}

HCURSOR CStrainDlg::OnQueryDragIcon()
{
return (HCURSOR) m_hIcon;
}
void CStrainDlg::OnButtonConnect()
{
CString csTemp;
int iCamera;
if (!m_bConnected)
{
iCamera=1;
m_hCameraA = LucamCameraOpen(iCamera);
m_hCameraB = LucamCameraOpen(iCamera+1);
LONG numCameras = LucamNumCameras();
LUCAM_VERSION pVersionsArray[20];
ULONG tt = LucamEnumCameras(pVersionsArray, numCameras);
if (pVersionsArray[0].serialnumber>pVersionsArray[1].serialnumber)
{
HANDLE swap;
swap=m_hCameraA;
m_hCameraA=m_hCameraB;
m_hCameraB=swap;
}
if ((m_hCameraA != NULL) && (m_hCameraB != NULL))
{
// Now connected to the camera
if (!LucamSetProperty(m_hCameraA, LUCAM_PROP_EXPOSURE, m_exposure, 0)) AfxMessageBox("Unable to
set exposure value.");
if (!LucamSetProperty(m_hCameraA, LUCAM_PROP_GAIN, m_gain, 0))  AfxMessageBox("Unable to set gain
value.");


if (!LucamSetProperty(m_hCameraB, LUCAM_PROP_EXPOSURE, m_exposure, 0)) AfxMessageBox("Unable to
set exposure value.");
```

```
if (!LucamSetProperty(m_hCameraB, LUCAM_PROP_GAIN, m_gain, 0))  AfxMessageBox("Unable to set gain
value.");
m_bConnected = TRUE;
m_cbConnect.SetWindowText(_T("Disconnect"));
m_cbPreview.EnableWindow(TRUE);
m_cbPreview.SetWindowText(_T("Preview"));
m_cbMeasure.EnableWindow(TRUE);
m_cbApply.EnableWindow(TRUE);
m_CalibrateIntensity.EnableWindow(TRUE);
if (!LucamGetFormat(m_hCameraA, &m_lffFormat, &m_fFrameRate))
{
MessageBox("Unable to get camera video format. Capture frames may not work properly.", "Get Fromat", MB_OK);
}
height=m_lffFormat.height;
width=m_lffFormat.width;
half_height=height/2;
half_width=width/2;
start_y=height/2-bs/2;
start_x=width/2-bs/2;
blockfilter = cvCreateMat(bs,bs,CV_32FC1);
CreateHanning(bs,bs,blockfilter,1,bs);
float fvar;
CStdioFile ppFile;
if ((pVersionsArray[0].serialnumber==30052108) &&  (pVersionsArray[1].serialnumber==30052152))
{
oldsensor=0;
if (ppFile.Open("C:\\Program Files\\Strain\\parameter_new sensor.txt", CFile::modeRead) != TRUE)
{

AfxMessageBox("Failed to load parameter file");
}
}
if ((pVersionsArray[0].serialnumber==30052090) &&  (pVersionsArray[1].serialnumber==30052184))
{
oldsensor=1;
if (ppFile.Open("C:\\Program Files\\Strain\\parameter_old sensor.txt", CFile::modeRead) != TRUE)
{
```

```
AfxMessageBox("Failed to load parameter file");
}
}
ppFile.SeekToBegin();
int cc=0;
CString tempString;
while(ppFile.ReadString(tempString) != FALSE)
{
fvar = (float) atof(tempString);
cc++;

switch(cc){
case 1: THRESHOLD=fvar;break;
case 2:thresholdhalf=fvar;break;
case 3:THRESHOLD_glass=fvar;break;
case 4: p1=fvar   ;break;
case 5: p2=fvar    ;break;
case 6:     p3=fvar   ;break;
case 7: p4=fvar   ; break;
case 8: g1=fvar   ;break;
case 9: g2=fvar    ;break;
case 10:    g3=fvar   ;break;
case 11: g4=fvar  ; break;
case 12: g5=fvar  ; break;

}

}
ppFile.Close();
img1_fft = ( fftwf_complex* )fftwf_malloc ( sizeof ( fftwf_complex ) * bs *
bs );
img2_fft =( fftwf_complex* ) fftwf_malloc ( sizeof ( fftwf_complex ) * bs *
bs );
res_fft =( fftwf_complex* ) fftwf_malloc ( sizeof ( fftwf_complex ) * bs *
bs);
img1 = ( fftwf_complex* )fftwf_malloc( sizeof( fftwf_complex ) * bs * bs );
img2 = ( fftwf_complex* )fftwf_malloc( sizeof( fftwf_complex ) * bs * bs );
res = ( fftwf_complex* )fftwf_malloc( sizeof( fftwf_complex ) * bs * bs );
```

```
img1_half=(float*) malloc ( sizeof ( float ) * bs * bs );
img1_fft_half = ( fftwf_complex* )fftwf_malloc ( sizeof ( fftwf_complex ) *
bs * (bs/2+1) );
img1_fft_halfL = ( fftwf_complex* )fftwf_malloc ( sizeof ( fftwf_complex ) *
bs * (bs/2+1) );
img1_fft_halfR = ( fftwf_complex* )fftwf_malloc ( sizeof ( fftwf_complex ) *
bs * (bs/2+1) );
img2_half =(float*) malloc ( sizeof ( float ) * bs * bs );
img2_fft_half =( fftwf_complex* ) fftwf_malloc ( sizeof ( fftwf_complex ) *
bs * (bs/2+1) );
res_half =(float*) malloc ( sizeof ( float ) * bs*bs );
res_fft_half =( fftwf_complex* ) fftwf_malloc ( sizeof ( fftwf_complex ) * bs
* (bs/2+1) );
FILE *planfile;
planfile= fopen( "plan.wisdom", "r" ) ;
if (planfile!=NULL)
{
fftwf_import_wisdom_from_file(planfile);
fclose(planfile);
}
fft_img1_halfsize = fftwf_plan_dft_r2c_2d( bs, bs, img1_half, img1_fft_half,
FFTW_ESTIMATE);
fft_img2_halfsize = fftwf_plan_dft_r2c_2d( bs, bs, img2_half, img2_fft_half,
FFTW_ESTIMATE);
ifft_res_halfsize = fftwf_plan_dft_c2r_2d( bs, bs, res_fft_half,res_half,
FFTW_ESTIMATE);

fft_img1 = fftwf_plan_dft_2d( bs, bs, img1, img1_fft,  FFTW_FORWARD,
FFTW_ESTIMATE);
fft_img2 = fftwf_plan_dft_2d( bs, bs, img2, img2_fft,  FFTW_FORWARD,
FFTW_ESTIMATE );
ifft_res = fftwf_plan_dft_2d( bs, bs, res_fft,res,
FFTW_BACKWARD,FFTW_ESTIMATE);
planfile= fopen( "plan.wisdom", "w" ) ;
if (planfile!=NULL)
{
fftwf_export_wisdom_to_file(planfile);
fclose(planfile);
```

```
}
}
else
{
MessageBox("Unable to connect to the camera.", "Connect", MB_OK);
}
}
else
{
if (m_bSnapping)
{
if (IDYES == AfxMessageBox("Currently running snapshot captures. Do you wish
to stop?", MB_YESNOCANCEL))
{
Sleep(1000);
}
else return;
}
if (m_bPreviewing)
{
}
if (!LucamCameraClose(m_hCameraA) && !LucamCameraClose(m_hCameraB))
{
MessageBox("Unable to disconnect to the camera. Closing application.",
"Disconnect", MB_OK);
}
else
{
m_bConnected = FALSE;
m_hCameraA = NULL;
m_hCameraB = NULL;
m_lffFormat.height = 0;
m_lffFormat.width = 0;
m_cbConnect.SetWindowText(_T("Connect"));
m_cbPreview.EnableWindow(FALSE);
m_cbPreview.SetWindowText(_T("Preview"));
m_cbMeasure.EnableWindow(FALSE);
m_cbApply.EnableWindow(FALSE);
```

```
}
}
OnEditchangeDataSetList() ;
}
void CStrainDlg::OnButtonPreview()
{
if (!m_bPreviewing)
{
FLOAT m_Lum;
LONG flags;
BOOL rt;
FLOAT m_Exp=2.0f;
m_Lum=60.0f;
flags = LUCAM_PROP_FLAG_AUTO;

rt = LucamSetProperty(m_hCameraA, LUCAM_PROP_EXPOSURE, m_Exp, flags);
if (!LucamSetProperty(m_hCameraA, LUCAM_PROP_AUTO_EXP_TARGET, m_Lum, flags))
{
MessageBox("Failed to set exposure target.");
}
flags = LUCAM_PROP_FLAG_AUTO;

rt = LucamSetProperty(m_hCameraB, LUCAM_PROP_EXPOSURE, m_Exp, flags);
if (!LucamSetProperty(m_hCameraB, LUCAM_PROP_AUTO_EXP_TARGET, m_Lum, flags))
{
MessageBox("Failed to set exposure target.");
}

if (LucamCreateDisplayWindow(m_hCameraA, "Preview A",
WS_OVERLAPPEDWINDOW|WS_VISIBLE, 0, 200, 640, 480, NULL, NULL)  &&
LucamCreateDisplayWindow(m_hCameraB, "Preview B",
WS_OVERLAPPEDWINDOW|WS_VISIBLE, 500, 300, 640, 480, NULL, NULL))
{
if (LucamStreamVideoControl(m_hCameraA, START_DISPLAY, NULL) &&
LucamStreamVideoControl(m_hCameraB, START_DISPLAY, NULL))
{
m_bPreviewing = TRUE;
m_cbPreview.EnableWindow(TRUE);
```

```
m_cbPreview.SetWindowText(_T("Stop"));
m_cbMeasure.EnableWindow(FALSE);
}
else
{
MessageBox("Unable start previewing video.", "Start Preview", MB_OK);
LucamDestroyDisplayWindow(m_hCameraA);
LucamDestroyDisplayWindow(m_hCameraB);
}
}
else
MessageBox("Unable create preview window.", "Start Preview", MB_OK);
}
else
{
// Stop the preview
if (LucamStreamVideoControl(m_hCameraA, STOP_STREAMING, NULL) &&
LucamStreamVideoControl(m_hCameraB, STOP_STREAMING, NULL))
{
m_cbPreview.EnableWindow(TRUE);
m_cbPreview.SetWindowText(_T("Preview"));
m_cbMeasure.EnableWindow(TRUE);
}
else
MessageBox("Unable STOP previewing video.", "Stop Preview", MB_OK);
LucamDestroyDisplayWindow(m_hCameraA);
LucamDestroyDisplayWindow(m_hCameraB);
m_bPreviewing = FALSE;
}
}
void CStrainDlg::CleanUp()
{
cvReleaseMat(&blockfilter);
if (m_bPreviewing)
{
if (IDYES == AfxMessageBox("Currently previewing. Do you wish to stop?",
MB_YESNOCANCEL)) OnButtonPreview();
else return;
```

```
}
if (m_hCameraA != NULL)
LucamCameraClose(m_hCameraA);
if (m_hCameraB != NULL)
LucamCameraClose(m_hCameraB);
if (img1_half != NULL)
{
fffwf_destroy_plan( fft_img1 );
fftwf_destroy_plan( fft_img2 );
fftwf_destroy_plan( ifft_res );
fftwf_destroy_plan( fft_img1_halfsize );
fftwf_destroy_plan( fft_img2_halfsize );
fftwf_destroy_plan( ifft_res_halfsize );
fftwf_free(img1);
fftwf_free(img2);
fftwf_free(res);
fftwf_free( img1_fft );
fftwf_free( img2_fft );
fftwf_free( res_fft );
fftwf_free(img1_fft_halfL);
fftwf_free(img1_fft_halfR);
free(img1_half);
free(img2_half);
free(res_half);
fftwf_free( img1_fft_half );
fftwf_free( img2_fft_half );
fftwf_free( res_fft_half );
}
if (File.m_hFile == CFile::hFileNull)
File.Close();
}
void CStrainDlg::OnClose()
{
CDialog::OnClose();
}

void CStrainDlg::OnButtonApply()
{
```

```
UpdateData(TRUE);
if (m_gain > 23 || m_gain < 0.1 || m_exposure < 0.001 )  return;

if (m_bPreviewing)
{
if (!LucamStreamVideoControl(m_hCameraA, STOP_STREAMING, NULL)
&& !LucamStreamVideoControl(m_hCameraB, STOP_STREAMING, NULL))
{
MessageBox("Unable to Apply.", "Update", MB_OK);
return;
}
LucamDestroyDisplayWindow(m_hCameraA);
LucamDestroyDisplayWindow(m_hCameraB);
}

if (!LucamSetProperty(m_hCameraA, LUCAM_PROP_EXPOSURE, m_exposure, 0))
AfxMessageBox("Unable to set exposure value.");

if (!LucamSetProperty(m_hCameraA, LUCAM_PROP_GAIN, m_gain, 0))
AfxMessageBox("Unable to set gain value.");

if (!LucamSetProperty(m_hCameraB, LUCAM_PROP_EXPOSURE, m_exposure, 0))
AfxMessageBox("Unable to set exposure value.");

if (!LucamSetProperty(m_hCameraB, LUCAM_PROP_GAIN, m_gain, 0))
AfxMessageBox("Unable to set gain value.");



}
void CStrainDlg::OnButtonSetfolder()
{
BROWSEINFO   browse;
ZeroMemory(&browse,sizeof(browse));
browse.hwndOwner   =   NULL;
browse.pszDisplayName   =   m_strPath.GetBuffer(MAX_PATH);
browse.lpszTitle   =   "Please select a folder";
LPITEMIDLIST   lpItem   =   SHBrowseForFolder(&browse);
if(lpItem   ==   NULL)   return   ;
```

```
m_strPath.ReleaseBuffer();
if(SHGetPathFromIDList(lpItem,m_strPath.GetBuffer(MAX_PATH))   ==   false)
return;
m_path.SetWindowText(m_strPath);
m_strPath.ReleaseBuffer();
}
void CStrainDlg::OnButtonMeasure()
{
UpdateData(TRUE);
b_keepgoing=TRUE;
if    ((m_measurementlist.GetSel(0)>0) && (m_measurementlist.GetCount()>1))
{
if (IDNO==AfxMessageBox("You are going to resume or retake the reference
image shots. Proceed?", MB_YESNO))
return;
}
pThread=AfxBeginThread(RUNTIME_CLASS(CUIThread));
while(b_keepgoing==TRUE)
{
b_redo=FALSE;
m_Spin.SetPos(m_pointnumber);
UpdateData(TRUE);
Measure();
pThread->PostThreadMessage(WM_CLOSEDIALOG,NULL,NULL);
Sleep(100);
if (m_pointnumber==datapointnumber && b_redo==FALSE)
{
break;
}
if (b_redo==FALSE && b_keepgoing==TRUE)
m_pointnumber++;
}
}
void CStrainDlg::OnButtonLock()
{
UpdateData(TRUE);
if (m_bLocked==1)
{
```

```
m_bLocked=0;
m_cbLock.SetWindowText(_T("Lock"));
GetDlgItem(IDC_ROUND1)->EnableWindow(TRUE);
GetDlgItem(IDC_ROUND2)->EnableWindow(TRUE);
GetDlgItem(IDC_ROUND3)->EnableWindow(TRUE);
GetDlgItem(IDC_ROUND4)->EnableWindow(TRUE);
GetDlgItem(IDC_ROUND5)->EnableWindow(TRUE);
GetDlgItem(IDC_ROUND6)->EnableWindow(TRUE);

}
else if (m_round>=0 && m_round<=5)
{
m_bLocked=1;
//m_cbRound.EnableWindow(FALSE);
m_cbLock.SetWindowText(_T("Unlock"));
GetDlgItem(IDC_ROUND1)->EnableWindow(FALSE);
GetDlgItem(IDC_ROUND2)->EnableWindow(FALSE);
GetDlgItem(IDC_ROUND3)->EnableWindow(FALSE);
GetDlgItem(IDC_ROUND4)->EnableWindow(FALSE);
GetDlgItem(IDC_ROUND5)->EnableWindow(FALSE);
GetDlgItem(IDC_ROUND6)->EnableWindow(FALSE);
switch(m_round)
{
case 0:
GetDlgItem(IDC_ROUND1)->EnableWindow(TRUE);
break;
case 1:
GetDlgItem(IDC_ROUND2)->EnableWindow(TRUE);
break;
case 2:
GetDlgItem(IDC_ROUND3)->EnableWindow(TRUE);
break;
case 3:
GetDlgItem(IDC_ROUND4)->EnableWindow(TRUE);
break;
case 4:
GetDlgItem(IDC_ROUND5)->EnableWindow(TRUE);
break;
```

```
case 5:
GetDlgItem(IDC_ROUND6)->EnableWindow(TRUE);
break;
}

}
}
void CStrainDlg::phase_correlation(IplImage *ref, IplImage *tpl, IplImage
*poc)
{
int   i, j, k;
float tmp;
int width    = ref->width;
int height   = ref->height;
int step     = ref->widthStep;
int fft_size = width * height;
float       *ref_data = ( float* ) ref->imageData;
float       *tpl_data = ( float* ) tpl->imageData;
float       *poc_data = ( float* )poc->imageData;
for( i = 0, k = 0 ; i < height ; i++ ) {
for( j = 0 ; j < width ; j++, k++ ) {
img1[k][0]= ref_data[k];
img1[k][1]=0;
img2[k][0] = tpl_data[k];
img2[k][1]=0;
}
}

fftwf_execute( fft_img1 );
fftwf_execute( fft_img2 );
// obtain the cross power spectrum
for( i = 0; i < height * width ; i++ ) {
res_fft[i][0] = ( img2_fft[i][0] * img1_fft[i][0] ) - ( img2_fft[i][1] * ( -
img1_fft[i][1] ) );
res_fft[i][1] = ( img2_fft[i][0] * ( -img1_fft[i][1] ) ) + ( img2_fft[i][1] *
img1_fft[i][0] );
tmp = sqrt(  pow(res_fft[i][0],2) + pow(res_fft[i][1],2));
res_fft[i][0] /= tmp;
```

```
res_fft[i][1] /= tmp;
}
fftwf_execute(ifft_res);
for( i = 0 ; i < fft_size ; i++ )
{
poc_data[i] = (res[i][0] / ( float )fft_size);
}
}

void CStrainDlg::phase_correlation_halfsize(IplImage *ref, IplImage *tpl,
IplImage *poc)
{
int   i, j, k;
float tmp;

int step     = ref->widthStep;
int fft_size = bs * bs;
uchar       *tpl_data = ( uchar* ) tpl->imageData;
float       *poc_data = ( float* )poc->imageData;
//load images' data to FFTW input
for( i = 0, k = 0 ; i < bs ; i++ ) {
for( j = 0 ; j < bs ; j++, k++ ) {
img2_half[k] = ( float )(( uchar* ) tpl_data)[(start_y+i) * step +(start_x+
j)];
}
}

// obtain the FFT of img2
fftwf_execute( fft_img2_halfsize );
for( i = 0; i < bs * (bs/2+1) ; i++ ) {
res_fft_half[i][0] = ( img2_fft_half[i][0] * img1_fft_half[i][0] ) -
( img2_fft_half[i][1] * ( -img1_fft_half[i][1] ) );
res_fft_half[i][1] = ( img2_fft_half[i][0] * ( -img1_fft_half[i][1] ) ) +
( img2_fft_half[i][1] * img1_fft_half[i][0] );
tmp = sqrt(  pow(res_fft_half[i][0],2) + pow(res_fft_half[i][1],2));
res_fft_half[i][0] /= tmp;
res_fft_half[i][1] /= tmp;
}
```

```
fftwf_execute(ifft_res_halfsize);
//normalize and copy to result image
for( i = 0 ; i < fft_size ; i++ )
{
poc_data[i] = (res_half[i] / ( float )fft_size);
}
}
void CStrainDlg::cvShiftDFT(CvArr *src_arr, CvArr *dst_arr)
{
CvMat * tmp;
CvMat q1stub, q2stub;
CvMat q3stub, q4stub;
CvMat d1stub, d2stub;
CvMat d3stub, d4stub;
CvMat * q1, * q2, * q3, * q4;
CvMat * d1, * d2, * d3, * d4;
CvSize size = cvGetSize(src_arr);
CvSize dst_size = cvGetSize(dst_arr);
Int cx, cy;
if(dst_size.width != size.width ||
dst_size.height != size.height){
cvError( CV_StsUnmatchedSizes, "cvShiftDFT", "Source and Destination arrays
must have equal sizes", __FILE__, __LINE__ );
}
if(src_arr==dst_arr){
tmp = cvCreateMat(size.height/2, size.width/2, cvGetElemType(src_arr));
}

cx = size.width/2;
cy = size.height/2; // image center
q1 = cvGetSubRect( src_arr, &q1stub, cvRect(0,0,cx, cy) );
q2 = cvGetSubRect( src_arr, &q2stub, cvRect(cx,0,cx,cy) );
q3 = cvGetSubRect( src_arr, &q3stub, cvRect(cx,cy,cx,cy) );
q4 = cvGetSubRect( src_arr, &q4stub, cvRect(0,cy,cx,cy) );
d1 = cvGetSubRect( src_arr, &d1stub, cvRect(0,0,cx,cy) );
d2 = cvGetSubRect( src_arr, &d2stub, cvRect(cx,0,cx,cy) );
d3 = cvGetSubRect( src_arr, &d3stub, cvRect(cx,cy,cx,cy) );
d4 = cvGetSubRect( src_arr, &d4stub, cvRect(0,cy,cx,cy) );
```

```
if(src_arr!=dst_arr){
if( !CV_ARE_TYPES_EQ( q1, d1 )){
cvError( CV_StsUnmatchedFormats, "cvShiftDFT", "Source and Destination arrays
must have the same format", __FILE__, __LINE__ );
}
cvCopy(q3, d1, 0);
cvCopy(q4, d2, 0);
cvCopy(q1, d3, 0);
cvCopy(q2, d4, 0);
}
else{
cvCopy(q3, tmp, 0);
cvCopy(q1, q3, 0);
cvCopy(tmp, q1, 0);
cvCopy(q4, tmp, 0);
cvCopy(q2, q4, 0);
cvCopy(tmp, q2, 0);
}
}
void CStrainDlg::OnButtonStop()
{
m_bStop=1;
}
void CStrainDlg::upsampling(CvArr* in, int factor, int roff, int coff,CvArr*
out ,int N)
{


// in:  input FT complex spetrum , 2 channels
//factor: upsampling factor
int i,j;
CvMat *Ma, *Mb, *Mc,*realtemp,*imaginarytemp,*temp;
float pi=3.14159f;
int nor=factor*N,noc=factor*N; //upsampled output matrix size
CvSize size;
size=cvGetSize(in);
int nr=size.height,nc=size.width;  //input matrix size
//int nr=4,nc=4;
```

```
CvMat* kr= cvCreateMat(nor,nr,CV_32FC2);
CvMat* kc= cvCreateMat(nc,noc,CV_32FC2);
cvZero(kc);cvZero(kr);
Ma= cvCreateMat(nor,1,CV_32FC1);
for(i=0;i<nor;i++)
cvmSet(Ma,i,0,(i+roff)*2*pi/(nr*factor));
Mb= cvCreateMat(1,nr,CV_32FC1);
for(i=0;i<nr;i++)
cvmSet(Ma,i+nr/2,0,((i+nr) % nr)-nr/2);
Mc= cvCreateMat(nor,nr,CV_32FC1);
cvMatMul(Ma, Mb, Mc);
realtemp= cvCreateMat(nor,nr,CV_32FC1);
imaginarytemp= cvCreateMat(nor,nr,CV_32FC1);
for(i=0;i<nor;i++)
{
for(j=0;j<nr;j++)
{
cvmSet(realtemp,i,j,cos(cvmGet(Mc,i,j)));
cvmSet(imaginarytemp,i,j,sin(cvmGet(Mc,i,j)));
}
}
cvReleaseMat(&Ma);
cvReleaseMat(&Mb);
cvReleaseMat(&Mc);
cvReleaseMat(&realtemp);
cvReleaseMat(&imaginarytemp);

Ma= cvCreateMat(nc,1,CV_32FC1);
for(i=0;i<nr;i++)
cvmSet(Ma,i+nr/2,0,((i+nr) % nr)-nr/2);
Mb= cvCreateMat(1,noc,CV_32FC1);
for(i=0;i<noc;i++)
cvmSet(Mb,0,i,(i+coff)*2*pi/(nc*factor));
Mc= cvCreateMat(nc,noc,CV_32FC1);
cvMatMul(Ma, Mb, Mc);
realtemp= cvCreateMat(nc,noc,CV_32FC1);
imaginarytemp= cvCreateMat(nc,noc,CV_32FC1);
for(i=0;i<nc;i++)
```

```
{
for(j=0;j<noc;j++)
{
cvmSet(realtemp,i,j,cos(cvmGet(Mc,i,j)));
cvmSet(imaginarytemp,i,j,sin(cvmGet(Mc,i,j)));
}
}
temp= cvCreateMat(nor,nc,CV_32FC2);
cvMatMul(kr, in, temp);
cvMatMul(temp, kc, out);
cvReleaseMat(&Ma);
cvReleaseMat(&Mb);
cvReleaseMat(&Mc);
cvReleaseMat(&realtemp);
cvReleaseMat(&imaginarytemp);
cvReleaseMat(&temp);
}
void CStrainDlg::fftwcopy(fftwf_complex* source, fftwf_complex* target, int
size)
{
int i;
for( i = 0; i < size ; i++ ) {
target[i][0] = source[i][0];
target[i][1] = source[i][1];

}

}
void CStrainDlg::OnCreateDataSet()
{
CNameInputDialog Dlg;
Dlg.m_DataPointNum=1;
Dlg.defaultfolder=defaultfolder;
if (Dlg.DoModal()==IDOK)
{
datapointnumber=Dlg.m_DataPointNum;
CComboBox* pCB = (CComboBox*) GetDlgItem(IDC_DataSetList);
pCB->ResetContent();
```

```
CStringArray files;
CFileFind finder;
BOOL bWorking = finder.FindFile(defaultfolder+"\\*.*");
while (bWorking)
{
bWorking = finder.FindNextFile();
if (finder.IsDirectory() && !finder.IsDots())
files.Add(finder.GetFilePath());
}
// now cycle through the array
for (int i=0; i<files.GetSize(); i++)
{
pCB->InsertString(-1, files[i].Right(files[i].GetLength()-
defaultfolder.GetLength()-1));
}
int nIndex = 0;
if ((nIndex=pCB->FindString(nIndex,Dlg.m_DataSetName )) != CB_ERR)
{
pCB->SetCurSel(nIndex );
}
if (File.m_hFile != CFile::hFileNull)
File.Close();
datapointnumber=Dlg.m_DataPointNum;
File.Open(defaultfolder+"\\"+Dlg.m_DataSetName
+"\\index.txt",CFile::modeCreate | CFile::modeWrite);
CString temp;
temp.Format("%d",datapointnumber);
File.WriteString(temp);
File.WriteString("\n");
File.Close();
OnSelchangeDataSetList() ;
}
}
void CStrainDlg::UpdateMeasurementList()
{
CString texttemp;
CString ReadMeasurementString;
while(m_measurementlist.GetCount()>0)
```

```
m_measurementlist.DeleteString( 0 );
int i=0;
if (File.m_hFile != CFile::hFileNull)
File.Close();
if (File.Open(defaultfolder+"\\"+datasetname+"\\index.txt", CFile::modeRead)
== TRUE)
{
File.SeekToBegin();
File.ReadString(ReadMeasurementString);
while(File.ReadString(ReadMeasurementString) != FALSE)
{
if (i==ref_index)
{
m_measurementlist.InsertString( i, ReadMeasurementString,RGB(255, 0, 0) );
texttemp= "Reference is  " +ReadMeasurementString;
m_refname.SetWindowText( texttemp );
}
else
m_measurementlist.InsertString( i, ReadMeasurementString );
i++;
measurementname=ReadMeasurementString ;
}
m_strPath=defaultfolder+"\\"+datasetname+"\\"+measurementname;
int n=m_measurementlist.GetCount();
m_measurementlist.SetCurSel(n-1);
}


OnSelchangeMeasurementList() ;
}
void CStrainDlg::OnEditchangeDataSetList()
{
}
void CStrainDlg::OnSelchangeDataSetList()
{
if (File.m_hFile != CFile::hFileNull)
File.Close();
CEdit* pED = (CEdit*) GetDlgItem(IDC_Description);
```

```
pED->Clear();
CComboBox* pCB = (CComboBox*) GetDlgItem(IDC_DataSetList);
pCB->UpdateData(TRUE);
int nIndex = pCB->GetCurSel();
pCB->GetLBText(nIndex, datasetname);
if (_access(defaultfolder+"\\"+datasetname +"\\index.txt",0) != -1)
{
if (File.Open(defaultfolder+"\\"+datasetname +"\\index.txt",
CFile::modeRead)==TRUE)
{
File.SeekToBegin();
CString temp;
File.ReadString(temp);
datapointnumber=_ttoi(temp);
CEdit* pED=(CEdit*)GetDlgItem(IDC_DataPointNumber);
CString pointnumber;
pointnumber.Format("%d",datapointnumber);
pED->SetWindowText(pointnumber);
m_Spin.SetRange(1, datapointnumber);
m_Spin.SetPos(1);
ref_index=0;
UpdateMeasurementList();
}
}
if (_access(defaultfolder+"\\"+datasetname +"\\description.txt",0) != -1)
{

CString temp2;
CString Description;
Description.Empty();
CStdioFile DescriptionFile;
DescriptionFile.Open(defaultfolder+"\\"+datasetname+"\\description.txt",CFile
::modeRead);
while(DescriptionFile.ReadString(temp2) != FALSE)
{
Description=Description+temp2+"\r\n";
}
pED->SetWindowText(Description);
```

```
DescriptionFile.Close();
}
CSpreadSheet SS(defaultfolder+"\\"+datasetname+".xls", "Sheet1");
SS.BeginTransaction();
CStringArray sampleArray;
sampleArray.RemoveAll();
CString ctemp;
sampleArray.Add("Point");
for(int i=1;i<datapointnumber+1;i++)
{
ctemp.Format("%d", i);
sampleArray.Add(ctemp);
}
SS.AddHeaders(sampleArray);
SS.Commit();
}
void CStrainDlg::OnNewMeasurement()
{
CMeasurementNameDialog Dlg;
if (Dlg.DoModal()==IDOK)
{
measurementname=Dlg.m_MeasurementName;
if (File.m_hFile != CFile::hFileNull)
File.Close();
if(File.Open(defaultfolder+"\\"+datasetname+"\\index.txt", CFile::modeWrite)
== TRUE)
{
File.SeekToEnd();
File.WriteString(measurementname);
File.WriteString("\n");
File.Close();
m_pointnumber=1;
m_Spin.SetPos(m_pointnumber);
UpdateMeasurementList();
}
}
}
void CStrainDlg::OnDeleteMeasurement()
```

```
{
CString ReadMeasurementString;
if (File.m_hFile != CFile::hFileNull)
File.Close();
CStdioFile temp;
if ((File.Open(defaultfolder+"\\"+datasetname+"\\index.txt",
CFile::modeReadWrite) == TRUE) &&
(temp.Open(defaultfolder+"\\"+datasetname+"\\temp.txt",CFile::modeCreate |
CFile::modeWrite)==TRUE))
{
File.SeekToBegin();
File.ReadString(ReadMeasurementString);
temp.WriteString(ReadMeasurementString);
temp.WriteString("\n");
while(File.ReadString(ReadMeasurementString) != FALSE)
{
if (ReadMeasurementString!=measurementname)
{
temp.WriteString(ReadMeasurementString);
temp.WriteString("\n");
}
}
File.Close();
temp.Close();
CFile::Remove(defaultfolder+"\\"+datasetname+"\\index.txt");

CFile::Rename(defaultfolder+"\\"+datasetname+"\\temp.txt",defaultfolder+"\\"+
datasetname+"\\index.txt");
}
UpdateMeasurementList();
}
BOOL CStrainDlg::Measure()
{
long lPixelSize=1;  //8 bits
int i,j,k;
CString cstemp;
UpdateData(TRUE);
m_Spin.SetPos(m_pointnumber);
```

```
CFileFind f;
CString cfilenameL,cfilenameR;
cfilenameL.Empty();
cfilenameL.Format("%s_%dL.bmp",m_strPath,m_pointnumber);
cfilenameR.Empty();
cfilenameR.Format("%s_%dR.bmp",m_strPath,m_pointnumber);
hCameras[0]=m_hCameraA;
hCameras[1]=m_hCameraB;
if          (m_measurementlist.GetSel(0)>0)
{
for (i = 0 ; i < CAMNUM ; i++)
{
params[i].format.height = height;
params[i].format.pixelFormat = LUCAM_PF_8;
params[i].format.subSampleX = 1;
params[i].format.subSampleY = 1;
params[i].format.width = width;
params[i].format.xOffset = 0;
params[i].format.yOffset = 0;
params[i].exposure = m_exposure;    // 50 ms exposure
params[i].gain =  23;
//          params[i].gainGrn1 = 1.0;
//          params[i].gainGrn2 = 1.0;
//          params[i].gainRed = 1.0;
params[i].strobeDelay = 0.0;  // unused
params[i].timeout = 3000.0;   // 3000 ms
params[i].useHwTrigger = FALSE;   // Set this to true for hardware triggered setup with daisy chaining
params[i].useStrobe = FALSE;      // Set this to true if daisy-chaining cameras
params[i].exposureDelay = 0;
params[i].shutterType = LUCAM_SHUTTER_TYPE_GLOBAL;
pParams[i] = &params[i];
}
params[0].exposure = m_exposureA;
params[1].exposure = m_exposureB;
pAllFrames = (UCHAR *)malloc((CAMNUM ) * width * height);
if (pAllFrames == NULL)
{
```

```
MessageBox("No memory for frames");
}
for (i = 0 ; i < CAMNUM ; i++)
{
ppFrames[i] = pAllFrames + i * width * height;
}
hSynchronousSnapshots = LucamEnableSynchronousSnapshots(CAMNUM, hCameras, pParams);
m_cbPreview.EnableWindow(FALSE);
m_cbPreview.SetWindowText(_T("Preview"));
m_cbApply.EnableWindow(FALSE);
UpdateWindow();
pThread->PostThreadMessage(WM_SHOWDIALOG,NULL,NULL);
CEdit* pEB = (CEdit*) GetDlgItem(IDC_DELAY);
pEB->UpdateData(TRUE);
if (m_delay<0) m_delay=0;
for(int k=0;k<m_delay;k++)
{
Sleep(1000);
if(b_keepgoing==FALSE || b_redo==TRUE) break;
}
if(b_keepgoing==TRUE && b_redo==FALSE)
{
LucamTakeSynchronousSnapshots(hSynchronousSnapshots, ppFrames);
PlaySound(MAKEINTRESOURCE(IDR_WAVE1),AfxGetResourceHandle(),SND_ASYNC|SND_RESOURCE|S
ND_NODEFAULT);
pThread->PostThreadMessage(WM_CLOSEDIALOG,NULL,NULL);
LucamSaveImage(width, height, LUCAM_PF_8, ppFrames[0], cfilenameL);
LucamSaveImage(width, height, LUCAM_PF_8, ppFrames[1], cfilenameR);
Sleep(100);
}
if (!LucamDisableSynchronousSnapshots(hSynchronousSnapshots))
{
MessageBox("Failed to unsetup synchronous snapshots");
}
if (pAllFrames)
{
free(pAllFrames);
```

```
}
}
else
{
for (i = 0 ; i < CAMNUM ; i++)
{
params[i].format.pixelFormat = LUCAM_PF_8;
params[i].format.subSampleX = 1;
params[i].format.subSampleY = 1;
params[i].format.height = height;
params[i].format.width = width;


params[i].format.xOffset = 0;
params[i].format.yOffset =0;
params[i].exposure = m_exposure;    // 50 ms exposure
params[i].gain = 23;
//          params[i].gainBlue = 1.0;
//          params[i].gainGrn1 = 1.0;
//          params[i].gainGrn2 = 1.0;
//          params[i].gainRed = 1.0;
params[i].strobeDelay = 0.0;  // unused
params[i].timeout = 3000.0;   // 3000 ms
params[i].useHwTrigger = FALSE;   // Set this to true for hardware triggered setup with daisy chaining
params[i].useStrobe = FALSE;      // Set this to true if daisy-chaining cameras
params[i].exposureDelay = 0;
params[i].shutterType = LUCAM_SHUTTER_TYPE_GLOBAL;
pParams[i] = &params[i];
}
params[0].exposure = m_exposureA;
params[1].exposure = m_exposureB;
pAllFrames = (UCHAR *)malloc((CAMNUM ) * width * height);
if (pAllFrames == NULL)
{
MessageBox("No memory for frames");
}
for (i = 0 ; i < CAMNUM ; i++)
```

```
{
ppFrames[i] = pAllFrames + i * width * height;
}
hSynchronousSnapshots = LucamEnableSynchronousSnapshots(CAMNUM, hCameras, pParams);
m_cbPreview.EnableWindow(FALSE);
m_cbPreview.SetWindowText(_T("Preview"));
m_cbApply.EnableWindow(FALSE);
CString refmeasurementname;

int n;
n = m_measurementlist.GetTextLen( ref_index );
m_measurementlist.GetText( ref_index, refmeasurementname.GetBuffer(n) );
refmeasurementname.ReleaseBuffer();
cRefFilenameL.Empty();
cRefFilenameL.Format("%s_%dL.bmp",defaultfolder+"\\"+datasetname+"\\"+refmeasurementname,m_pointnumbe
r);
cRefFilenameR.Empty();
cRefFilenameR.Format("%s_%dR.bmp",defaultfolder+"\\"+datasetname+"\\"+refmeasurementname,m_pointnumbe
r);
if(!f.FindFile(cRefFilenameL))
{
AfxMessageBox("Left Reference image doesn't exist. Can't do correlation.");
LucamDisableSynchronousSnapshots(hSynchronousSnapshots);
free(pAllFrames);
b_keepgoing=FALSE;
return FALSE;
}
if(!f.FindFile(cRefFilenameR))
{
AfxMessageBox("Right Reference image doesn't exist. Can't do correlation.");
LucamDisableSynchronousSnapshots(hSynchronousSnapshots);
free(pAllFrames);
b_keepgoing=FALSE;
return FALSE;
}
int         colindex,rowindex;
IplImage *poc_halfL = 0;
```

```
IplImage *tplL = 0;
IplImage *refL = 0;
IplImage *poc_halfR = 0;
IplImage *tplR = 0;
IplImage *refR = 0;
IplImage *poc = 0;
IplImage *refblockL=0;
IplImage *refblockR=0 ;
IplImage *reffiltered=0;
IplImage *tplfiltered=0;
IplImage *tplLtemp = 0;
IplImage *tplRtemp = 0;
IplImage *tplL_backup = 0;
IplImage *tplR_backup = 0;
tplLtemp=cvCreateImage( cvSize( bs, bs ), IPL_DEPTH_8U, 1 ) ;
tplRtemp=cvCreateImage( cvSize( bs, bs ), IPL_DEPTH_8U, 1 ) ;
poc = cvCreateImage( cvSize( bs, bs ), IPL_DEPTH_32F, 1 );
refblockL=cvCreateImage( cvSize( bs, bs ), IPL_DEPTH_8U, 1 );
refblockR=cvCreateImage( cvSize( bs, bs ), IPL_DEPTH_8U, 1 ) ;
reffiltered=cvCreateImage( cvSize( bs, bs ), IPL_DEPTH_32F, 1 );
tplfiltered=cvCreateImage( cvSize( bs, bs ), IPL_DEPTH_32F, 1 );
tplL_backup=cvCreateImage( cvSize( bs, bs ), IPL_DEPTH_8U, 1 );
tplR_backup =cvCreateImage( cvSize( bs, bs ), IPL_DEPTH_8U, 1 );
pThread->PostThreadMessage(WM_SHOWDIALOG,NULL,NULL);
/* load reference image */
refL = cvLoadImage( cRefFilenameL, CV_LOAD_IMAGE_GRAYSCALE );
poc_halfL = cvCreateImage( cvSize( bs, bs ), IPL_DEPTH_32F, 1 );
refR = cvLoadImage( cRefFilenameR, CV_LOAD_IMAGE_GRAYSCALE );
poc_halfR = cvCreateImage( cvSize( bs, bs ), IPL_DEPTH_32F, 1 );
tplL = cvCreateImage( cvSize( width, height ), IPL_DEPTH_8U, 1 );
tplR = cvCreateImage( cvSize( width, height ), IPL_DEPTH_8U, 1 );
int stepsize=192;
int colnum=(width-bs)/stepsize+1;
int rownum=(height-bs)/stepsize+1;
CvRect rect ;
for( colindex=0;colindex<colnum;colindex++)
{
```

```
for(rowindex=0;rowindex<rownum;rowindex++)
{
rect= cvRect(colindex*stepsize, rowindex*stepsize,bs,bs );
cvSetImageROI(refL , rect);
cvCopy(refL , refblockL, NULL);
filterproduct(refblockL,blockfilter,reffiltered);
memcpy (img1_half,( float* )reffiltered->imageData,bs*bs*sizeof ( float ));
fftwf_execute( fft_img1_halfsize );
fft_halfL[colindex][rowindex] = ( fftwf_complex* )fftwf_malloc ( sizeof ( fftwf_complex ) * bs * (bs/2+1) );
fftwcopy(img1_fft_half,fft_halfL[colindex][rowindex],bs* (bs/2+1) );
cvSetImageROI(refR , rect);
cvCopy(refR , refblockR, NULL);
filterproduct(refblockR,blockfilter,reffiltered);
memcpy (img1_half,( float* )reffiltered->imageData,bs*bs*sizeof ( float ));
fftwf_execute( fft_img1_halfsize );
fft_halfR[colindex][rowindex] = ( fftwf_complex* )fftwf_malloc ( sizeof ( fftwf_complex ) * bs * (bs/2+1) );
fftwcopy(img1_fft_half,fft_halfR[colindex][rowindex],bs* (bs/2+1) );
}}
CvPoint minlocL, maxlocL,minlocR, maxlocR, maxlocLhalf,maxlocRhalf;
CvPoint minlocLtemp, minlocRtemp, maxlocLhalftemp,maxlocRhalftemp;
double  minvalL, maxvalL,minvalR, maxvalR, maxvalLhalf, maxvalRhalf;
double  minvalLtemp, minvalRtemp, maxvalLhalftemp, maxvalRhalftemp;
int colL, rowL,colR,rowR;
int colindex_store,rowindex_store;
CvPoint oldstartL,oldstartR,startL,startR;
oldstartL=cvPoint(0,0);
oldstartR=cvPoint(0,0);
startL=cvPoint(0,0);
startR=cvPoint(0,0);
BOOL peakflag,workmode;
peakflag=FALSE;
double oldLpeak,oldRpeak;
oldLpeak=0;oldRpeak=0;
maxvalLhalf=0;maxvalRhalf=0;
colL=0;rowL=0;colR=0;rowR=0;
CButton* pCBmode = (CButton*) GetDlgItem(IDC_HANDHOLD);
pCBmode->UpdateData(TRUE);
```

```
if (pCBmode->GetCheck()==BST_CHECKED)
workmode=0;
else workmode=1;
m_tStartTime = GetTickCount();//clock();
while(b_keepgoing==1 && b_redo==FALSE)
{
m_tEndTime = GetTickCount();//clock();
dElapsed =  (m_tEndTime - m_tStartTime);
if (   ((peakflag==TRUE) && (dElapsed>0)) ||   ( (peakflag==TRUE) &&  ((maxvalLhalf>thresholdhalf) &&
(maxvalRhalf>thresholdhalf) ) ) )
{
pThread->PostThreadMessage(WM_CLOSEDIALOG,NULL,NULL);
PlaySound(MAKEINTRESOURCE(IDR_WAVE1),AfxGetResourceHandle(),SND_ASYNC|SND_RESOURCE|S
ND_NODEFAULT);
break;
}
LucamTakeSynchronousSnapshots(hSynchronousSnapshots, ppFrames);
tplL->imageData=(char*)ppFrames[0];
rect= cvRect(width/2-bs/2, height/2-bs/2,bs,bs );
cvSetImageROI(tplL , rect);
cvCopy(tplL, tplLtemp, NULL);
filterproduct(tplLtemp,blockfilter,tplfiltered);
memcpy (img1_half,( float* )tplfiltered->imageData,bs*bs*sizeof ( float ));
fftwf_execute( fft_img1_halfsize );
maxvalLhalf=0;
colindex_store=0;
rowindex_store=0;
for(colindex=0;colindex<colnum;colindex++)
{
for(rowindex=0;rowindex<rownum;rowindex++)
{
fftwcopy (img1_fft_halfL,img1_fft_half,bs * (bs/2+1) );
phase_correlation_block( fft_halfL[colindex][rowindex], img1_fft_half, poc_halfL );
cvMinMaxLoc( poc_halfL, &minvalLtemp, &maxvalLhalftemp, &minlocLtemp, &maxlocLhalftemp, 0 );
if (maxvalLhalftemp>maxvalLhalf)
{
maxvalLhalf=maxvalLhalftemp;
```

```
maxlocLhalf=maxlocLhalftemp;
colindex_store=colindex;
rowindex_store=rowindex;
}
}
}
if (maxlocLhalf.x>bs/2)
startL.x=colindex_store*stepsize+bs-maxlocLhalf.x;
else
startL.x=colindex_store*stepsize-maxlocLhalf.x;
if (maxlocLhalf.y>bs/2)
startL.y=rowindex_store*stepsize+bs-maxlocLhalf.y;
else
startL.y=rowindex_store*stepsize-maxlocLhalf.y;
if(  (maxvalLhalf>THRESHOLD) )   {
tplR->imageData=(char*)ppFrames[1];
rect= cvRect(width/2-bs/2, height/2-bs/2,bs,bs );
cvSetImageROI(tplR , rect);
cvCopy(tplR, tplRtemp, NULL);
filterproduct(tplRtemp,blockfilter,tplfiltered);
memcpy (img1_half,( float* )tplfiltered->imageData,bs*bs*sizeof ( float ));
fftwf_execute( fft_img1_halfsize );
maxvalRhalf=0;
colindex_store=0;
rowindex_store=0;
for( colindex=0;colindex<colnum;colindex++)
{
for(rowindex=0;rowindex<rownum;rowindex++)
{
phase_correlation_block( fft_halfR[colindex][rowindex], img1_fft_half,
poc_halfR );
cvMinMaxLoc( poc_halfR, &minvalRtemp, &maxvalRhalftemp, &minlocRtemp,
&maxlocRhalftemp, 0 );
if (maxvalRhalftemp>maxvalRhalf)
{
maxvalRhalf=maxvalRhalftemp;
maxlocRhalf=maxlocRhalftemp;
```

```
colindex_store=colindex;
rowindex_store=rowindex;
}
}
}
if (maxlocRhalf.x>bs/2)
startR.x=colindex_store*stepsize+bs-maxlocRhalf.x;
else
startR.x=colindex_store*stepsize-maxlocRhalf.x;
if (maxlocRhalf.y>bs/2)
startR.y=rowindex_store*stepsize+bs-maxlocRhalf.y;
else
startR.y=rowindex_store*stepsize-maxlocRhalf.y;
if  (maxvalRhalf>THRESHOLD)  {
if ( (  (maxvalLhalf>oldLpeak) && (maxvalRhalf>oldRpeak) ) ||
((maxvalLhalf>thresholdhalf) && (maxvalRhalf>thresholdhalf) )  )
{
peakflag=TRUE;
oldLpeak=maxvalLhalf;
oldRpeak=maxvalRhalf;
oldstartL=startL;
oldstartR=startR;
cvCopy( tplRtemp, tplR_backup, NULL );
cvCopy( tplLtemp, tplL_backup, NULL );
m_tStartTime = GetTickCount();//clock();
}
}
}
}
if(b_keepgoing==TRUE && b_redo==FALSE)
{
if (oldstartL.x<0)
oldstartL.x=0;
if (oldstartL.y<0)
oldstartL.y=0;
if (oldstartR.x<0)
oldstartR.x=0;
if (oldstartR.y<0)
```

```
oldstartR.y=0;
if (oldstartL.x+bs>width)
oldstartL.x=width-bs-1;
if (oldstartL.y+bs>height)
oldstartL.y=height-bs-1;
oldstartR.x=width-bs-1;
if (oldstartR.y+bs>height)
oldstartR.y=height-bs-1;
rect= cvRect(oldstartL.x, oldstartL.y,bs,bs );
cvSetImageROI(refL , rect);
cvCopy(refL , refblockL, NULL);
filterproduct(refblockL,blockfilter,reffiltered);
filterproduct(tplL_backup,blockfilter,tplfiltered);
phase_correlation( reffiltered, tplfiltered, poc_halfL );
cvMinMaxLoc( poc_halfL, &minvalL, &maxvalL, &minlocL, &maxlocL, 0 );
int xx,yy;
if (maxlocL.x>bs/2)
xx=oldstartL.x+bs-maxlocL.x;
else
xx=oldstartL.x-maxlocL.x;
if (maxlocL.y>bs/2)
yy=oldstartL.y+bs-maxlocL.y;
else
yy=oldstartL.y-maxlocL.y;

int    x=maxlocL.x;
int  y=maxlocL.y;
CvMat* real=cvCreateMat(bs, bs, CV_32FC1);
CvMat* im=cvCreateMat(bs, bs, CV_32FC1);
for( i = 0, k = 0 ; i < bs ; i++ ) {
for( j = 0 ; j < bs ; j++, k++ ) {
cvmSet(real,i,j,(float)res_fft[k][0]);
cvmSet(im,  i,j,(float)res_fft[k][1]);
}
}
CvMat* in= cvCreateMat(bs,bs,CV_32FC2);
int factor=25;
CvMat* out= cvCreateMat(2*factor,2*factor,CV_32FC2);
```

```
upsampling(in, factor,(y-1)*factor, (x-1)*factor,out,2);
cvReleaseMat(&real);
cvReleaseMat(&im);
real=cvCreateMat(factor*2, factor*2, CV_32FC1);
im=cvCreateMat(factor*2, factor*2, CV_32FC1);
cvSplit( out, real, im, 0, 0 );
// Compute the magnitude of the spectrum Mag = sqrt(Re^2 + Im^2)
cvPow( real, real, 2.0);
cvPow( im, im, 2.0);
cvAdd( real, im , real, NULL);
cvPow( real, real, 0.5 );
cvMinMaxLoc( real, &minvalL, &maxvalL, &minlocL, &maxlocL, 0 );
cvReleaseMat(&real);
cvReleaseMat(&im);
float subxL, subyL;
subxL=width/2-bs/2-xx-1+(float)maxlocL.x/factor;
subyL=yy-(height/2-bs/2)-(-1+(float)maxlocL.y/factor);
float subxR,subyR;
rect= cvRect(oldstartR.x, oldstartR.y,bs,bs );
cvSetImageROI(refR , rect);
cvCopy(refR , refblockR, NULL);
filterproduct(refblockR,blockfilter,reffiltered);
filterproduct(tplR_backup,blockfilter,tplfiltered);
phase_correlation( reffiltered, tplfiltered, poc_halfR );
cvMinMaxLoc( poc_halfR, &minvalR, &maxvalR, &minlocR, &maxlocR, 0 );
if (maxlocR.x>bs/2)
xx=oldstartR.x+bs-maxlocR.x;
else
xx=oldstartR.x-maxlocR.x;
if (maxlocR.y>bs/2)
yy=oldstartR.y+bs-maxlocR.y;
else
yy=oldstartR.y-maxlocR.y;
x=maxlocR.x;
y=maxlocR.y;
real=cvCreateMat(bs, bs, CV_32FC1);
im=cvCreateMat(bs, bs, CV_32FC1);
for( i = 0, k = 0 ; i < bs ; i++ ) {
```

```
for( j = 0 ; j < bs ; j++, k++ ) {
cvmSet(real,i,j,(float)res_fft[k][0]);
cvmSet(im,  i,j,(float)res_fft[k][1]);
}
}
upsampling(in, factor,(y-1)*factor, (x-1)*factor,out,2);
cvReleaseMat(&real);
cvReleaseMat(&im);
real=cvCreateMat(factor*2, factor*2, CV_32FC1);
im=cvCreateMat(factor*2, factor*2, CV_32FC1);
cvSplit( out, real, im, 0, 0 );
cvPow( real, real, 2.0);
cvPow( im, im, 2.0);
cvAdd( real, im , real, NULL);
cvPow( real, real, 0.5 );
cvReleaseMat(&in);
cvReleaseMat(&out);
cvMinMaxLoc( real, &minvalR, &maxvalR, &minlocR, &maxlocR, 0 );
cvReleaseMat(&real);
cvReleaseMat(&im);
subxR=width/2-bs/2-xx-1+(float)maxlocR.x/factor;
subyR=yy-(height/2-bs/2)-(-1+(float)maxlocR.y/factor);
if ( (maxvalL<THRESHOLD) || (maxvalR<THRESHOLD) )
AfxMessageBox("might be fake peak, measure again!");

float deflection;
float secondorder;
deflection=p1*subxL+p2*subyL+p3*subxR+p4*subyR;
secondorder=(-p2*subxL+p1*subyL-p4*subxR+p3*subyR)*(-p2*subxL+p1*subyL-
p4*subxR+p3*subyR)/(2*25.4*m_gl);
CStdioFile DataFile;
cstemp.Format("%f  %f  %5.4f %5.4f %5.4f  %5.4f  %f %f",oldLpeak,
oldRpeak,subxL,subyL,subxR,subyR,deflection,secondorder);
if(DataFile.Open("c:\\data_fitting.txt",CFile::modeWrite|
CFile::modeNoTruncate | CFile::modeCreate ) == TRUE)
{
DataFile.SeekToEnd();
DataFile.WriteString(cstemp);
```

```
DataFile.WriteString("\n");
DataFile.Close();
}
deflection=deflection+secondorder;
CSpreadSheet SS(defaultfolder+"\\"+datasetname+".xls", "Sheet1");
SS.BeginTransaction();
if (ref_index!=0)
{
SS.ReadCell(cstemp, m_pointnumber+1,ref_index+1);
float ref_deflection;
ref_deflection=atof((LPCSTR)cstemp);
deflection=deflection+ref_deflection;
}
CComboBox* pCBunit = (CComboBox*) GetDlgItem(IDC_UNIT);
pCBunit->UpdateData(TRUE);
int nUnit = pCBunit->GetCurSel();
switch (nUnit)
{
case 2:
cstemp.Format("Distance change= %5.4fmm",deflection);
break;
case 0:
cstemp.Format("Distance change= %5.5finch",deflection/25.4);
break;
case 1:
CEdit* pEgl = (CEdit*) GetDlgItem(IDC_GL);
pEgl->UpdateData(TRUE);
cstemp.Format("strain=%5.1f micro Strain", deflection/25.4/m_gl*1000000);
;
break;
}
if (m_duration>0)
{
CDelayMessageBox mbox(this);
mbox.MessageBox(cstemp,    m_duration,
TRUE,CDelayMessageBox::MBIcon::MBICONNONE);
}
cstemp.Format("%5.4f",deflection);
```

```
SS.AddCell(cstemp, m_pointnumber+1,m_measurementlist.GetCurSel()+1);
SS.Commit();
LucamSaveImage(width, height, LUCAM_PF_8, ppFrames[0], cfilenameL);
LucamSaveImage(width, height, LUCAM_PF_8, ppFrames[1], cfilenameR);
cvReleaseMat(&real);
cvReleaseMat(&im);
cvReleaseMat(&in);
cvReleaseMat(&out);
}
else
{
LucamSaveImage(width, height, LUCAM_PF_8, ppFrames[0], cfilenameL);
LucamSaveImage(width, height, LUCAM_PF_8, ppFrames[1], cfilenameR);
}
for(colindex=0;colindex<colnum;colindex++)
{
for(rowindex=0;rowindex<rownum;rowindex++)
{
fftwf_free( fft_halfL[colindex][rowindex]);
fftwf_free( fft_halfR[colindex][rowindex]);
}
}
cvReleaseImage( &poc );
cvReleaseImage(&refblockL);
cvReleaseImage(&refblockR);
cvReleaseImage(&reffiltered);
cvReleaseImage(&tplfiltered);
cvReleaseImage(&tplL_backup);
cvReleaseImage(&tplR_backup);
cvReleaseImage(&tplRtemp);
cvReleaseImage(&tplLtemp);
cvReleaseImage( &tplR );
cvReleaseImage( &refR );
cvReleaseImage( &poc_halfR );
cvReleaseImage( &tplL );
cvReleaseImage( &refL );
cvReleaseImage( &poc_halfL );
if (!LucamDisableSynchronousSnapshots(hSynchronousSnapshots))
```

```
{
MessageBox("Failed to unsetup synchronous snapshots");
}
if (pAllFrames)
{
free(pAllFrames);
}
}
m_cbPreview.EnableWindow(TRUE);
m_cbPreview.SetWindowText(_T("Preview"));
m_cbApply.EnableWindow(TRUE);
return TRUE;
}
void CStrainDlg::OnSelchangeMeasurementList()
{
int n;
CString str;
for (int i=0;i < m_measurementlist.GetCount();i++)
{
if (m_measurementlist.GetSel(i)>0)
{
n = m_measurementlist.GetTextLen( i );
m_measurementlist.GetText( i, str.GetBuffer(n) );
str.ReleaseBuffer();

measurementname=str;
m_strPath=defaultfolder+"\\"+datasetname+"\\"+measurementname;
}
}
m_pointnumber=1;
m_Spin.SetPos(m_pointnumber);
if (m_measurementlist.GetCurSel()>0)
{
CSpreadSheet SS(defaultfolder+"\\"+datasetname+".xls", "Sheet1");
SS.BeginTransaction();
SS.AddCell(measurementname, 1,m_measurementlist.GetCurSel()+1);
SS.Commit();
}
```

```
}
void CStrainDlg::PostNcDestroy()
{
CleanUp();
CDialog::PostNcDestroy();
}
BOOL CStrainDlg::CreateHanning(int M,int N,CvMat* filter,BOOL flag, int d)
{
CvMat* largefilter;
CvRect rect ;
largefilter = cvCreateMat(M/2*3,N/2*3,CV_32FC1);
CreateLargeHanning(M/2*3,N/2*3,largefilter);
IplImage *img, img_header;
img = cvGetImage(largefilter, &img_header);
rect= cvRect(M/4, N/4,M,N );
cvSetImageROI(img , rect);
cvCopy(img , filter, NULL);
cvResetImageROI(img);
cvReleaseMat(&largefilter);
return TRUE;
}
void CStrainDlg::filterproduct(IplImage *img, CvMat *filter, IplImage
*productimg)
{

int   i, j, k;
float tmp;
CvScalar s;
// get image properties
int width    = img->width;
int height   = img->height;
uchar       *img_data = ( uchar* ) img->imageData;
float       *productimg_data= ( float* )productimg->imageData;
for(i=0,k=0; i<height; i++)
for(j=0; j<width; j++,k++)
{
tmp=cvmGet(filter,i,j);
s=cvGet2D(img,i,j);
```

```
productimg_data[k]=tmp* s.val[0];
}
}
void CStrainDlg::converttofloat(IplImage *img, CvMat *filter, IplImage
*productimg, int shiftx, int shifty)
{
int   i, j, k;
float tmp;
// get image properties
int width    = img->width;
int height   = img->height;
uchar       *img_data = ( uchar* ) img->imageData;
float       *productimg_data= ( float* )productimg->imageData;
for(i=0,k=0; i<height; i++)
for(j=0; j<width; j++,k++)
{
if (  ((i+shifty>(height-1)) || ((i+shifty)<0)) || ((j+shiftx)>(width-1)) ||
((j+shiftx)<0) )
tmp=0;
else
tmp=1.0;
productimg_data[k]=tmp* ( float )img_data[k];
}
}

void CStrainDlg::OnConcrete()
{
m_exposure=4;
CEdit* pEd = (CEdit*) GetDlgItem(IDC_EXPOSURE);
pEd->SetWindowText("4");
}
void CStrainDlg::OnSteel()
{
m_exposure=18;
CEdit* pEd = (CEdit*) GetDlgItem(IDC_EXPOSURE);
pEd->SetWindowText("18");
}
```

```
void CStrainDlg::INTfilter(IplImage *img, CvMat *filter, IplImage *productimg,
int shiftx, int shifty)
{
int   i, j, k;
float tmp;
// get image properties
int width    = img->width;
int height   = img->height;
uchar       *img_data = ( uchar* ) img->imageData;
uchar       *productimg_data= ( uchar* )productimg->imageData;
for(i=0,k=0; i<height; i++)
for(j=0; j<width; j++,k++)
{
if (  ((i+shifty>(height-1)) || ((i+shifty)<0)) || ((j+shiftx)>(width-1)) ||
((j+shiftx)<0) )
tmp=0;
else
tmp=cvmGet(filter,i+shifty,j+shiftx);
productimg_data[k]=(uchar)(tmp* ( float )img_data[k]+0.5);
}
}
void CStrainDlg::OnOpendatafile()
{
ShellExecute(NULL,"open",defaultfolder+"\\"+datasetname+".xls",NULL,NULL,SW_S
HOWNORMAL);

}
void CStrainDlg::OnCalibrateIntensity()
{
if (!m_bPreviewing)
{
FLOAT m_Lum;
LONG flags;
BOOL rt;
FLOAT m_Exp=2.0f;
UpdateData(TRUE);
switch (m_surfacetype)
{
```

```
case 0:
m_Lum=50.0f;
break;
case 1:
m_Lum=70.0f;
break;
}
flags = LUCAM_PROP_FLAG_AUTO;
BOOL AutoA=1;
rt = LucamSetProperty(m_hCameraA, LUCAM_PROP_EXPOSURE, m_Exp, flags);
if (!LucamSetProperty(m_hCameraA, LUCAM_PROP_AUTO_EXP_TARGET, m_Lum, flags))
{
MessageBox("Failed to set exposure target.");
AutoA=0;
}
flags = LUCAM_PROP_FLAG_AUTO;
rt = LucamSetProperty(m_hCameraB, LUCAM_PROP_EXPOSURE, m_Exp, flags);
if (!LucamSetProperty(m_hCameraB, LUCAM_PROP_AUTO_EXP_TARGET, m_Lum, flags)) {
MessageBox("Failed to set exposure target.");
}
// Start the preview
if (LucamCreateDisplayWindow(m_hCameraA, "Preview A", WS_OVERLAPPEDWINDOW|WS_VISIBLE, 0,
200, 640, 480, this->m_hWnd, NULL)  && LucamCreateDisplayWindow(m_hCameraB, "Preview B",
WS_OVERLAPPEDWINDOW|WS_VISIBLE, 500, 300, 640, 480, this->m_hWnd, NULL))
{
if (LucamStreamVideoControl(m_hCameraA, START_DISPLAY, NULL) &&
LucamStreamVideoControl(m_hCameraB, START_DISPLAY, NULL))
{m_bPreviewing = TRUE;
m_cbPreview.EnableWindow(TRUE);
m_cbPreview.SetWindowText(_T("Stop"));
m_cbMeasure.EnableWindow(FALSE);
}
else
{
MessageBox("Unable start previewing video.", "Start Preview", MB_OK);
LucamDestroyDisplayWindow(m_hCameraA);
LucamDestroyDisplayWindow(m_hCameraB);
```

```
}
}
else
MessageBox("Unable create preview window.", "Start Preview", MB_OK);
CDelayMessageBox mbox(this);
mbox.MessageBox("Calibating Intensity...",    5,    TRUE,CDelayMessageBox::MBIcon::MBICONNONE);
long dumb=0;
LucamGetProperty(m_hCameraA, LUCAM_PROP_EXPOSURE, &m_exposureA, &dumb);
LucamGetProperty(m_hCameraB, LUCAM_PROP_EXPOSURE, &m_exposureB, &dumb);
if (AutoA==0)
m_exposureA=m_exposureB;
if (LucamStreamVideoControl(m_hCameraA, STOP_STREAMING, NULL) &&
LucamStreamVideoControl(m_hCameraB, STOP_STREAMING, NULL))
{
m_cbPreview.EnableWindow(TRUE);
m_cbPreview.SetWindowText(_T("Preview"));
m_cbMeasure.EnableWindow(TRUE);
}
else
MessageBox("Unable STOP previewing video.", "Stop Preview", MB_OK);
LucamDestroyDisplayWindow(m_hCameraA);
LucamDestroyDisplayWindow(m_hCameraB);
m_bPreviewing = FALSE;
}
}
void CStrainDlg::phase_correlation_block(fftwf_complex *fft1, fftwf_complex *fft2, IplImage *poc)
{
float      tmp;
// get image properties
float fft_size = (float)bs * bs;
// setup pointers to images
float      *poc_data = ( float* )poc->imageData;
for(int i = 0; i < bs * (bs/2+1) ; i++ ) {
res_fft_half[i][0] = ( fft2[i][0] * fft1[i][0] ) - ( fft2[i][1] * ( -fft1[i][1] ) );
res_fft_half[i][1] = ( fft2[i][0] * ( -fft1[i][1] ) ) + ( fft2[i][1] * fft1[i][0] );
tmp = sqrt(  pow(res_fft_half[i][0],2) + pow(res_fft_half[i][1],2));
res_fft_half[i][0] /= tmp;
```

```
res_fft_half[i][1] /= tmp;
}
// obtain the phase correlation array
fftwf_execute(ifft_res_halfsize);
//normalize and copy to result image
for( i = 0 ; i < bs * bs ; i++ )
{
poc_data[i] = (res_half[i] /fft_size);
}
// deallocate FFTW arrays and plans
}
void CStrainDlg::ShowImage(IplImage *img)
{

int width               = img->width;
int height   = img->height;
IplImage *img_temp;
img_temp = cvCreateImage( cvSize( width, height ), IPL_DEPTH_32F, 1 );
double minv, maxv;
CvPoint minl, maxl;
cvMinMaxLoc( img, &minv, &maxv, &minl, &maxl, 0 );
cvScale(img, img_temp, 1.0/(maxv-minv), 1.0*(-minv)/(maxv-minv));
cvNamedWindow( "image", 0 );
cvShowImage( "image", img_temp);
cvResizeWindow("image",width, height);
cvWaitKey( 0 );
cvDestroyWindow( "image" );
cvReleaseImage( &img_temp);
}
void CStrainDlg::CreateLargeHanning(int M, int N, CvMat *filter)
{double pi=3.1415926;
float temp;
CvMat* Ma = cvCreateMat(M,1,CV_32FC1);
CvMat* Mb = cvCreateMat(1,N,CV_32FC1);
for(int row=0;row<M/2;row++)
{
temp=(float)(0.5*(1-cos( pi*(((float)row)/((float)M/2)) )));
```

```
cvmSet(Ma,row,1, temp);
cvmSet(Ma,M-row-1,1, temp);
}
for(int col=0;col<N/2;col++)
{
temp=(float)(0.5*(1-cos(pi*(((float)col)/((float)N/2)))));
cvmSet(Mb,1,col,temp);
cvmSet(Mb,1,N-col-1, temp);
}
cvMatMul(Ma, Mb, filter);

cvReleaseMat(&Ma);
cvReleaseMat(&Mb);
//          return TRUE;
}
void CStrainDlg::OnSetreference()
{
int selindex,nIndex ;
selindex=m_measurementlist.GetCurSel();
CString texttemp;
m_measurementlist.GetText(ref_index, texttemp);
m_measurementlist.DeleteString(ref_index);
nIndex = m_measurementlist.InsertString(ref_index, texttemp);
m_measurementlist.GetText(selindex, texttemp);
m_measurementlist.DeleteString(selindex);
nIndex = m_measurementlist.InsertString(selindex, texttemp, RGB(255, 0, 0));
ref_index=selindex;
int n=m_measurementlist.GetCount();
m_measurementlist.SetCurSel(n-1);
texttemp= "Reference is  " +texttemp;
m_refname.SetWindowText( texttemp );
//          UpdateData(FALSE);
}
void CStrainDlg::Subpixel(IplImage *in, double *x, double *y, int factor)
{
CvPoint minl,maxl;
double minv,maxv;
```

```
int         h=64;
int         w=64;
CvRect rect;
IplImage* peakarea = cvCreateImage(cvSize(w,h ), IPL_DEPTH_32F, 1);



cvMinMaxLoc( in, &minv, &maxv, &minl, &maxl, 0 );
int intx=maxl.x;
int inty=maxl.y;
rect= cvRect(maxl.x-w/2, maxl.y-h/2,w,h );
cvSetImageROI(in , rect);
cvCopy(in, peakarea, NULL);
cvResetImageROI(in);
IplImage* fftImg = cvCreateImage(cvSize(w, h), IPL_DEPTH_32F, 2);
IplImage* complexInput = cvCreateImage(cvSize(w, h), IPL_DEPTH_32F, 2);
IplImage* imaginaryInput = cvCreateImage(cvSize(w, h), IPL_DEPTH_32F, 1);
cvZero(imaginaryInput);
cvDFT(complexInput, fftImg, CV_DXT_FORWARD/*|CV_DXT_SCALE*/,complexInput->height);
cvMinMaxLoc( peakarea, &minv, &maxv, &minl, &maxl, 0 );
CvMat* out= cvCreateMat(2*factor,2*factor,CV_32FC2);
upsampling(fftImg, factor,(maxl.y-1)*factor, (maxl.x-1)*factor,out,2);
IplImage* real = cvCreateImage(cvSize(factor*2, factor*2), IPL_DEPTH_32F, 1);
IplImage* im = cvCreateImage(cvSize(factor*2, factor*2), IPL_DEPTH_32F, 1);
cvSplit( out, real, im, 0, 0 );
// Compute the magnitude of the spectrum Mag = sqrt(Re^2 + Im^2)
cvPow( real, real, 2.0);
cvPow( im, im, 2.0);
cvAdd( real, im , real, NULL);
cvPow( real, real, 0.5 );
cvMinMaxLoc( real, &minv, &maxv, &minl, &maxl, 0 );
*x=intx-1+(double)(maxl.x)/(double)factor;
*y=inty-1+(double)(maxl.y)/(double)factor;
cvReleaseImage( &real);
cvReleaseImage( &im);
cvReleaseImage( &peakarea);
cvReleaseImage( &fftImg);
cvReleaseImage( &complexInput);
```

```
cvReleaseImage( &imaginaryInput);
cvReleaseMat(&out);
}

void CStrainDlg::PreProcess(IplImage *input, IplImage *output)
{
cvSmooth( input,output,          CV_MEDIAN,          3, 3 );
AdaptiveHist(output,output);
UpdateData(TRUE);
if (m_invert==TRUE)
{
cvXorS(output, cvScalar(255), output);
cvThreshold( output,output, 120,    0, CV_THRESH_TOZERO );
}
cvEqualizeHist( output, output );
}
void CStrainDlg::AdaptiveHist(IplImage *input, IplImage *output)
{
int histsize=4;
CvRect rect;
int width          = input->width;
int height   = input->height;
int colnum=floor(width/histsize);
int rownum=1;
for(int colindex=0;colindex<colnum;colindex++)
{
for(int rowindex=0;rowindex<rownum;rowindex++)
{
rect= cvRect(colindex*histsize, rowindex*histsize, histsize,height );
cvSetImageROI(input , rect);
cvEqualizeHist( input, input );
cvResetImageROI(input);
}
}

cvEqualizeHist( input, output );
}
```

```
BOOL CStrainDlg::Blurcheck(IplImage *img1, IplImage *img2)
{
IplImage *diff = 0;
diff= cvCreateImage( cvGetSize( img1 ), IPL_DEPTH_8U, 1 );
cvAbsDiff(img1,img2,diff);
CvScalar d=cvAvg(diff);
cvReleaseImage(&diff);
if (d.val[0]<16)
return 0;
else return 1;
}
void CStrainDlg::MaxLoc(IplImage *image, double &max, CvPoint &location)
{
float* data;
int step;
CvSize size;
int x, y;
cvGetRawData( image, (uchar**)&data, &step, &size );
step /= sizeof(data[0]);
max = 0;
location.x = 0;
location.y = 0;
for( y = 0; y < size.height; y++, data += step )
for( x = 0; x < size.width; x++ )
{
if( data[x] > max )
{
max = (double)data[x];
location.x = x;
location.y = y;
}
}
}
void CStrainDlg::MinLoc(IplImage *image, double &min, CvPoint &location)
{
float* data;
int step;
```

```
CvSize size;
int x, y;
cvGetRawData( image, (uchar**)&data, &step, &size );
step /= sizeof(data[0]);
min = (double)data[0];
location.x = 0;
location.y = 0;
for( y = 0; y < size.height; y++, data += step )
for( x = 0; x < size.width; x++ )
{
if( data[x] < min )
{
min = (double)data[x];
location.x = x;
location.y = y;
}
}
}
void CStrainDlg::MultipleMaxLoc(IplImage *image, CvPoint location[])
{
float* data;
int step;
CvSize size;
int x, y, i, j;
int iNumPoints=1;
double dMax[1];
cvGetRawData( image, (uchar**)&data, &step, &size );
step /= sizeof(data[0]);
for( i = 0; i < iNumPoints; i++ )
dMax[i] = 0;
for( y = 0; y < size.height; y++, data += step )
{
for( x = 0; x < size.width; x++ )
{
for( i = 0; i < iNumPoints; i++ )
{
if( data[x] >= dMax[i] )
```

```
{
for( j = iNumPoints - 1; j > i; j-- )
{
dMax[j] = dMax[j-1];
location[j] = location[j-1];
}
dMax[i] = (double)data[x];
location[i].x = x;
location[i].y = y;
break;
}
}
}
}
}
void CStrainDlg::MultipleMinLoc(IplImage *image, CvPoint location[])
{
float* data;
int step;
CvSize size;
int x, y, i, j;
int iNumPoints=1;
double dMin[1];
cvGetRawData( image, (uchar**)&data, &step, &size );
step /= sizeof(data[0]);
for( i = 0; i < iNumPoints; i++ )
dMin[i] = 1;
for( y = 0; y < size.height; y++, data += step )
{
for( x = 0; x < size.width; x++ )
{
for( i = 0; i < iNumPoints; i++ )
{
if( data[x] <= dMin[i] )
{
for( j = iNumPoints - 1; j > i; j-- )
{
```

```
dMin[j] = dMin[j-1];
location[j] = location[j-1];
}
dMin[i] = (double)data[x];
location[i].x = x;
location[i].y = y;
break;
}
}
}
}
}
void CStrainDlg::OnCalibration()
{
double subxL,subyL,subxR,subyR;
CString cstemp;
int N=15;
double    baseb=-0.004447;

LONG numCameras = LucamNumCameras();
LUCAM_VERSION pVersionsArray[20];
ULONG tt = LucamEnumCameras(pVersionsArray, numCameras);
UpdateData(TRUE);
CvMat* X = cvCreateMat(N,3,CV_32FC1);
CvMat* Y = cvCreateMat(N,1,CV_32FC1);
CvMat* b = cvCreateMat(3,1,CV_32FC1);
CvMat* Xt = cvCreateMat(3,N,CV_32FC1);
CvMat* XtX = cvCreateMat(3,3,CV_32FC1);
CvMat* tempM  = cvCreateMat(3,N,CV_32FC1);
b_keepgoing=TRUE;
//take initial reading
pThread=AfxBeginThread(RUNTIME_CLASS(CUIThread));
TakeInitialReading();
pThread->PostThreadMessage(WM_CLOSEDIALOG,NULL,NULL);
Sleep(100);
Sleep(2000);
int         i=0;
```

```
while(b_keepgoing==1 && i<N)
{b_keepgoing=TRUE;
pThread=AfxBeginThread(RUNTIME_CLASS(CUIThread));
b_redo=FALSE;
CalibrationReadingSpeckle(&subxL,&subyL,&subxR,&subyR);
pThread->PostThreadMessage(WM_CLOSEDIALOG,NULL,NULL);
Sleep(1000);
cvmSet(Y,i,0,subxL*(-baseb));
cvmSet(X,i,0,subyL);
cvmSet(X,i,1,subxR);
cvmSet(X,i,2,subyR);
i++;
}
cvTranspose(X, Xt);
cvMatMul(Xt, X, XtX);
cvInvert(XtX, XtX);
cvMatMul(XtX, Xt, tempM );
cvMatMul(tempM, Y, b );
CvMat* Xb  = cvCreateMat(N,1,CV_32FC1);
cvMatMul(X, b, Xb);
cvSub(Xb,Y,Xb);
cvAbs(Xb,Xb);
float residue=0;
int maxindex=-1;
for(i=0;i<N;i++)
{
if (residue<cvmGet(Xb,i,0))
{
residue=cvmGet(Xb,i,0);
maxindex=i;
}
}
cvmSet(Y,maxindex,0,0);
cvmSet(X,maxindex,0,0);
cvmSet(X,maxindex,1,0);
cvmSet(X,maxindex,2,0);
cvMatMul(X, b, Xb);
```

```
cvSub(Xb,Y,Xb);
cvAbs(Xb,Xb);
residue=0;
maxindex=-1;
for(i=0;i<N;i++)
{
if (residue<cvmGet(Xb,i,0))
{
residue=cvmGet(Xb,i,0);
maxindex=i;
}
}
cvmSet(Y,maxindex,0,0);
cvmSet(X,maxindex,0,0);
cvmSet(X,maxindex,1,0);
cvmSet(X,maxindex,2,0);
cvTranspose(X, Xt);
cvMatMul(Xt, X, XtX);
cvInvert(XtX, XtX);
cvMatMul(XtX, Xt, tempM );
cvMatMul(tempM, Y, b );
cvReleaseMat(&Xb);
CStdioFile DataFile;
cstemp.Format("%8.8f \n%8.8f \n%8.8f\n%8.8f\n  ",baseb, cvmGet(b,0,0),
cvmGet(b,0,1),cvmGet(b,0,2)   );
if(DataFile.Open("c:\\para.txt",CFile::modeWrite| CFile::modeNoTruncate |
CFile::modeCreate ) == TRUE)
{
DataFile.SeekToEnd();
DataFile.WriteString(cstemp);
DataFile.WriteString("\n");
DataFile.Close();
}
CStdioFile ppFile;
if ((pVersionsArray[0].serialnumber==30052108) &&
(pVersionsArray[1].serialnumber==30052152))
{
```

```
if (ppFile.Open("C:\\Program Files\\Strain\\parameter_new sensor.txt",
CFile::modeReadWrite) != TRUE)
{
AfxMessageBox("Failed to load parameter file");
}
}
if ((pVersionsArray[0].serialnumber==30052090) &&
(pVersionsArray[1].serialnumber==30052184))
{
if (ppFile.Open("C:\\Program Files\\Strain\\parameter_old sensor.txt",
CFile::modeReadWrite) != TRUE)
{
AfxMessageBox("Failed to load parameter file");
}
}

float fvar;
ppFile.SeekToBegin();
int cc=0;
CString tempString;
while(ppFile.ReadString(tempString) != FALSE)
{
fvar = (float) atof(tempString);
cc++;
switch(cc){
case 1: THRESHOLD=fvar;break;
case 2:thresholdhalf=fvar;break;
case 3:THRESHOLD_glass=fvar;break;
case 4: p1=fvar   ;break;
case 5: p2=fvar    ;break;
case 6:     p3=fvar   ;break;
case 7: p4=fvar   ; break;
case 8: g1=fvar   ;break;
case 9: g2=fvar    ;break;
case 10:    g3=fvar   ;break;
case 11: g4=fvar  ; break;
case 12: g5=fvar  ; break;
}
```

```
}
ppFile.SeekToBegin();
CString cstemp_thres,cstemp_speckle,cstemp_paint;
cstemp_thres.Format("%5.4f\n%5.4f\n%5.4f\n",THRESHOLD,thresholdhalf,THRESHOLD
_glass);
cstemp_speckle.Format("%8.8f\n%8.8f\n%8.8f\n",p1,p2,p3,p4);
cstemp_paint.Format("%8.8f\n%8.8f\n%8.8f\n%8.8f\n%8.8f\n",g1,g2,g3,g4,0);
switch (m_surfacetype)
{
case 0:
cstemp_speckle.Format("%8.8f\n%8.8f \n%8.8f\n%8.8f\n  ",baseb, cvmGet(b,0,0),
cvmGet(b,0,1),cvmGet(b,0,2)   );
break;
case 1:
cstemp_paint.Format("%8.8f\n%8.8f\n%8.8f\n%8.8f\n%8.8f\n",baseb,
cvmGet(b,0,0), cvmGet(b,0,1),cvmGet(b,0,2) ,0  );
break;
}
cstemp.Empty();
cstemp= cstemp_thres+cstemp_speckle+cstemp_paint;
ppFile.WriteString(cstemp);
ppFile.Close();
AfxMessageBox("Calibration Done");
cvReleaseMat(&X);
cvReleaseMat(&Y);
cvReleaseMat(&b);
cvReleaseMat(&Xt);
cvReleaseMat(&XtX);
cvReleaseMat(&tempM);
}
BOOL CStrainDlg::TakeInitialReading()
{
long lPixelSize=1;  //8 bits
int i,j;
BOOL flag=0;
CString cstemp;
UpdateData(TRUE);
CFileFind f;
```

```
CString cfilenameL,cfilenameR;
cfilenameL.Empty();
cfilenameL=defaultfolder+"\\"+"L.bmp";
cfilenameR.Empty();
cfilenameR=defaultfolder+"\\"+"R.bmp";
hCameras[0]=m_hCameraA;
hCameras[1]=m_hCameraB;
for (i = 0 ; i < CAMNUM ; i++)
{params[i].format.height = height;
params[i].format.pixelFormat = LUCAM_PF_8;
params[i].format.subSampleX = 1;
params[i].format.subSampleY = 1;
params[i].format.width = width;
params[i].format.xOffset = 0;
params[i].format.yOffset = 0;

params[i].exposure = m_exposure;    // 50 ms exposure
params[i].gain =  23;
params[i].strobeDelay = 0.0;  // unused
params[i].timeout = 3000.0;   // 3000 ms
params[i].useHwTrigger = FALSE;       // Set this to true for hardware
triggered setup with daisy chaining
params[i].useStrobe = FALSE;      // Set this to true if daisy-chaining
cameras
params[i].exposureDelay = 0;
params[i].shutterType = LUCAM_SHUTTER_TYPE_GLOBAL;
pParams[i] = &params[i];
}
params[0].exposure = m_exposureA;
params[1].exposure = m_exposureB;
pAllFrames = (UCHAR *)malloc((CAMNUM ) * width * height);
if (pAllFrames == NULL)
{
MessageBox("No memory for frames");
}
for (i = 0 ; i < CAMNUM ; i++)
{
ppFrames[i] = pAllFrames + i * width * height;
```

```
}
hSynchronousSnapshots = LucamEnableSynchronousSnapshots(CAMNUM, hCameras,
pParams);
m_cbPreview.EnableWindow(FALSE);
m_cbPreview.SetWindowText(_T("Preview"));
m_cbApply.EnableWindow(FALSE);
UpdateWindow();
pThread->PostThreadMessage(WM_SHOWDIALOG,NULL,NULL);
//    int delay;
CEdit* pEB = (CEdit*) GetDlgItem(IDC_DELAY);
pEB->UpdateData(TRUE);
if (m_delay<0) m_delay=0;
for(int k=0;k<m_delay;k++)
{
Sleep(1000);
if(b_keepgoing==FALSE || b_redo==TRUE) break;

}
if(b_keepgoing==TRUE && b_redo==FALSE)
{
IplImage *rL = 0;
IplImage *rR = 0;
rL = cvCreateImage( cvSize( width, height ), IPL_DEPTH_8U, 1 );
rR = cvCreateImage( cvSize( width, height ), IPL_DEPTH_8U, 1 );
IplImage *rL_blurcheck = 0;
IplImage *rR_blurcheck = 0;
rL_blurcheck = cvCreateImage( cvSize( width, height ), IPL_DEPTH_8U, 1 );
rR_blurcheck = cvCreateImage( cvSize( width, height ), IPL_DEPTH_8U, 1 );
cvZero(rL_blurcheck );
cvZero(rR_blurcheck );
BOOL no_blur=0;
while (no_blur==0)
{if (b_keepgoing==0 || b_redo==TRUE)
break;
m_tStartTime = GetTickCount();
LucamTakeSynchronousSnapshots(hSynchronousSnapshots, ppFrames);
rL->imageData=(char*)ppFrames[0];
rR->imageData=(char*)ppFrames[1];
```

```
if ((Blurcheck(rL,rL_blurcheck)==0) && (Blurcheck(rR,rR_blurcheck)==0))
no_blur=1;
cvCopy(rL, rL_blurcheck, NULL);
cvCopy(rR, rR_blurcheck, NULL);
}
PlaySound(MAKEINTRESOURCE(IDR_WAVE1),AfxGetResourceHandle(),SND_ASYNC|SND_RES
OURCE|SND_NODEFAULT);
pThread->PostThreadMessage(WM_CLOSEDIALOG,NULL,NULL);
LucamSaveImage(width, height, LUCAM_PF_8, ppFrames[0], cfilenameL);
LucamSaveImage(width, height, LUCAM_PF_8, ppFrames[1], cfilenameR);
Sleep(100);
cvReleaseImage(&rL);
cvReleaseImage(&rR);
cvReleaseImage(&rL_blurcheck);
cvReleaseImage(&rR_blurcheck);

}
if (!LucamDisableSynchronousSnapshots(hSynchronousSnapshots))
{
MessageBox("Failed to unsetup synchronous snapshots");
}
if (pAllFrames)
{
free(pAllFrames);
}
m_cbPreview.EnableWindow(TRUE);
m_cbPreview.SetWindowText(_T("Preview"));
m_cbApply.EnableWindow(TRUE);
return true;
}
BOOL CStrainDlg::CalibrationReadingSpeckle(double *subxL, double *subyL,
double *subxR, double *subyR)
{
long lPixelSize=1;  //8 bits
int i,j,k;
CString cstemp;
UpdateData(TRUE);
CFileFind f;
```

```
hCameras[0]=m_hCameraA;
hCameras[1]=m_hCameraB;
for (i = 0 ; i < CAMNUM ; i++)
{
params[i].format.pixelFormat = LUCAM_PF_8;
params[i].format.subSampleX = 1;
params[i].format.subSampleY = 1;
params[i].format.height = height;
params[i].format.width = width;
params[i].format.xOffset = 0;
params[i].format.yOffset =0;
params[i].exposure = m_exposure;    // 50 ms exposure
params[i].gain = 23;
params[i].strobeDelay = 0.0;  // unused
params[i].timeout = 3000.0;   // 3000 ms
params[i].useHwTrigger = FALSE;       // Set this to true for hardware
triggered setup with daisy chaining
params[i].useStrobe = FALSE;      // Set this to true if daisy-chaining
cameras
params[i].exposureDelay = 0;
params[i].shutterType = LUCAM_SHUTTER_TYPE_GLOBAL;
pParams[i] = &params[i];
}
params[0].exposure = m_exposureA;
params[1].exposure = m_exposureB;
pAllFrames = (UCHAR *)malloc((CAMNUM ) * width * height);
if (pAllFrames == NULL)
{
MessageBox("No memory for frames");
}
for (i = 0 ; i < CAMNUM ; i++)
{ppFrames[i] = pAllFrames + i * width * height;
}
hSynchronousSnapshots = LucamEnableSynchronousSnapshots(CAMNUM, hCameras,
pParams);
m_cbPreview.EnableWindow(FALSE);
m_cbPreview.SetWindowText(_T("Preview"));
m_cbApply.EnableWindow(FALSE);
```

```
int n;
CString refmeasurementname;
cRefFilenameL.Empty();
cRefFilenameL=defaultfolder+"\\"+"L.bmp";
cRefFilenameR.Empty();
cRefFilenameR=defaultfolder+"\\"+"R.bmp";
if(!f.FindFile(cRefFilenameL))
{
AfxMessageBox("Left Reference image doesn't exist. Can't do correlation.");
LucamDisableSynchronousSnapshots(hSynchronousSnapshots);
free(pAllFrames);
b_keepgoing=FALSE;
return FALSE;
}

if(!f.FindFile(cRefFilenameR))
{
AfxMessageBox("Right Reference image doesn't exist. Can't do correlation.");
LucamDisableSynchronousSnapshots(hSynchronousSnapshots);
free(pAllFrames);
b_keepgoing=FALSE;
return FALSE;
}
int   colindex,rowindex;
IplImage *poc_halfL = 0;
IplImage *tplL = 0;
IplImage *refL = 0;
IplImage *poc_halfR = 0;
IplImage *tplR = 0;
IplImage *refR = 0;
IplImage *poc = 0;
IplImage *refblockL=0;
IplImage *refblockR=0 ;
IplImage *reffiltered=0;
IplImage *tplfiltered=0;
IplImage *tplLtemp = 0;
IplImage *tplRtemp = 0;
IplImage *tplL_backup = 0;
```

```
IplImage *tplR_backup = 0;
tplLtemp=cvCreateImage( cvSize( bs, bs ), IPL_DEPTH_8U, 1 ) ;
tplRtemp=cvCreateImage( cvSize( bs, bs ), IPL_DEPTH_8U, 1 ) ;
poc = cvCreateImage( cvSize( bs, bs ), IPL_DEPTH_32F, 1 );
refblockL=cvCreateImage( cvSize( bs, bs ), IPL_DEPTH_8U, 1 );
refblockR=cvCreateImage( cvSize( bs, bs ), IPL_DEPTH_8U, 1 ) ;
reffiltered=cvCreateImage( cvSize( bs, bs ), IPL_DEPTH_32F, 1 );
tplfiltered=cvCreateImage( cvSize( bs, bs ), IPL_DEPTH_32F, 1 );
tplL_backup=cvCreateImage( cvSize( bs, bs ), IPL_DEPTH_8U, 1 );
tplR_backup =cvCreateImage( cvSize( bs, bs ), IPL_DEPTH_8U, 1 );
pThread->PostThreadMessage(WM_SHOWDIALOG,NULL,NULL);
/* load reference image */
refL = cvLoadImage( cRefFilenameL, CV_LOAD_IMAGE_GRAYSCALE );
/* create an image to store phase correlation result */


poc_halfL = cvCreateImage( cvSize( bs, bs ), IPL_DEPTH_32F, 1 );
refR = cvLoadImage( cRefFilenameR, CV_LOAD_IMAGE_GRAYSCALE );
/* create an image to store phase correlation result */
poc_halfR = cvCreateImage( cvSize( bs, bs ), IPL_DEPTH_32F, 1 );
/* create a image template for new imge */
tplL = cvCreateImage( cvSize( width, height ), IPL_DEPTH_8U, 1 );
int stepsize=192;
int colnum=(width-bs)/stepsize+1;
int rownum=(height-bs)/stepsize+1;
CvRect rect ;
fftwf_complex *fft_halfL[100][100],*fft_halfR[100][100];
for( colindex=0;colindex<colnum;colindex++)  // 0 -> 6
{
for(rowindex=0;rowindex<rownum;rowindex++)
{
rect= cvRect(colindex*stepsize, rowindex*stepsize,bs,bs );
cvSetImageROI(refL , rect);
cvCopy(refL , refblockL, NULL);
cvResetImageROI(refL);
filterproduct(refblockL,blockfilter,reffiltered);
memcpy (img1_half,( float* )reffiltered->imageData,bs*bs*sizeof ( float ));
fftwf_execute( fft_img1_halfsize );
```

```
fft_halfL[colindex][rowindex] = ( fftwf_complex* )fftwf_malloc ( sizeof
( fftwf_complex ) * bs * (bs/2+1) );
fftwcopy(img1_fft_half,fft_halfL[colindex][rowindex],bs* (bs/2+1) );
cvSetImageROI(refR , rect);
cvCopy(refR , refblockR, NULL);
cvResetImageROI(refR);
filterproduct(refblockR,blockfilter,reffiltered);
memcpy (img1_half,( float* )reffiltered->imageData,bs*bs*sizeof ( float ));
fftwf_execute( fft_img1_halfsize );
fft_halfR[colindex][rowindex] = ( fftwf_complex* )fftwf_malloc ( sizeof
( fftwf_complex ) * bs * (bs/2+1) );
fftwcopy(img1_fft_half,fft_halfR[colindex][rowindex],bs* (bs/2+1) );
}
}

CvPoint minlocL, maxlocL,minlocR, maxlocR, maxlocLhalf,maxlocRhalf;
CvPoint minlocLtemp, minlocRtemp, maxlocLhalftemp,maxlocRhalftemp;
double  minvalL, maxvalL,minvalR, maxvalR, maxvalLhalf, maxvalRhalf;
double  minvalLtemp, minvalRtemp, maxvalLhalftemp, maxvalRhalftemp;
int colL, rowL,colR,rowR;
int colindex_store,rowindex_store;
CvPoint oldstartL,oldstartR,startL,startR;
oldstartL=cvPoint(0,0);
oldstartR=cvPoint(0,0);
startL=cvPoint(0,0);
startR=cvPoint(0,0);
BOOL peakflag,workmode;
peakflag=FALSE;
double oldLpeak,oldRpeak;
oldLpeak=0;oldRpeak=0;
maxvalLhalf=0;maxvalRhalf=0;
colL=0;rowL=0;colR=0;rowR=0;
CButton* pCBmode = (CButton*) GetDlgItem(IDC_HANDHOLD);
pCBmode->UpdateData(TRUE);
if (pCBmode->GetCheck()==BST_CHECKED)
workmode=0;
else workmode=1;
m_tStartTime = GetTickCount();//clock();
```

```
while(b_keepgoing==1 && b_redo==FALSE)
{
m_tEndTime = GetTickCount();//clock();
dElapsed =  (m_tEndTime - m_tStartTime);
if (   ((peakflag==TRUE) && (dElapsed>0)) ||   ( (peakflag==TRUE) &&
((maxvalLhalf>thresholdhalf) && (maxvalRhalf>thresholdhalf) ) ) )
{
pThread->PostThreadMessage(WM_CLOSEDIALOG,NULL,NULL);
PlaySound(MAKEINTRESOURCE(IDR_WAVE1),AfxGetResourceHandle(),SND_ASYNC|SND_RES
OURCE|SND_NODEFAULT);
break;
}
LucamTakeSynchronousSnapshots(hSynchronousSnapshots, ppFrames);


tplL->imageData=(char*)ppFrames[0];
rect= cvRect(width/2-bs/2, height/2-bs/2,bs,bs );
cvSetImageROI(tplL , rect);
cvCopy(tplL, tplLtemp, NULL);
cvResetImageROI(tplL);
filterproduct(tplLtemp,blockfilter,tplfiltered);
memcpy (img1_half,( float* )tplfiltered->imageData,bs*bs*sizeof ( float ));
fftwf_execute( fft_img1_halfsize );
maxvalLhalf=0;
colindex_store=0;
rowindex_store=0;
for(colindex=0;colindex<colnum;colindex++)
{
for(rowindex=0;rowindex<rownum;rowindex++)
{
phase_correlation_block( fft_halfL[colindex][rowindex], img1_fft_half,
poc_halfL );
cvMinMaxLoc( poc_halfL, &minvalLtemp, &maxvalLhalftemp, &minlocLtemp,
&maxlocLhalftemp, 0 );
if (maxvalLhalftemp>maxvalLhalf)
{
maxvalLhalf=maxvalLhalftemp;
maxlocLhalf=maxlocLhalftemp;
```

```
colindex_store=colindex;
rowindex_store=rowindex;
}
}
}
if (maxlocLhalf.x>bs/2)
startL.x=colindex_store*stepsize+bs-maxlocLhalf.x;
else
startL.x=colindex_store*stepsize-maxlocLhalf.x;
if (maxlocLhalf.y>bs/2)
startL.y=rowindex_store*stepsize+bs-maxlocLhalf.y;
else
startL.y=rowindex_store*stepsize-maxlocLhalf.y;



if(  (maxvalLhalf>THRESHOLD) )   {
tplR->imageData=(char*)ppFrames[1];
rect= cvRect(width/2-bs/2, height/2-bs/2,bs,bs );
cvSetImageROI(tplR , rect);
cvCopy(tplR, tplRtemp, NULL);
cvResetImageROI(tplR);
filterproduct(tplRtemp,blockfilter,tplfiltered);
memcpy (img1_half,( float* )tplfiltered->imageData,bs*bs*sizeof ( float ));
fftwf_execute( fft_img1_halfsize );
maxvalRhalf=0;
colindex_store=0;
rowindex_store=0;
for( colindex=0;colindex<colnum;colindex++)
{
for(rowindex=0;rowindex<rownum;rowindex++)
{
phase_correlation_block( fft_halfR[colindex][rowindex], img1_fft_half,
poc_halfR );
cvMinMaxLoc( poc_halfR, &minvalRtemp, &maxvalRhalftemp, &minlocRtemp,
&maxlocRhalftemp, 0 );
if (maxvalRhalftemp>maxvalRhalf)
{
```

```
maxvalRhalf=maxvalRhalftemp;
maxlocRhalf=maxlocRhalftemp;
colindex_store=colindex;
rowindex_store=rowindex;
}
}
}
if (maxlocRhalf.x>bs/2)
startR.x=colindex_store*stepsize+bs-maxlocRhalf.x;
else
startR.x=colindex_store*stepsize-maxlocRhalf.x;
if (maxlocRhalf.y>bs/2)
startR.y=rowindex_store*stepsize+bs-maxlocRhalf.y;
else
startR.y=rowindex_store*stepsize-maxlocRhalf.y;
if  (maxvalRhalf>THRESHOLD)  {
if ( (  (maxvalLhalf>oldLpeak) && (maxvalRhalf>oldRpeak) ) ||
((maxvalLhalf>thresholdhalf) && (maxvalRhalf>thresholdhalf) )  )
{
peakflag=TRUE;
oldLpeak=maxvalLhalf;
oldRpeak=maxvalRhalf;
oldstartL=startL;
oldstartR=startR;
cvCopy( tplRtemp, tplR_backup, NULL );
cvCopy( tplLtemp, tplL_backup, NULL );
m_tStartTime = GetTickCount();//clock();
}
}
}
}
if(b_keepgoing==TRUE && b_redo==FALSE)
{
if (oldstartL.x<0)
oldstartL.x=0;
if (oldstartL.y<0)
oldstartL.y=0;
if (oldstartR.x<0)
```

```
oldstartR.x=0;
if (oldstartR.y<0)
oldstartR.y=0;
if (oldstartL.x+bs>width)
oldstartL.x=width-bs-1;
if (oldstartL.y+bs>height)
oldstartL.y=height-bs-1;
if (oldstartR.x+bs>width)
oldstartR.x=width-bs-1;
if (oldstartR.y+bs>height)
oldstartR.y=height-bs-1;
rect= cvRect(oldstartL.x, oldstartL.y,bs,bs );
cvSetImageROI(refL , rect);
cvCopy(refL , refblockL, NULL);
cvResetImageROI(refL);
filterproduct(refblockL,blockfilter,reffiltered);
filterproduct(tplL_backup,blockfilter,tplfiltered);
phase_correlation( reffiltered, tplfiltered, poc_halfL );
cvMinMaxLoc( poc_halfL, &minvalL, &maxvalL, &minlocL, &maxlocL, 0 );
int xx,yy;
if (maxlocL.x>bs/2)
xx=oldstartL.x+bs-maxlocL.x;
else
xx=oldstartL.x-maxlocL.x;
if (maxlocL.y>bs/2)
yy=oldstartL.y+bs-maxlocL.y;
else
yy=oldstartL.y-maxlocL.y;
int    x=maxlocL.x;
int  y=maxlocL.y;
CvMat* real=cvCreateMat(bs, bs, CV_32FC1);
CvMat* im=cvCreateMat(bs, bs, CV_32FC1);
for( i = 0, k = 0 ; i < bs ; i++ ) {
for( j = 0 ; j < bs ; j++, k++ ) {
cvmSet(real,i,j,(float)res_fft[k][0]);
cvmSet(im,  i,j,(float)res_fft[k][1]);
}
}
```

```
CvMat* in= cvCreateMat(bs,bs,CV_32FC2);
int factor=25;
CvMat* out= cvCreateMat(2*factor,2*factor,CV_32FC2);
upsampling(in, factor,(y-1)*factor, (x-1)*factor,out,2);
cvReleaseMat(&real);
cvReleaseMat(&im);
real=cvCreateMat(factor*2, factor*2, CV_32FC1);
im=cvCreateMat(factor*2, factor*2, CV_32FC1);
cvSplit( out, real, im, 0, 0 );
// Compute the magnitude of the spectrum Mag = sqrt(Re^2 + Im^2)
cvPow( real, real, 2.0);
cvPow( im, im, 2.0);
cvAdd( real, im , real, NULL);
cvPow( real, real, 0.5 );
cvMinMaxLoc( real, &minvalL, &maxvalL, &minlocL, &maxlocL, 0 );
cvReleaseMat(&real);
cvReleaseMat(&im);
*subxL=width/2-bs/2-xx-1+(float)maxlocL.x/factor;
*subyL=yy-(height/2-bs/2)-(-1+(float)maxlocL.y/factor);
rect= cvRect(oldstartR.x, oldstartR.y,bs,bs );
cvSetImageROI(refR , rect);
cvCopy(refR , refblockR, NULL);
cvResetImageROI(refL);
filterproduct(refblockR,blockfilter,reffiltered);
filterproduct(tplR_backup,blockfilter,tplfiltered);
phase_correlation( reffiltered, tplfiltered, poc_halfR );
cvMinMaxLoc( poc_halfR, &minvalR, &maxvalR, &minlocR, &maxlocR, 0 );
if (maxlocR.x>bs/2)
xx=oldstartR.x+bs-maxlocR.x;
else
xx=oldstartR.x-maxlocR.x;
if (maxlocR.y>bs/2)
yy=oldstartR.y+bs-maxlocR.y;
else
yy=oldstartR.y-maxlocR.y;
x=maxlocR.x;
y=maxlocR.y;
real=cvCreateMat(bs, bs, CV_32FC1);
```

```
im=cvCreateMat(bs, bs, CV_32FC1);
for( i = 0, k = 0 ; i < bs ; i++ ) {
for( j = 0 ; j < bs ; j++, k++ ) {
cvmSet(real,i,j,(float)res_fft[k][0]);
cvmSet(im,  i,j,(float)res_fft[k][1]);
}
}
upsampling(in, factor,(y-1)*factor, (x-1)*factor,out,2);
cvReleaseMat(&real);
cvReleaseMat(&im);
real=cvCreateMat(factor*2, factor*2, CV_32FC1);
im=cvCreateMat(factor*2, factor*2, CV_32FC1);
cvSplit( out, real, im, 0, 0 );
// Compute the magnitude of the spectrum Mag = sqrt(Re^2 + Im^2)
cvPow( real, real, 2.0);
cvPow( im, im, 2.0);
cvAdd( real, im , real, NULL);
cvPow( real, real, 0.5 );
cvReleaseMat(&in);
cvReleaseMat(&out);
cvMinMaxLoc( real, &minvalR, &maxvalR, &minlocR, &maxlocR, 0 );
cvReleaseMat(&real);
cvReleaseMat(&im);
*subxR=width/2-bs/2-xx-1+(float)maxlocR.x/factor;
*subyR=yy-(height/2-bs/2)-(-1+(float)maxlocR.y/factor);
if ( (maxvalL<THRESHOLD) || (maxvalR<THRESHOLD) )
AfxMessageBox("might be fake peak, measure again!");
float deflection;
CStdioFile DataFile;
cstemp.Format("%5.4f %5.4f %5.4f  %5.4f ",*subxL,*subyL,*subxR,*subyR);
if(DataFile.Open("c:\\data_fitting.txt",CFile::modeWrite|
CFile::modeNoTruncate | CFile::modeCreate ) == TRUE)
{
DataFile.SeekToEnd();
DataFile.WriteString(cstemp);
DataFile.WriteString("\n");
DataFile.Close();
}
```

```
cvReleaseMat(&real);
cvReleaseMat(&im);
cvReleaseMat(&in);
cvReleaseMat(&out);
}
for(colindex=0;colindex<colnum;colindex++)
{
for(rowindex=0;rowindex<rownum;rowindex++)
{
fftwf_free( fft_halfL[colindex][rowindex]);
fftwf_free( fft_halfR[colindex][rowindex]);
}
}
cvReleaseImage( &poc );
cvReleaseImage(&refblockL);
cvReleaseImage(&refblockR);
cvReleaseImage(&reffiltered);
cvReleaseImage(&tplfiltered);
cvReleaseImage(&tplL_backup);
cvReleaseImage(&tplR_backup);
cvReleaseImage(&tplRtemp);
cvReleaseImage(&tplLtemp);
cvReleaseImage( &tplR );
cvReleaseImage( &refR );
cvReleaseImage( &poc_halfR );
cvReleaseImage( &tplL );
cvReleaseImage( &refL );
cvReleaseImage( &poc_halfL );
if (!LucamDisableSynchronousSnapshots(hSynchronousSnapshots))
{
MessageBox("Failed to unsetup synchronous snapshots");
}
if (pAllFrames)
{
free(pAllFrames);
}
m_cbPreview.EnableWindow(TRUE);
m_cbPreview.SetWindowText(_T("Preview"));
```

```
m_cbApply.EnableWindow(TRUE);
return true;
}
```